A STUDY OF THE TRANSITION AT THE RABI FREQUENCY IN THE DRIVEN TWO LEVEL ATOM

By

Andrew S.M. Windsor

A Thesis Submitted for the Degree of Doctor of Philosophy at The Australian National University.
2001

Declaration

THE AUSTRALIAN
LIBRARY
NATIONAL UNIVERSITY

The research described in this thesis is my own work except where indicated. The work was carried out while I was a full time postgraduate student at the Australian National University.

This thesis has never been submitted to another university or similar institution.

Andrew S.M. Windsor
Canberra, 2001

ACKNOWLEDGEMENTS

First and foremost, I would like to thank my principal supervisor, Dr. Neil Manson. His commitment and professionalism is second to none. His contribution to this thesis was enormous, and a student couldn't ask for a better supervisor. I would also like to thank my other two supervisors, Dr. Nail Akhmediev and Dr. John Martin, who were sources of great support and advice during the time of this thesis.

Also in the group, I very much enjoyed working with Dr. Changjiang Wei, Dr. Andrew Greentree and, in the early stages of my project, Dr. Scott Holmstrom. These physicists helped a great deal with my work, and I enjoyed many fruitful discussions with them.

On a personal note, I would like to thank Dr. Max Bott, Dr. Hugo Giordano, Mr. Tim Dyke and Ms. Kylie Waring for being great friends and colleagues during my time at the Laser Physics Centre.

Finally, I would like to thank Cathy for her unwavering support. Without her, I could not have done it. Thanks again.

ABSTRACT

The strongly driven two level atom exhibits a transition at the Rabi frequency when it has a permanent dipole moment. In this circumstance, a **z** polarised field can interact with this transition, the Rabi transition. In chapter 1, the basic concepts are introduced, and the geometrical model of the two level atom is used to motivate the study of the Rabi transition.

In Chapter 2, a fully quantum mechanical calculation is performed to model the situation when a strong **z** polarised pump field interacts with the Rabi transition. It is found that the situation can be modelled by employing the doubly dressed states, a natural extension to the singly dressed states. The new probe beam absorption resonances that then arise (both at the driven Rabi transition, and at the original transition) are seen to be due to transitions between the doubly dressed states.

The calculation is refined in chapter 3. The semiclassical calculation is performed, which provides a more accurate solution than the one presented in chapter 2. Solutions for both **z** polarised and **x** polarised probe beams are produced, and the spectral features are explained in terms of the doubly dressed states. Higher order interactions then become evident, at the Rabi of the Rabi transition for instance. The origin of these interactions is discussed, as well as further refinements to the theoretical basis of the theoretical framework, including introducing the possibility of triply, quadruply and further dressed states.

In Chapter 4, the experimental results that examine the Rabi transition are presented, and compared with theoretical predictions. There is excellent agreement with the theoretical treatment. Higher order interactions are examined, as well as a novel triply driven Two Level Atom and it shown that triply dressed states can be used to explain these results.

Contents

Chapter 1

Introduction

This chapter introduces the ideas that are central to this thesis. Firstly, the commonly used two level atom model [1] is explained, with some remarks on the spectroscopic methods used to probe this simple theoretical model. The two level atom can also be represented using the so called vector model, and this model will be used to demonstrate the existence of a new resonance, the *Rabi resonance.* The relation of this resonance with systems that have a permanent dipole moment is developed. The dressed state analysis is presented which provides the theoretical backbone of this thesis as well as an elegant explanation for the emergence of the Rabi resonance.

1.1 The Two Level Atom

The two level atom (henceforth referred to as the TLA) is the most fundamental system in the study of how light interacts with matter. Most of the important concepts in quantum optics can be understood in terms of this simple model. The "matter" in this approximation becomes an atom with only two energy levels, the ground state $|g\rangle$ with energy 0 and the excited state $|e\rangle$ with energy $\hbar\omega_0$. The radiation that is coupled to this simple quantum system can be either a classical field (the *semiclassical* regime) or a fully quantum mechanical one. The coupling is assumed to be via the familiar dipole interaction.

The solutions of this system provide a powerful explanation for many phenomena in modern quantum optics and in particular spectroscopy, with notable examples including the Mollow

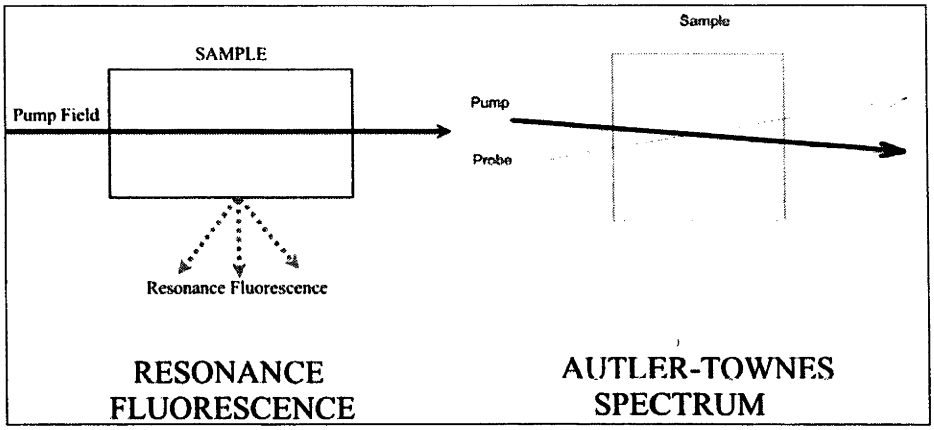

Figure 1-1: Diagramatic representations of the Resonance Fluorescence (left) and Autler-Townes (or Mollow) absorption spectra (right).

spectrum [3]-[4], Resonance Fluorescence [6]-[8] and the Autler-Townes Spectra [2]. All of these spectroscopic techniques involve driving the TLA with a strong *pump* field, and then observing the spectral characteristics of the fluorescence (Resonance Fluorescence) or the effect on the absorption spectrum of a weak probe field coupled to either the driven transition itself (Mollow spectrum), or to a third, weakly coupled transition (Autler Townes Spectroscopy).

The spectra obtained from these methods give valuable insight into the dynamics of the driven atom, including the populations of the atomic levels, the energy level scheme of the combined 'atom+field' system, and so on. A schematic representation of the two methods is shown in Fig 1-1. In the resonance fluorescence case , the photodetector conventionally observes fluorescence photons emitted at right angles to the incident pump field, and in the absorption case, the detector counts probe field photons. Note that these two methods do not in principle provide different information (in fact are very similar in the mathematical details) so the choice of which spectroscopic method is used is one of experimental convenience. In this thesis, it is the probe absorption spectrum that is the experimentally verifiable one, so much more emphasis is placed on it.

Obviously, a real system has many more energy levels that just the two considered in this simplified system, however the effects of these extra transitions can be ignored if the strong field is nearly resonant with the transition in question. Under these quasi-resonant conditions,

the TLA model provides excellent results, with the benefits of the system being mathematically simple and intuitive in its properties. In fact the experimental system that this thesis deals with is remarkable in its closeness to the ideal two level atom scenario, and provides excellent agreement with the theoretical predictions of the TLA.

1.2 The Dressed State Formalism

The results of all of the above spectroscopic techniques can be nicely explained using the elegant dressed state formalism. The dressed states are the Eigenstates of the fully quantum mechanical Hamiltonian that describes the driven two level system [9]-[12] (for the semiclassical treatment, see [13]-[15]). In this circumstance, the light is modelled as a fully quantum mechanical superposition of Fock states $|n\rangle$, characterised by photon number n. The dressed states are a central theme of this thesis, and in particular a natural progression of them, the *doubly dressed states* are used to explain the phenomena examined in this thesis.

1.2.1 The fully quantum mechanical atom-light interaction

To start with, the atom is considered to be a simple TLA and the light will be modelled quantum mechanically. Under these circumstances, the Hamiltonian for the system becomes

$$\mathcal{H}_0 = \mathcal{H}_A + \mathcal{H}_F + \mathcal{H}_{AF}$$

where the components of the Hamiltonian include the bare atom and the "bare" field Hamiltonians

$$\begin{aligned} \mathcal{H}_A &= \hbar\omega_0 |e\rangle \langle e| \\ \mathcal{H}_F &= \hbar\omega_x \left(a^\dagger a + \frac{1}{2}\right) \end{aligned} \tag{1.1a}$$

where ω_0 represents the TLA interaction frequency, ω_1 is the frequency of the light and a

and $a^\dagger$ are the annihilation and creation operators for the light field. The third term $\mathcal{H}_{AF}$ is the dipole interaction for this system

$$\mathcal{H}_{AF} = \hbar g \left(a + a^\dagger\right)\left(\sigma^+ + \sigma^-\right) \tag{1.2}$$

with the definitions

$$\begin{aligned} g &= -\overrightarrow{\epsilon}\cdot\overrightarrow{d}_{eg}\sqrt{\frac{\omega_1}{2\hbar\epsilon_0 V}} \\ \sigma^+ &= |e\rangle\langle g| \\ \sigma^- &= |g\rangle\langle e| \end{aligned}$$

where $\overrightarrow{\epsilon}$ gives the polarisation vector of the applied field, and $\overrightarrow{d}_{eg}$ is the dipole moment of the system. Implicit in this is the assumption that the size of the atom is such that the spatial variation of the field is negligible over the atomic area.

1.2.2 The Quantum mechanical Rotating Wave approximation

To proceed, a well known and fundamental approximation known as the *rotating wave approximation* (RWA) needs to be applied. The interaction term $\mathcal{H}_{AF}$ can be broken up into a resonant (energy conserving, $\mathcal{H}_r$) and an anti-resonant (non energy conserving, $\mathcal{H}_{ar}$) term

$$\begin{aligned} \mathcal{H}_{AF} &= \mathcal{H}_r + \mathcal{H}_{ar} \\ \mathcal{H}_r &= \hbar g\left(a\sigma^+ + a^\dagger\sigma^-\right) && \text{(1.3a)} \\ \mathcal{H}_{ar} &= \hbar g\left(a\sigma^- + a^\dagger\sigma^+\right) && \text{(1.3b)} \end{aligned}$$

Equation 1.3*a* refers to a process where the atom goes from the ground state to the excited state coupled with a loss of a photon from the field (and vice versa). These terms are physically significant for a near resonant driving field, and remain. However, 1.3*b* represents processes such as the absorption of a photon at the same time that the TLA goes from the excited to the ground state. These terms are discarded as they are not energy conserving, and won't be

significant. These terms do in fact have an impact (the well known Bloch-Siegert shift [16]) which will be examined within the context of this thesis in chapter 3.

Finally then, after the RWA has been taken, the form of the Hamiltonian becomes

$$\mathcal{H}_0 = \hbar\omega_0 |e\rangle \langle e| + \hbar\omega_1 \left(a^\dagger a + \frac{1}{2}\right) + \hbar g \left(a\sigma^+ + a^\dagger\sigma^-\right) \tag{1.4}$$

and it is this Hamiltonian that is diagonalised by the dressed states.

1.2.3 The Dressed State Basis

The Hamiltonian 1.4 can be written in terms of the basis states

$$\begin{aligned} |e,n\rangle &= |e\rangle \otimes |n\rangle \\ |g,n\rangle &= |g\rangle \otimes |n\rangle \end{aligned}$$

It is noted that, in this basis, equation 1.4 can be written as the infinite sum of separate energy level doublet *manifolds*

$$\mathcal{H}_0 = \sum_{n=1}^{\infty} \mathcal{H}_n$$

where

$$\begin{aligned} \mathcal{H}_n &= \hbar\left(\delta |e,n-1\rangle \langle e,n-1| + \left(n\omega_1 + \frac{1}{2}\right)\hat{I}_n\right) \\ &\quad +\hbar g\sqrt{n}\left(|e,n-1\rangle \langle g,n| + |g,n\rangle \langle e,n-1|\right) \end{aligned} \tag{1.6}$$

where $\delta = \omega_0 - \omega_1$ is the detuning of the light field from the atomic resonance, and the identity operator $\hat{I}_n$ is given by

$$\hat{I}_n = |e,n-1\rangle \langle e,n-1| + |g,n\rangle \langle g,n|$$

so the Hamiltonian manifolds now form a *closed system* which is easily diagonalised by the so called *dressed states*

$$|1,n\rangle = \cos\theta_n |e,n-1\rangle + \sin\theta_n |g,n\rangle$$
$$|2,n\rangle = -\sin\theta_n |e,n-1\rangle + \cos\theta_n |g,n\rangle$$

The following definitions have been used

$$\cos 2\theta_n = -\frac{\delta}{\Omega_n}, \sin 2\theta_n = \frac{\chi_n}{\Omega_n}$$

where the positive quantum mechanical *Rabi frequency* is defined $\chi_n = |-2g\sqrt{n}|$ and the *generalised Rabi frequency* $\Omega_n^2 = \delta^2 + \chi_n^2$. Note that the angle θ can take values from 0 to $\frac{\pi}{2}$. The Rabi frequency thus characterises the strength of the interaction of the applied field with the TLA, and the generalised Rabi frequency characterises the energy level splitting of the new levels. The new eigenlevels of the system (and hence the energy levels) are

$$\mathcal{H}_n |1,n\rangle = \left((n+1/2)\omega_1 + \frac{\delta}{2} - \frac{\Omega_n}{2}\right)|1,n\rangle$$
$$\mathcal{H}_n |2,n\rangle = \left((n+1/2)\omega_1 + \frac{\delta}{2} + \frac{\Omega_n}{2}\right)|2,n\rangle$$

A final assumption that simplifies the above is that the radiation field is very strong $n \gg 1$, implying that $\Omega_n \approx \Omega_{n-1}$ so the dependence on n of the generalised Rabi frequency above is then ignored (i.e. $\Omega_n \rightarrow \Omega$). The final energy levels then become

$$\mathcal{H}_n |1,n\rangle = \left((n+1/2)\omega_1 + \frac{\delta}{2} - \frac{\Omega}{2}\right)|1,n\rangle$$
$$\mathcal{H}_n |2,n\rangle = \left((n+1/2)\omega_1 + \frac{\delta}{2} + \frac{\Omega}{2}\right)|2,n\rangle$$

The energy levels of the "TLA + radiation" system is therefore given by an infinite ladder of doublets, indexed by n (the Fock number), where the *inter-doublet* separation is given by the radiation frequency ω_1, and the *intra-doublet* separation is given by the generalised Rabi frequency Ω. In fig 1-2, the energy level diagram is shown, firstly of the bare system, then of the dressed system.

This dressed state picture enables a convenient explanation of the major spectroscopic

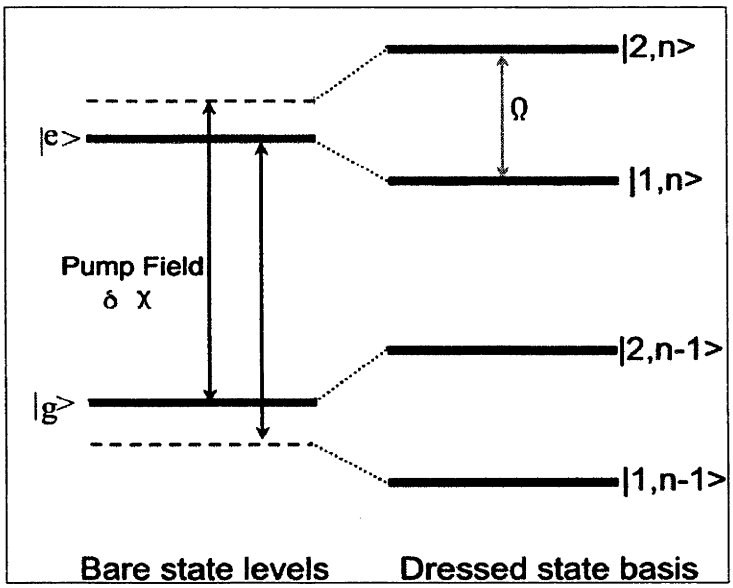

Figure 1-2: The dressed state basis (right) generated by the driving field (detuning δ, Rabi frequency χ) interacting with the bare state TLA (left). The dressed state basis is a infinite ladder of energy level doublets, with inter-doublet separation ω_1 and intra-doublet separation Ω, of which two manifolds are shown here.

features associated with the driven TLA as transitions between the dressed states, rather than between the bare state levels $|e\rangle$ and $|g\rangle$. To understand this, refer to the well known work of Cohen-Tannoudji [9]-[12], where an analysis of the dressed state formalism gives for the steady state populations of the dressed states

$$P_2 = \frac{\sin^4\theta}{\cos^4\theta + \sin^4\theta}$$
$$P_1 = \frac{\cos^4\theta}{\cos^4\theta + \sin^4\theta}$$

where $P_{1,2}$ denotes the population of dressed state $|1,2,n\rangle$. This shows that in the case of resonance ($\delta = 0$), the populations are equalized. In the case where the system is negatively detuned (i.e. $\delta < 0$), there is a higher population in the 'excited' dressed state $|2,n\rangle$ than the 'ground' dressed state $|1,n\rangle$ and vice versa. With a bare state relaxation rate of Γ included in the model, the relaxation rates for the transitions between the excited states and the ground

states are given by

$$\begin{aligned}\Gamma_{coh} &= \Gamma\left(\frac{1}{2}+\cos^2\theta\sin^2\theta\right)\\ \Gamma_{pop} &= \Gamma\left(\cos^4\theta+\sin^4\theta\right)\end{aligned}$$

where Γ_{coh} refers to the coherence relaxation rate, and Γ_{pop} the population relaxation rate. These results then give the basic dynamics of the driven system. A more thorough treatment of these results, with the extension to the doubly dressed states, is presented in chapter 2.

1.3 Results from Spectroscopy

1.3.1 Resonance Fluorescence

The well known Resonance Fluorescence spectrum [6]-[8] for the on-resonant case is shown in Fig 1-3. This spectrum demonstrates three transitions, the one at ω_1 is simply the emission from $|1,n\rangle$ to $|1,n-1\rangle$ and $|2,n\rangle$ to $|2,n-1\rangle$, between the energy level doublets. The side bands, at $\omega_1 \pm \Omega$ are due to interactions between energy level doublets as well. $\omega_1+\Omega$ is due to emission from $|2,n\rangle$ to $|1,n-1\rangle$, and the peak at $\omega_1-\Omega$ is induced by emission from $|1,n\rangle$ to $|2,n-1\rangle$. This is presented in figure 1-3. The integrated areas of the peak represent the product of the populations of the excited state and the transition rate, and the widths are related to the moment between the dressed states.

1.3.2 Autler-Townes Spectrum

In this case [2], the probe beam (frequency ω_p) is coupled to the transition between the two level atom's ground state $|g\rangle$ and a weakly interacting third level $|c\rangle$ (transition frequency ω_c). The on resonance case is shown in Fig 1-4, showing two peaks at $\omega_c-\omega_g \pm \frac{1}{2}\Omega$. Denoting the third energy level by $|c\rangle$, these peaks are given by transitions induced by the probe beam between $|1,n\rangle$ and $|c,n\rangle$ for the resonance at $\omega_c-\omega_g+\frac{1}{2}\Omega$, and between $|2,n\rangle$ and $|c,n\rangle$ for the resonance at $\omega_c-\omega_g-\frac{1}{2}\Omega$. The relative peak heights are then given by the relative populations of the dressed states $|1,n\rangle$ and $|2,n\rangle$, and their widths are given by the relaxation rate of the

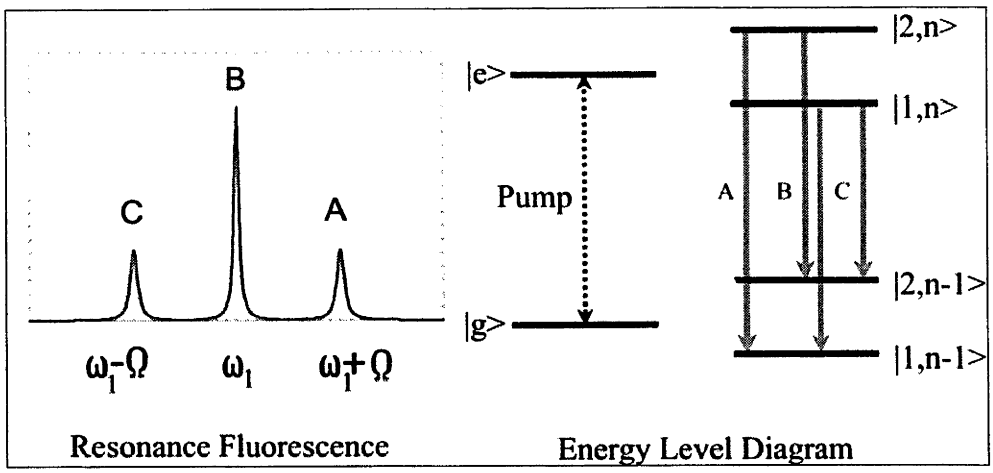

Figure 1-3: Fluorescence spectrum (left) with on-resonant driving field of frequency ω_1 and Rabi frequency Ω. Energy level diagram (right) shows the transitions associated with the peaks on the left.

probe beam transition.

1.3.3 Mollow Spectrum

This configuration [3]-[4] sees a probe beam applied to the same transition over which the pump beam is applied. Since the resonance condition causes the populations of the upper and lower dressed states to equalize, there is no net absorption of the probe beam (in the first order calculation - at higher orders coherences give a small absorption signal [5]). It makes more sense, then, to look at the absorption of the probe beam in the special case where the pump field is off resonance. Say the beam is negatively detuned ($\delta < 0$, $\omega_1 > \omega_0$), then there is more population in the $|2, n\rangle$ dressed state than the $|1, n-1\rangle$ state, so the transition of the $\omega_1 + \Omega$ line is emissive in nature, and (for analogous reasons) the $\omega_1 - \Omega$ line is absorptive in nature. The line weights are given by the product of the population difference between the appropriate levels and the transition strength between them. Fig 1-5 shows the spectrum in this case, with the energy level diagram and relative populations shown.

The dressed state model has many advantages, but much of the work in this thesis will concentrate on an alternative method of modelling this scenario. The semiclassical model in which the atom is treated quantum mechanically, but the radiation is considered to be a

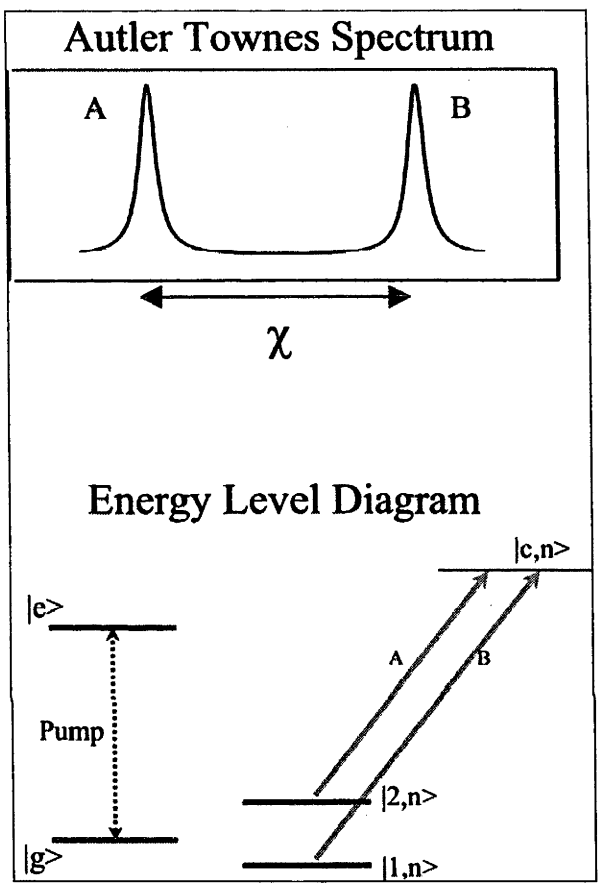

Figure 1-4: Autler Townes Spectrum, showing two peaks where the probe beam weakly interacts betweent the third level and the dressed states. This results in the two transitions shown in the energy level diagram, and their coresponding peaks in the absorption spectrum.

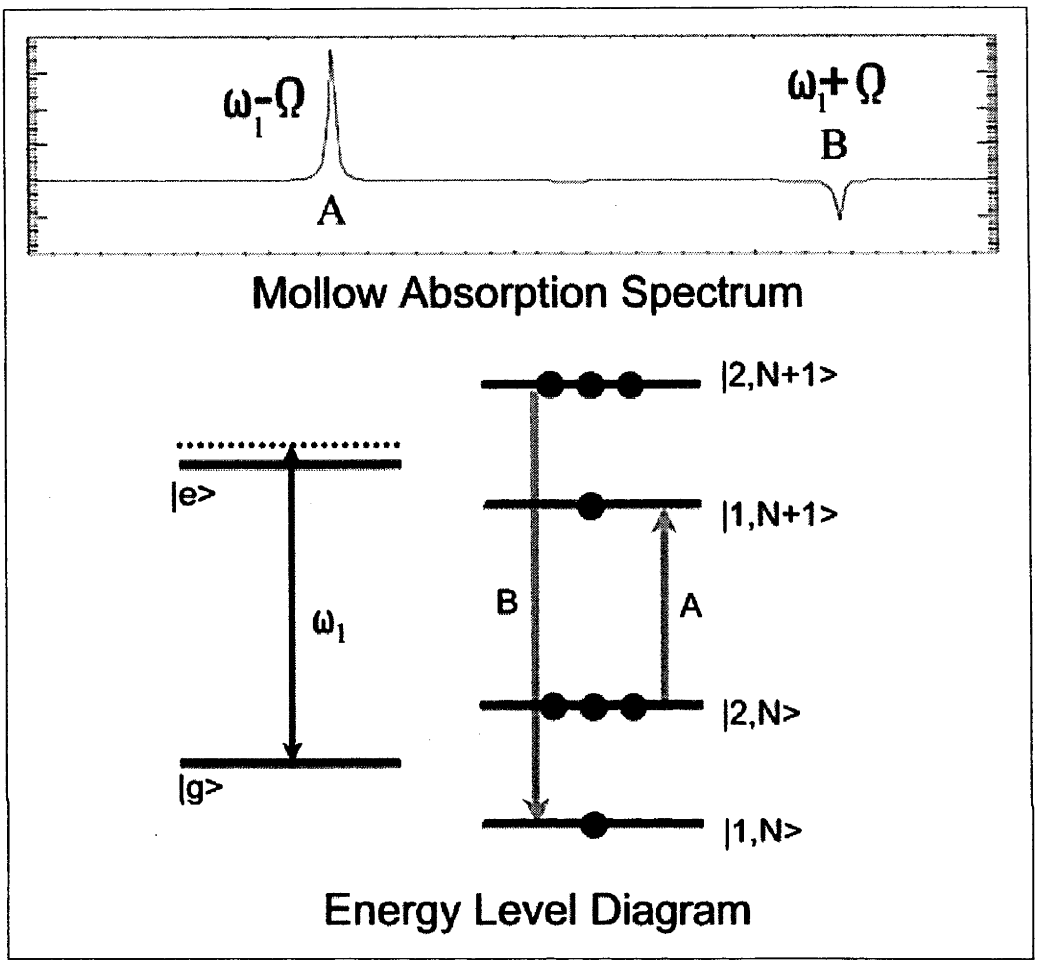

Figure 1-5: Off-resonance Mollow spectrum. Off resonant energy level diagram displays the relative populations in the dressed state basis by the number of circles. The two resonances in the spectrum labelled A and B are then shown as transitions between the dressed state levels, with the arrow directions denoting absorptive (upwards) or emissive (downwards) spectral lines. Note that there is generally a very small central dispersive feature, however this is too weak to be seen in this picture.

classical field, allows a somewhat more powerful analysis even if it is not as intuitive. The Mollow spectrum will be presented in more detail later in the chapter.

1.4 The Semiclassical Two Level Atom

In the semiclassical TLA model, the atom is treated as a two level quantum system, while the coupled radiation is modelled as a classical field. The radiation is coupled to the two level atom via the familiar dipole coupling. The formalism is well known, so only a brief introduction is presented here.

1.4.1 Density Matrix Formalism

Firstly, the well known density matrix formalism is presented, which is used to study systems in quantum statistics. The wave function for the system $|\Psi(t)\rangle$, which is a solution of the time-dependent Schrodinger equation, is given by

$$i\hbar\frac{\partial}{\partial t}|\Psi(t)\rangle = (\mathcal{H}_0 + V(t))|\Psi(t)\rangle$$

where the total Hamiltonian is made up of a time dependent part $V(t)$ and a time independent part $\mathcal{H}_0$. Once the eigenstates of $\mathcal{H}_0$ (call them $|n\rangle$) have been found, the total wave function can be written

$$|\Psi(t)\rangle = \sum_n c_n(t)|n\rangle \tag{1.7}$$

In a complex system (for example a collection of atoms in thermal equilibrium), then each atom may be found in one of various atomic states, and the system is said to be in a mixed state. Under these conditions, it is useful then to model the system as a statistical ensemble of pure wave functions, where it can be said that the atom has a certain probability of residing in one of the state. It is more convenient to use the so called *density matrix* operator to describe the statistical nature of of the system. This operator is defined as

$$\rho = \sum_\Psi P_\Psi |\Psi\rangle\langle\Psi| \tag{1.8}$$

where the sum is over all of the statistically accessible states $|\Psi\rangle$ and P_Ψ gives the probability that the system is described by that particular statistically accessible state $|\Psi\rangle$. If there is no statistical mixing of the state, then the system is said to be in a *pure* state, and the system is known to be described by a single state $|\Psi\rangle$. Then, eq. 1.8 becomes

$$\rho = |\Psi\rangle \langle\Psi|$$

and using the expansion in eq. 1.7

$$\rho = \sum_{n,m} \rho_{nm} |n\rangle \langle m|$$

where the density operator matrix elements become $\rho_{nm} = c_n c_m^\star$. This allows a simple physical interpretation of the density matrix components. When $n = m$ (the diagonal terms), $\rho_{nn} = |c_n|^2$ gives the probability that the system will be found to be in basis state $|n\rangle$ after a measurement. It is clear that ρ_{nn} can be thought of as the *population* of state $|n\rangle$. When $n \neq m$ then the density matrix component represents the way that the two states $|n\rangle$ and $|m\rangle$ are correlated, which corresponds to the *coherence* of the system.

The density matrix formalism is particularly useful for calculating the expectation values of Hermitian operators (e.g. A)

$$\begin{aligned} \langle A \rangle &= \langle \Psi | A | \Psi \rangle \\ &= Tr(\rho A) \end{aligned}$$

The time evolution of the density matrix operator is given (according to the time-dependent Schrodinger equation) by the Liouville equation

$$\dot{\rho} = -\frac{i}{\hbar} [\mathcal{H}, \rho]$$

where $\mathcal{H} = \mathcal{H}_0 + V(t)$ is the total Hamiltonian. To model more complex systems of TLAs in solids, where external environmental factors induce damping, the Liouville equation can be

expanded to introduce phenomenological damping terms

$$\dot{\rho} = -\frac{i}{\hbar}[\mathcal{H}, \rho] + \text{damping terms} \tag{1.9}$$

which is useful where the damping mechanisms of the total system are too complex to be reliably modelled, or the details of the damping are not known.

1.4.2 Density Matrix Equations of motion for the driven TLA

In the semiclassical system, the atom is again modelled as a pair of energy states, the ground state $|g\rangle$ and excited state $|e\rangle$ with energy $\hbar\omega_0$. The Hamiltonian of the uncoupled atom is then simply given by

$$\mathcal{H}_A = \hbar\omega_0 |e\rangle \langle e|$$

The radiation field is modelled as a simple classical electrical field of strength E, polarised along the $\hat{x}$ axis and with frequency ω_x. The subscript x here is used to indicate that the field in question is $\hat{x}$ polarised.

$$\overrightarrow{E} = E_x \hat{x} \cos \omega_x t$$

$\hat{x}$ here is defined to be at right angles to the axis of the two level atom, which is defined to lie along the $\hat{z}$ axis. The interaction of the radiation with the TLA is given by the dipole interaction,

$$V(t) = -\overrightarrow{\mu} \bullet \overrightarrow{E}$$

with the electric dipole moment operator $\overrightarrow{\mu}$ defined

$$\overrightarrow{\mu} = \mu\hat{x}(|g\rangle \langle e| + |e\rangle \langle g|)$$

where it is assumed that $\mu_{eg} = \mu_{ge}$. The total Hamiltonian is thus given by

$$\begin{aligned}\mathcal{H}' &= \hbar\omega_0 |e\rangle\langle e| - \mu E\left(|g\rangle\langle e| + |e\rangle\langle g|\right)\cos\omega_x t \\ &= \hbar\omega_0 |e\rangle\langle e| + \hbar\chi_x\left(|g\rangle\langle e| + |e\rangle\langle g|\right)\cos\omega_x t\end{aligned}$$

where the *Rabi frequency* χ_x is defined as

$$\chi_x = -\frac{\mu E_x}{\hbar}$$

Note the use of the x subscript. This is not usually employed but as the thesis is developed, its usefulness will become clear. For the moment, suffice it to say that the x refers to the polarisation of the incident field. This thesis will deal with the interaction of differently polarised fields with the TLA, so the distinction of polarisation will become important later on. Substituting this Hamiltonian into the Liouville equation eq. 1.9 the semiclassical equations of motion for the driven TLA (with phenomenological relaxation terms included) become

$$\begin{aligned}\dot{\rho}_{gg} &= -i\chi_x\left(\rho_{eg} - \rho_{ge}\right)\cos\omega_x t - \gamma\left(\rho_{gg} - \rho_{gg}^{eq}\right) \\ \dot{\rho}_{ee} &= i\chi_x\left(\rho_{eg} - \rho_{ge}\right)\cos\omega_x t - \gamma\left(\rho_{ee} - \rho_{ee}^{eq}\right) \\ \dot{\rho}_{ge} &= \left(i\omega_0 - \Gamma\right)\rho_{ge} - i\chi_x\cos\omega_x t\left(\rho_{ee} - \rho_{gg}\right)\end{aligned} \tag{1.10}$$

Here the longitudinal and transverse relaxation rates, γ and Γ respectively, have been introduced. It is assumed that the coherence of the system in the undriven system will tend to relax to zero, and that the populations will relax to some equilibrium, ρ_{ee}^{eq} and ρ_{gg}^{eq}. Note that $\rho_{eg} = \rho_{ge}^{\star}$ so that eq. 1.10 also provides the equation of motion for ρ_{eg}. To simplify this a little, define the population difference $W = \rho_{ee} - \rho_{gg}$, leading to

$$\begin{aligned}\dot{\rho}_{ge} &= \left(i\omega_0 - \Gamma\right)\rho_{ge} - i\chi_x\cos\omega_x t W \\ \dot{W} &= -2i\chi_x\left(\rho_{ge} - \rho_{eg}\right)\cos\omega_x t - \gamma\left(W - W^{eq}\right)\end{aligned} \tag{1.11}$$

where the equilibrium population difference $W^{eq} = \rho_{ee}^{eq} - \rho_{gg}^{eq}$ has been defined. Note that $W^{eq} < 0$ in standard systems in the absence of a driving field, so in general it is expected

that the population of the excited state to be less than that of the ground state in equilibrium conditions.

1.4.3 Semiclassical Rotating Wave Approximation

The Rotating Wave Approximation (RWA) is one of the most important approximations that can be made to simplify the above equations. It is exactly analogous to the RWA taken in the dressed state basis. To apply the approximation, a transformation to the rotating frame is firstly performed

$$\rho_{ge} = \tilde{\rho}_{ge} e^{i\omega_x t}$$

which transforms eq. 1.11 to

$$\begin{aligned} \frac{d}{dt}\tilde{\rho}_{ge} &= (i\delta_x - \Gamma)\,\tilde{\rho}_{ge} - \frac{i\chi_x}{2}\left(1 + e^{-2i\omega_x t}\right) W \\ \dot{W} &= -2i\chi_x \left(\tilde{\rho}_{ge} e^{i\omega_x t} - \tilde{\rho}_{eg} e^{-i\omega_x t}\right) \cos\omega_x t - \gamma\left(W - W^{eq}\right) \end{aligned}$$

The detuning $\delta_x = \omega_0 - \omega_x$ gives the difference between the natural frequency of the TLA ω_0 and the frequency of the applied field ω_x. The RWA involves discarding the rapidly varying terms in this equation. This reflects the fact that the classical field is composed of a resonant rotating component and an anti-resonant counter-rotating term. The effect of this second term is expected to be negligible and so it is ignored (they affect of this approximation is examined in section 3.5.1). The resultant equations of motion therefore become

$$\begin{aligned} \tfrac{d}{dt}\tilde{\rho}_{ge} &= (i\delta_x - \Gamma)\,\tilde{\rho}_{ge} - \tfrac{i\chi_x}{2} W \\ \dot{W} &= -i\chi_x\left(\tilde{\rho}_{ge} - \tilde{\rho}_{eg}\right) - \gamma\left(W - W^{eq}\right) \end{aligned} \tag{1.12}$$

which are the basic Bloch [1] equations that facilitate the study of the TLA. These equations describe the dynamics of the simple TLA, when strongly driven by a quasi-resonant classical magnetic field. They provide the basis for the bulk of the theoretical work that makes up the backbone of this thesis. To provide insight into these equations, they can be rewritten in another form which allows a simple geometrical interpretation of the resultant dynamics of the

system.

1.4.4 Spherical Coordinates

To see this graphical interpretation, which will be useful later for motivating the Rabi transition, a transformation to *spherical coordinates* is required [1]. These are defined

$$U = (\rho_{12} + \rho_{21})$$
$$V = i(\rho_{21} - \rho_{12})$$

so it is immediately obvious that these quantities are now real. Transforming the Bloch equations (eq.1.12) into this basis gives

$$\begin{aligned} \dot{U} &= -\delta_x V - \Gamma U \\ \dot{V} &= \delta_x U - \Gamma V - \chi_x W \\ \dot{W} &= \chi_x V - \gamma(W - W^{eq}) \end{aligned} \tag{1.13}$$

This new description of the Bloch equations allows for physical interpretation of these spherical coordinates. W is the population difference, U is the dispersion and V is the absorption. The steady state solutions for eq. 1.13 is given by

$$\begin{aligned} U^{ss} &= \frac{W^{eq}\gamma\chi_x\delta_x}{D} \\ V^{ss} &= -\frac{W^{eq}\gamma\chi_x\Gamma}{D} \\ W^{ss} &= \frac{W^{eq}\gamma\left(\delta_x^2 + \Gamma^2\right)}{D} \end{aligned} \tag{1.14}$$

where

$$D = \gamma\left(\Gamma^2 + \delta_x^2\right) + \Gamma\chi_x^2$$

These provide the familiar *dispersive* and *absorptive* curves. They are shown in figure 1-6. The Bloch equations in spherical coordinates may be written out in matrix form

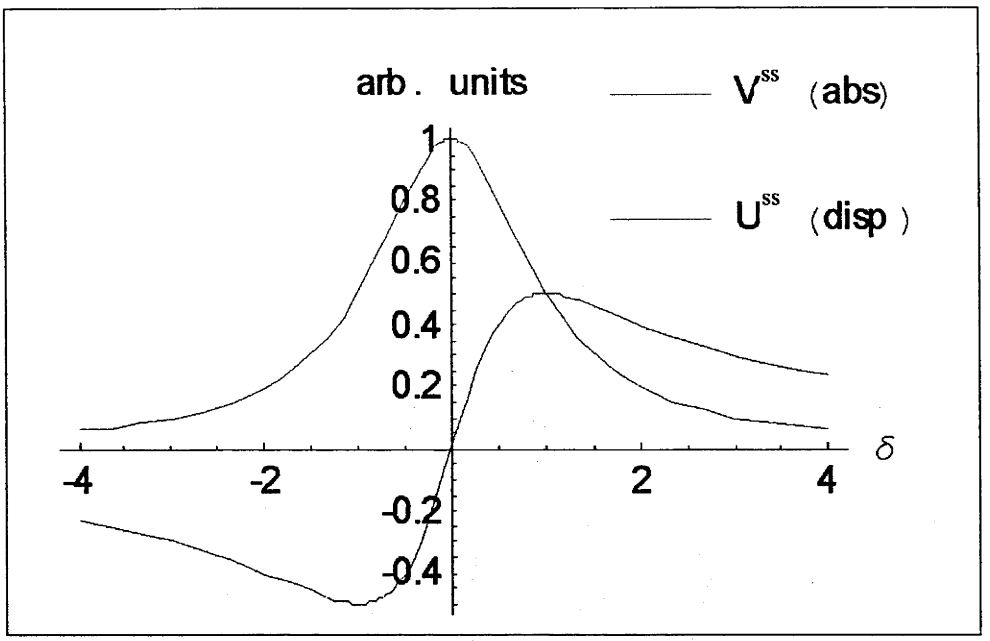

Figure 1-6: The steady state solutions for the driven TLA. The absorption is given in red, the dispersion in blue.

$$\frac{d}{dt}\begin{pmatrix} U \\ V \\ W \end{pmatrix} = \begin{pmatrix} -\Gamma & -\delta_x & 0 \\ \delta_x & -\Gamma & -\chi_x \\ 0 & \chi_x & -\gamma \end{pmatrix}\begin{pmatrix} U \\ V \\ W \end{pmatrix} + \begin{pmatrix} 0 \\ 0 \\ \gamma W^{eq} \end{pmatrix} \tag{1.15}$$

Ignoring the relaxation terms for the point of demonstration and defining the *Bloch vector* $\overrightarrow{m} = [U, V, W]$ then eq.1.15 is equivalent to

$$\frac{d}{dt}\overrightarrow{m} = -\overrightarrow{m} \times \overrightarrow{\Omega}$$

where

$$\overrightarrow{\Omega} = [\chi_x, 0, \delta_x]$$

There is an obvious similarity between this equation and the well known equation of motion for the fully classical magnetic dipole $\overrightarrow{\mu}$ with gyromagnetic ratio γ_m in a static magnetic field

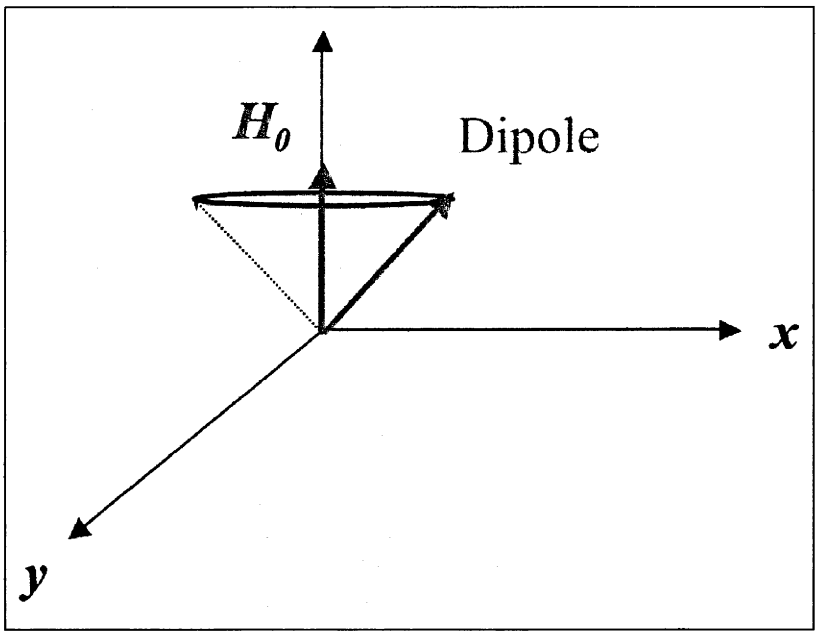

Figure 1-7: The Magnetic Dipole μ precesses about the static field H_0 with frequency given by the Larmor frequency ω_0.

$\overrightarrow{H}_0$;

$$\frac{d}{dt}\overrightarrow{\mu} = -\gamma_m \overrightarrow{\mu} \times \overrightarrow{H}_0$$

The connection between the entirely classical case of the magnetic dipole and the semiclassical driven TLA is then clear. In the classical case, the magnetic dipole precesses about the static magnetic field with a frequency given by the Larmor frequency $\omega_0 = \gamma_m \left|\overrightarrow{H_0}\right|$, as shown in fig 1-7.

Likewise, in the semiclassical driven atom, the Bloch vector $\overrightarrow{m}$ will precess about the $\overrightarrow{\Omega}$ vector (see Fig 1-8), and the frequency of its precession is given then by $\left|\overrightarrow{\Omega}\right| = \sqrt{\delta_x^2 + \chi_x^2}$. This frequency, which is obviously related to the Rabi frequency χ_x which characterised the strength of the dipole interaction, is the *Generalised Rabi frequency.* It characterises in a fundamental way the dynamics of the driven TLA, as can be seen from these results. In particular, since the Bloch vector component W is simply the population difference between the excited and ground states, the dipole interaction will cause the state populations to cycle at a frequency given by Ω,

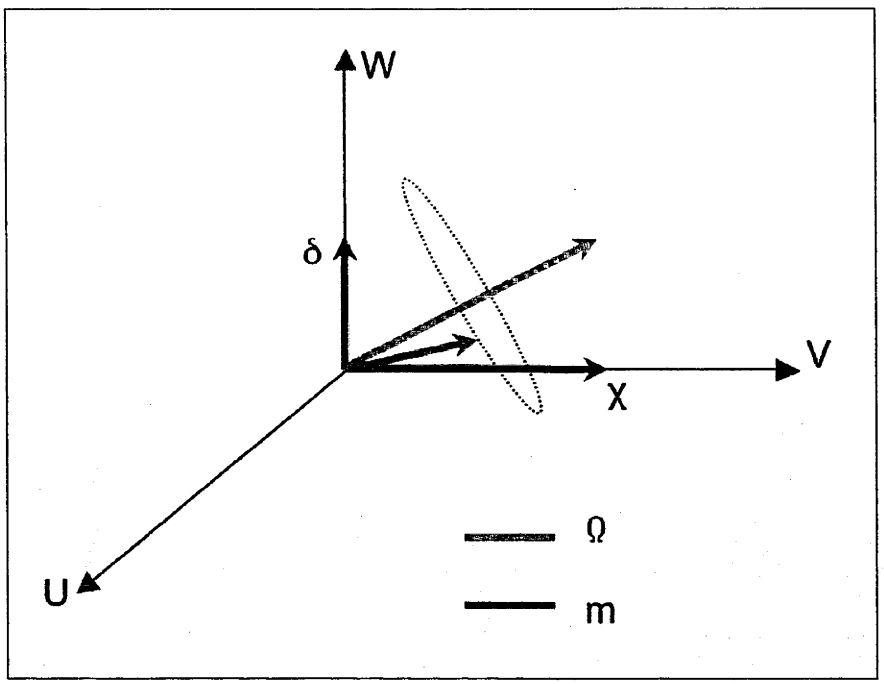

Figure 1-8: The precession of the Bloch vector m about the vector Ω, with the frequency of the precession equal to the generalised Rabi frequency.

the generalised Rabi frequency. Intuitively, it can be seen that the phenomenological damping terms will tend to damp the vector until it lies along the population axis, with a length given by the equilibrium population difference, W^{eq}.

Shortly the Bloch vector model will be used to demonstrate very effectively the existence of a new transition, the *Rabi transition*, the study of which forms the basis for this work.

1.4.5 Semiclassical Dressed State Basis

In a manner completely analogous to the fully quantum mechanical dressed state basis, it is possible to define a semiclassical dressed state basis that will solve the Bloch equations (eq 1.12). It is employable in the circumstance where $\Gamma = \gamma$, i.e. the transverse and population relaxation rates are the same. Note that for purely radiative dampening $\Gamma = 2\gamma$. The case of more general dampening is considered in section 3.5.3. To see this, define the *semiclassical dressed states*

$$
\begin{aligned}
|1\rangle &= \cos\theta\,|g\rangle - \sin\theta\,|e\rangle \\
|2\rangle &= \sin\theta\,|g\rangle + \cos\theta\,|e\rangle
\end{aligned}
$$

with the definitions

$$
\cos 2\theta = \frac{\delta_x}{\Omega_x} \qquad \sin 2\theta = \frac{\chi_x}{\Omega_x}
$$

These states are the semiclassical analogs to the quantum mechanical dressed states employed earlier. Under this transformation, the Bloch equation becomes (with $\Gamma = \gamma$)

$$
\begin{aligned}
\dot{\rho}_{12} &= i\Omega_x \rho_{12} - \Gamma\left(\rho_{12} - \rho_{12}^{eq}\right) \\
\dot{W}_d &= -\Gamma\left(W_d - W_d^{eq}\right)
\end{aligned}
$$

where

$$
\begin{aligned}
W_d &= \rho_{22} - \rho_{11} \\
\rho_{12}^{eq} &= \frac{\chi_x \Gamma W^{eq}}{2\Omega_x} = -\frac{1}{2}\Gamma W^{eq} \sin 2\theta \\
W_d^{eq} &= \frac{\delta_x}{\Omega_x} W^{eq} = W^{eq} \cos 2\theta
\end{aligned}
$$

Here, ρ_{12} refers to the coherence in the dressed state basis, and W_d refers to the population difference between the dressed state basis states. The transformed Bloch equations are easily solved, giving for the steady state solutions

$$
\begin{aligned}
\rho_{12}^{ss} &= \rho_{12}^{eq} L\left(-\Omega\right) \\
W_d^{ss} &= W_d^{eq}
\end{aligned}
$$

Here, the Lorentzian function $L(\alpha)$ is defined, and will be used extensively throughout this thesis.

$$L(\alpha) = L_A(\alpha) - iL_D(\alpha)$$

with the absorptive (L_A) and dispersive (L_D) Lorentzians

$$\begin{aligned} L_A(\alpha) &= \frac{\Gamma}{\Gamma^2 + \alpha^2} \\ L_D(\alpha) &= \frac{\alpha}{\Gamma^2 + \alpha^2} \end{aligned}$$

These steady state limits then give the steady state solutions for the dressed states. In the original basis (bare state basis), the results become

$$\begin{aligned} \rho_{ge}^{ss} &= \cos^2\theta\rho_{12}^{ss} - \sin^2\theta\rho_{21}^{ss} + \cos\theta\sin\theta W_d^{ss} \\ W^{ss} &= \left(\cos^2\theta - \sin^2\theta\right) W_d^{ss} - 2\cos\theta\sin\theta(\rho_{12}^{ss} + \rho_{21}^{ss}) \end{aligned}$$

1.4.6 Geometrical Interpretation of the Dressed States

As has been seen, the Optical Bloch equations leads to a simple geometrical interpretation, completely analogous to the fully classical magnetic dipole. Recall the basic dynamics of the TLA as being represented by the vector equations

$$\frac{d}{dt}\vec{m} = -\vec{m} \times \vec{\Omega}$$

This can be extended to include homogeneous damping terms

$$\frac{d}{dt}\vec{m} = -\vec{m} \times \vec{\Omega} - \Gamma\left(\vec{m} - \vec{m}_{eq}\right)$$

where

$$\vec{m}_{eq} = [0, 0, W_{eq}]$$

The dressed state basis is then simply a rotation that aligns the transformed z' axis with $\vec{\Omega}$, simplifying the system. In this basis, the Bloch vector $\vec{m}'$ precesses about the z' axis, relaxing to the steady state $\vec{m}'_{eq} = [-\sin 2\theta, 0, \cos 2\theta]\, W_{eq}$.

1.4.7 The Mollow Spectrum

The semiclassical dressed state basis is used extensively throughout this thesis and so to introduce its use, a calculation of the standard Mollow spectrum can be performed [3]. This sort of calculation will be used frequently, and so it is useful to see it used in a simple circumstance. In the Mollow spectrum, a strong pump field is applied to the TLA, and then a weak probe field (frequency ω_p and small Rabi frequency α) is scanned across the transition, and its absorption measured. The equations of motion that describe this are given by

$$\begin{aligned} \frac{d}{dt}\tilde{\rho}_{ge} &= (i\delta_x - \Gamma)\,\tilde{\rho}_{ge} - i\frac{\chi_x}{2}W - i\frac{\alpha}{2}We^{i\delta_p t} \\ \dot{W} &= 2i\chi\left(\tilde{\rho}_{eg} - \tilde{\rho}_{ge}\right) + 2i\alpha\left(\tilde{\rho}_{eg}e^{i\delta_p t} - \tilde{\rho}_{ge}e^{-i\delta_p t}\right) - \Gamma\left(W - W^{eq}\right) \end{aligned}$$

where the probe field detuning $\delta_p = \omega_p - \omega_x$. The solutions can be written as a power series in the weak parameter α

$$\begin{aligned} \tilde{\rho}_{ge} &= \rho_{ge}^{(0)} + \alpha\rho_{ge}^{(1)} + \alpha^2\rho_{ge}^{(2)} + \ldots \\ W &= W^{(0)} + \alpha W^{(1)} + \alpha^2 W^{(2)} + \ldots \end{aligned}$$

The zeroth order equations are simply Eq. 1.12, and have been solved above, to give solutions $\rho_{eg}^{(0)}$ and $W^{(0)}$. The equations in the first order in α then are

$$\begin{aligned}
\dot{\rho}_{ge}^{(1)} &= \left(i\delta_x - \Gamma\right)\rho_{ge}^{(1)} - i\frac{\chi_x}{2}W^{(1)} - i\frac{1}{2}W^{(0)}e^{i\delta_p t} \\
\dot{W}^{(1)} &= 2i\chi\left(\rho_{eg}^{(1)} - \rho_{ge}^{(1)}\right) + 2i\left(\rho_{eg}^{(0)}e^{i\delta_p t} - \rho_{ge}^{(0)}e^{-i\delta_p t}\right) - \Gamma W^{(1)}
\end{aligned}$$

To proceed, transform these equations into the dressed state basis

$$\begin{aligned}
\rho_{12}^{(1)} &= \left(i\Omega_x - \Gamma\right)\rho_{12}^{(1)} + i\frac{1}{2}\sin 2\theta\left(e^{i\delta_p t} + e^{-i\delta_p t}\right)\rho_{12}^{(0)} - i\frac{1}{2}\left(\cos^2\theta e^{i\delta_p t} - \sin^2\theta e^{-i\delta_p t}\right)W_d^{(0)} \\
\dot{W}_d^{(1)} &= -\Gamma W_d^{(1)} + i\left(\cos^2\theta e^{i\delta_p t} - \sin^2 e^{-i\delta_p t}\right)\rho_{21}^{(0)} - i\left(\cos^2\theta e^{-i\delta_p t} - \sin^2\theta e^{i\delta_p t}\right)\rho_{12}^{(0)}
\end{aligned}$$

which is easily solved by substituting in the zeroth order solutions. After putting in the zeroth order solutions, the solutions to the first order in the probe beam power become

$$\begin{aligned}
\rho_{12}^{(1)} &= \rho_+ e^{i\delta_p t} + \rho_- e^{-i\delta_p t} \\
W_d^{(1)} &= W_d^+ e^{i\delta_p t} + W_d^- e^{-i\delta_p t}
\end{aligned}$$

where

$$\begin{aligned}
\rho_+ &= -i\frac{1}{2}\left(\frac{1}{2}\sin^2 2\theta\Gamma W^{eq}L\left(-\Omega_x\right) + \cos^2\theta\cos 2\theta W^{eq}\right)L\left(\delta_p - \Omega_x\right) \\
\rho_- &= -i\frac{1}{2}\left(\frac{1}{2}\sin^2 2\theta\Gamma W^{eq}L\left(-\Omega_x\right) - \sin^2\theta\cos 2\theta W^{eq}\right)L\left(-\delta_p - \Omega_x\right) \\
W_d^+ &= -\frac{1}{2}i\alpha\sin 2\theta\Gamma W^{eq}\left(\cos^2\theta L\left(\Omega_x\right) + \sin^2\theta L\left(-\Omega_x\right)\right)L\left(\delta_p\right) \\
W_d^- &= \frac{1}{2}i\alpha\sin 2\theta\Gamma W^{eq}\left(\cos^2\theta L\left(-\Omega_x\right) + \sin^2\theta L\left(\Omega_x\right)\right)L\left(-\delta_p\right)
\end{aligned}$$

To recover the final probe absorption spectrum, it is necessary to calculate the component of the bare state coherence rotating at frequency δ_p i.e.

$$
\begin{aligned}
\tilde{\rho}_{ge}(\delta_p) &= \cos^2\theta\rho_+ - \sin^2\theta\rho_-^\star + \frac{1}{2}\sin 2\theta W_d^+ \\
&= -i\frac{\alpha}{2}\cos^2\theta\left(\frac{1}{2}\sin^2 2\theta\Gamma W^{eq}L(-\Omega_x) + \cos^2\theta\cos 2\theta W^{eq}\right)L(\delta_p - \Omega_x) \\
&\quad -i\frac{\alpha}{2}\sin^2\theta\left(\frac{1}{2}\sin^2 2\theta\Gamma W^{eq}L(\Omega_x) - \sin^2\theta\cos 2\theta W^{eq}\right)L(\delta_p + \Omega_x) \\
&\quad -\frac{1}{4}i\alpha\sin^2 2\theta\Gamma W^{eq}\left(\cos^2\theta L(\Omega_x) + \sin^2\theta L(-\Omega_x)\right)L(\delta_p)
\end{aligned}
$$

The familiar solution is then a series of three Lorentzians at $\delta_p = 0, \pm\Omega_x$, each having a weight summarised in the following table

Lorentzian	**Weight**
$L(\delta_p - \Omega_x)$	$-i\frac{1}{2}\cos^2\theta\left(\cos^2\theta W_d^{eq} - \sin 2\theta\rho_{12}^{eq}L(-\Omega_x)\right)$
$L(\delta_p + \Omega_x)$	$i\frac{1}{2}\sin^2\theta\left(\sin^2\theta W_d^{eq} + \sin 2\theta\rho_{12}^{eq}L(\Omega_x)\right)$
$L(\delta_p)$	$\frac{1}{2}i\sin 2\theta\rho_{12}^{eq}\left(\cos^2\theta L(\Omega_x) + \sin^2\theta L(-\Omega_x)\right)$

Notice that the sidebands ($\delta_p = \pm\Omega_x$) have a weight that is broken up into two parts. The first part is proportional to the equilibrium population difference in the dressed states, W_d^{eq}, and the second part is due to a contribution from the steady state coherence that is set up by the driving field ρ_{12}^{eq}. As well there is a component at $\delta_p = 0$ that is proportional to the coherence.

In the limit of well separated peaks, i.e. $\Omega_x \gg \Gamma$, it is possible to make the following simplification

$$
L(\Omega_x) \sim -iL_D(\Omega_x)
$$

and since $L_D(\Omega_x) \propto 1/\Omega_x$, it can be noted that when the pump field is *off resonance*

$$
|L_D(\Omega_x)| \ll |W_d^{eq}|
$$

and the weights become

Lorentzian	Weight
$L(\delta_p - \Omega_x)$	$-i\frac{1}{2}\cos^4\theta W_d^{eq}$
$L(\delta_p + \Omega_x)$	$i\frac{1}{2}\sin^4\theta W_d^{eq}$
$L(\delta_p)$	$\frac{1}{2}\sin 2\theta\rho_{12}^{eq}\cos 2\theta L_D(\Omega_x)$

The actual absorption and dispersion spectra are given by

$$\begin{aligned} A(\delta_p) &= -\Im\rho_{ge}(\delta_p) \\ &= \frac{1}{2}\cos^4\theta W_d^{eq} L_A(\delta_p - \Omega_x) - \frac{1}{2}\sin^4\theta W_d^{eq} L_A(\delta_p + \Omega_x) \\ &\quad + \frac{1}{2}\sin 2\theta\rho_{12}^{eq}\cos 2\theta L_D(\Omega_x) L_D(\delta_p) \\ D(\delta_p) &= \Re\rho_{ge}(\delta_p) \\ &= -\frac{1}{2}\cos^4\theta W_d^{eq} L_D(\delta_p - \Omega_x) + \frac{1}{2}\sin^4\theta W_d^{eq} L_D(\delta_p + \Omega_x) \\ &\quad - \frac{1}{2}\sin 2\theta\rho_{12}^{eq}\cos 2\theta L_D(\Omega_x) L_D(\delta_p) \end{aligned}$$

This is the familiar off-resonance Mollow spectrum (in the high power limit). Three peaks are evident. The two oppositely signed peaks $L_A(\delta_p - \Omega_x)$ and $L_A(\delta_p + \Omega_x)$ are due to transitions between the dressed states, just as in the fully quantum mechanical case. The third peak, much smaller since it is proportional to $L_D(\Omega_x)$, is a dispersive shaped peak centered at $\delta_p = 0$. This peak is due to the steady state coherence that arises in the driven system ρ_{12}^{eq}.

The on-resonance ($\delta_x = 0$) case leads to the result (to the same approximation as above)

Lorentzian	Weight
$L(\delta_p - \Omega_x)$	$\frac{1}{8}\Gamma W^{eq} L_D(\Omega_x)$
$L(\delta_p + \Omega_x)$	$-\frac{1}{8}\Gamma W^{eq} L_D(\Omega_x)$
$L(\delta_p)$	$-\frac{1}{2}i\Gamma W^{eq} L_A(\Omega_x)$

which corresponds to the familiar on-resonance Mollow spectrum.

1.5 The Rabi Transition

The TLA uses only the transverse dipole moment as the light-matter interaction. In this case, the incident radiation is polarised at right angles to the axis of the TLA and the population cycles between the ground and excited states at a rate given by the generalised Rabi frequency. A natural extension of this is to then study the effects of applying more strong fields and to study the effects of this on the dressed state formalism. While this has been studied extensively theoretically [17]-[31], there is a paucity of experimental results [32]-[38],[45]-[46],[47]-[50]. *Ficek and Freedhoff* [51] have also written an excellent review article that sums up much of the work to date. Most of these studies centre on the idea of using another $\hat{x}$ polarised field as the second driving field. In this thesis, a different scenario will be examined, that of driving the driven TLA with a $\hat{z}$ polarised field.

It has been shown theoretically [56]-[58],[39]-[42]and experimentally [43]-[44] that if a field polarised in parallel with the population axes is applied, then a resonance at the generalised Rabi frequency can be seen. To see this, modify the "light+matter" interaction to include a *permanent dipole moment.* This allows the TLA to couple with $\hat{z}$ polarised fields. To see how this will generate the Rabi transition, consider the geometrical model shown above.

Previously, a single $\hat{x}$ polarised field (call it Field_x) is coupled to the transition via the standard (see Fig 1-9a) transverse dipole moment interaction. Now add an additional $\hat{z}$ polarised field (Field_z), coupled to the transition via the permanent dipole moment (the theoretical details will be expanded later). Go to the rotating frame, as before, and discard the anti-resonant term (the RWA). Note that since the rotation is around the $\hat{z}$ axis, Field_z is unaffected. Fig 1-9b shows the picture as it stands.

Recall then that the dressed states basis transformation rotates the axis so that it is in line with $\overrightarrow{\Omega}$. Once this is done, note that there are now two components to Field_z in this frame. One is perpendicular to the new z′ axis, and the other is parallel. The field perpendicular to the z′ will then drive the transition which is characterised by the vector $\overrightarrow{\Omega}$, in exactly the same way that the original Field_x drove the transition characterised by the original transition frequency ω_0. This new transition has a resonant frequency of Ω, the generalised Rabi frequency. Thus, if a z polarised field is applied to a driven TLA with a permanent dipole moment, then this field will interact with a transition at the Rabi frequency, the so called *Rabi transition.* It is

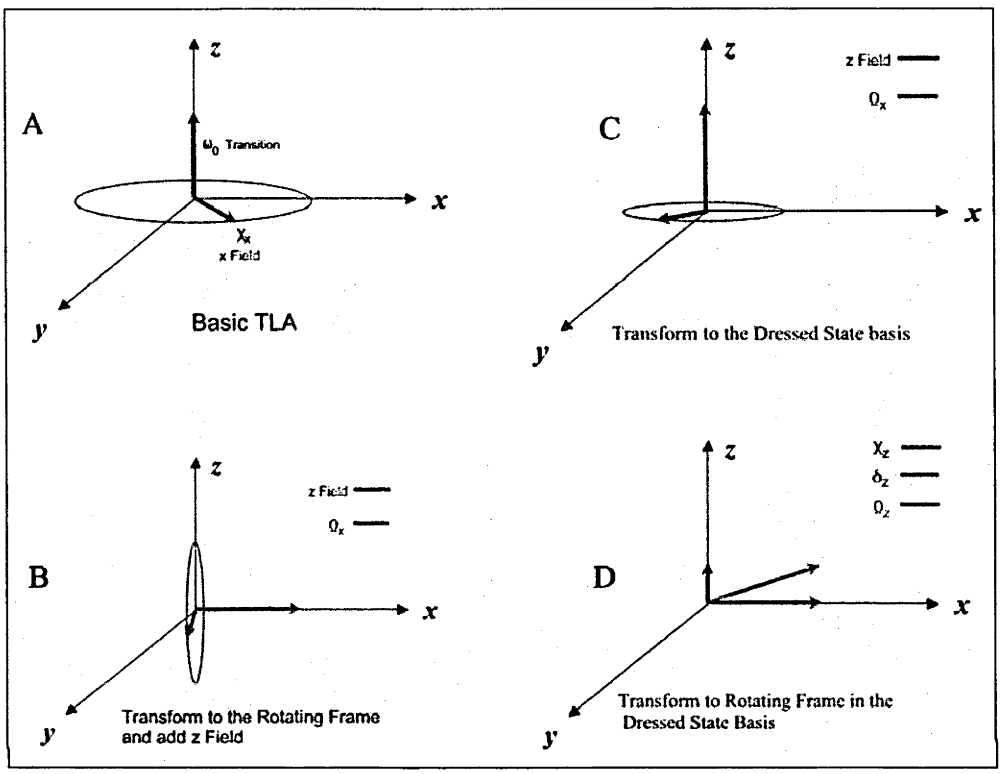

Figure 1-9: The four stages towards understanding the Rabi transition. In (A), the standard TLA is presented, with an on-resonance $\hat{x}$ polarised field (Rabi frequency χ_x) interacting with the bare transition of frequency ω_0. (B) sees the system transformed to the rotating frame produces an effective field lying along the $\hat{x}$ axis. Now, the $\hat{z}$ polarised field (Rabi frequency χ_z) is applied, with a component that rotates about the $\hat{x}$ axis as shown. In (C), the transformation to the dressed state basis rotates the z axis to lie along the effective field from (B). Notice the similarity with diagram (A). In (D), finally, transform to the rotating frame to produce the final effective field about which the Bloch vector precesses.

the study of this transition that forms the bulk of the work of this thesis. Fig 1-9c shows this transition geometrically in the case where Field_x is resonant.

The second component of Field_z in this basis, the one parallel to $\overrightarrow{\Omega}$, is part of a higher order process which will be studied in more detail later. Actually, at this point, it is plain in what direction the theoretical analysis should proceed. There is now, in this new basis, a system which is completely analogous to the original system, where Field_x was driving the original transition. Clearly, then, a similar set of transformations (rotating frame, RWA, dressed state basis) can be applied to shed insight into this system, which is in fact performed in Chapters 2,3.

The Rabi transition behaves in a similar fashion to the normal TLA, allowing for many of the same analysis techniques to be applied. In fact, the Rabi transition can be driven by a strong pump field, and then examined using a probe beam that studies either the original transition itself, or the Rabi transition. The details of this will be covered in a later chapter. Again, this system is theoretically accessible to relatively simple analysis, which employs the *Doubly Dressed States*, a natural extension of the dressed state analysis.

The doubly dressed states formalism is not a new concept, and has been used recently to study interactions of TLAs with polychromatic radiation [51]. The formalism has been used to successfully study the case of two Field_x's interacting with a TLA (much of it since 1998, when this work was performed), however the complexity of the interactions mean that in general the solution is perturbative in nature though there are special circumstances where a more accurate solution is gained. However, what makes the calculation in this thesis different is the orthogonal nature of the interacting fields, Field_x and Field_z. As will be seen, this naturally lends itself to an elegant symmetry in the dynamics, where Field_x and Field_z interact in entirely distinct regimes. This enables the doubly dressed states to be used very naturally and accurately, and they remain a good form of analysis for a broad range of experimental parameters. It will also be shown that the extension of the work to include the concept of triply, quadruply and so on dressed states is equally intuitive and natural. To appreciate this, it will be worthwhile to carefully present the calculations in their entirety.

In chapter 2, the doubly dressed state theory is introduced, with the results shown for the major spectroscopic techniques. Chapter 3 shows the semiclassical analysis of the basic doubly

driven system. Chapter 3 also refines the theory somewhat, using numerical techniques to calculate higher order terms, the Bloch Siegert shift associated with the Rabi transition and so forth. The experimental results (the experimental system is introduced in Chapter 1) are then compared with the theoretical results in Chapter 4.

The Rabi transition is then studied by applying a $\hat{z}$ polarised field to the driven system. To examine this transition, first assume that the $\hat{z}$ field is weak. That is, the TLA is strongly driven with a Field$_x$ and then probe the system with a weak Field$_z$. So the system is coupled to one classical $\hat{x}$ polarised field,

$$\overrightarrow{E}_x = \hat{x} E_x \cos \omega_x t$$

and one $\hat{z}$ polarised probe field

$$\overrightarrow{E_z} = \hat{z} E_z \cos \omega_z t$$

The Field$_z$ is coupled to the TLA by the permanent dipole moment, with Hamiltonian

$$\begin{aligned} H &= -\overrightarrow{\mu} \bullet \left(\overrightarrow{E}_x + \overrightarrow{E_z} \right) \\ &= \hbar \begin{pmatrix} 0 & \chi_x \\ \chi_x & 0 \end{pmatrix} \cos \omega_x t + \hbar \begin{pmatrix} 0 & 0 \\ 0 & 2\chi_z \end{pmatrix} \cos \omega_z t \end{aligned}$$

where the semiclassical Rabi frequencies are defined by

$$\begin{aligned} \chi_x &= -\frac{\mu_x E_x}{\hbar} \\ \chi_z &= -\frac{\mu_z E_z}{\hbar} \end{aligned}$$

Here, μ_z is taken to be the component of the dipole moment parallel to the $\hat{z}$ axis (as defined in section 1.4.2). u_x is then the component of the dipole moment perpendicular to this, lying along the $\hat{x}$ axis. Using this Hamiltonian in the standard fashion, the Optical Bloch Equations

(in the rotating frame) become

$$\begin{aligned}\frac{d}{dt}\tilde{\rho}_{ge} &= \left\{i\left(\delta_x + 2\chi_z\cos\omega_z t\right) - \Gamma\right\}\tilde{\rho}_{ge} - i\frac{\chi_x}{2}W \\ \dot{W} &= i\chi_x\left(\tilde{\rho}_{eg} - \tilde{\rho}_{ge}\right) - \Gamma\left(W - W^{eq}\right)\end{aligned}$$

To examine the Rabi transition using a probe beam, assume that χ_z is small. The solutions are then written as a power series expansion in χ_z, e.g.

$$\tilde{\rho}_{ge} = \rho^0_{ge} + \chi_z\rho^1_{ge} + \chi^2_z\rho^2_{ge} + ...$$

The steady state zero order terms have already been calculated above, and expressed in the semiclassical dressed state basis they become

$$\begin{aligned}\rho^{(0)}_{12} &= \rho^{eq}_{12}L\left(-\Omega_x\right) \\ W^{(0)} &= W^{eq}_d\end{aligned}$$

Writing out the first order equation, the first order term equations of motion are obtained

$$\begin{aligned}\dot{\rho}^{(1)}_{ge} &= \left(i\delta_x - \Gamma\right)\rho^{(1)}_{ge} + 2i\chi_z\cos\omega_z t\rho^{(0)}_{ge} - i\frac{\chi_x}{2}W^{(1)} \\ \dot{W}^{(1)} &= i\chi_x\left(\rho^{(1)}_{eg} - \rho^{(1)}_{ge}\right) - \Gamma W^{(1)}\end{aligned}$$

These are then converted to the semiclassical dressed state basis as above

$$\begin{aligned}\dot{\rho}^{(1)}_{12} &= \left(i\Omega_x - \Gamma\right)\rho^{(1)}_{12} + 2i\chi''_z\cos\omega_z t\rho^{(0)}_{12} - i\chi'_z\cos\omega_z tW^{(0)}_d \\ \dot{W}^{(1)}_d &= 2i\chi'_z\cos\omega_z t\left(\rho^{(0)}_{21} - \rho^{(0)}_{12}\right) - \Gamma W^{(1)}_d\end{aligned}$$

with the definitions

$$\begin{aligned}\chi_z' &= -\sin 2\theta \chi_z = -\frac{\chi_x}{\Omega_x}\chi_z \\ \chi_z'' &= \cos 2\theta \chi_z = \frac{\delta_x}{\Omega_x}\chi_z\end{aligned}$$

Then these can be easily solved for the first order solutions

$$\begin{aligned}\rho_{12}^{(1)} &= a^1 e^{i\omega_z t} + a^{-1} e^{-i\omega_z t} \\ W_d^{(1)} &= c^1 e^{i\omega_z t} + c^{-1} e^{-i\omega_z t}\end{aligned}$$

The coefficients then become

$$\begin{aligned}a^1 &= \frac{i}{2}\left(2\chi_z'\rho_{12}^{(0)} - \chi_z'\omega^{(0)}\right) L\left(\omega_z - \Omega_x\right) \\ &= \frac{i}{2}\cos 2\theta \sin 2\theta \chi_z W^{eq}\left(1 - \Gamma L\left(-\Omega_x\right)\right) L\left(\omega_z - \Omega_x\right) \\ a^{-1} &= \frac{i}{2}\cos 2\theta \sin 2\theta \chi_z W^{eq}\left(1 - \Gamma L\left(-\Omega_x\right)\right) L\left(-\omega_z - \Omega_x\right) \\ c^1 &= -\Gamma \sin^2 2\theta \chi_z W^{eq} L_D\left(\Omega_x\right) L\left(\omega_z\right) \\ c^{-1} &= -\Gamma \sin^2 2\theta \chi_z W^{eq} L_D\left(\Omega_x\right) L\left(-\omega_z\right)\end{aligned}$$

These results are transformed back into the bare state basis (for the population)

$$\begin{aligned}W &= -\sin 2\theta\left(\rho_{12} + \rho_{21}\right) + \cos 2\theta W_d \\ &= W^0 + W^1 e^{i\omega_z t} + W^{-1} e^{-i\omega_z t}\end{aligned}$$

The probe beam is $\hat{z}$ polarised, so the probe absorption spectrum is derived from the component of the population that rotates with the probe beam field frequency ω_z (dropping the probe beam power χ_z):

$$
\begin{aligned}
W^1 &= -\sin 2\theta a^1 - \sin 2\theta \left(a^{-1\star}\right) + \cos 2\theta c^1 \\
&= \kappa\left(\frac{i}{2}\left(\left(1-\Gamma L\left(-\Omega_x\right)\right) L\left(\omega_z-\Omega_x\right)+\left(1-\Gamma L\left(\Omega_x\right)\right) L\left(\omega_z+\Omega_x\right)\right)-\Gamma L_D\left(\Omega_x\right) L\left(\omega_z\right)\right)
\end{aligned}
$$

where

$$\kappa = \cos 2\theta \sin^2 2\theta \chi_z W^{eq}$$

Examining the high power limit (i.e. $\Omega_x \gg \Gamma$), it is possible to simplify

$$L\left(\Omega_x\right) = L_A\left(\Omega_x\right) - iL_D\left(\Omega_x\right)$$

by noting that $L_D\left(\Omega_x\right) \gg L_A\left(\Omega_x\right)$; hence

$$L\left(\Omega_x\right) \sim -iL_D\left(\Omega_x\right)$$

and so

$$\Gamma L_D\left(\Omega_x\right) \ll 1$$

leading finally to the equations

$$W^1 = \kappa\frac{i}{2}\left(L\left(\omega_z-\Omega_x\right)+L\left(\omega_z+\Omega_x\right)\right)$$

This obviously shows a resonance at the Rabi frequency. Looking at that component in particular, the absorption and dispersion are calculated:

$$
\begin{aligned}
abs &= \Im W^1 = \frac{\kappa}{2} L_A\left(\omega_z-\Omega_x\right) \\
disp &= \Re W^1 = \frac{\kappa}{2} L_D\left(\omega_z-\Omega_x\right)
\end{aligned}
$$

The weight of the probe absorption spectrum at the Rabi frequency is then given by

$$\begin{aligned}\frac{\kappa}{2} &= \frac{1}{2}\cos 2\theta \sin^2 2\theta \chi_z W^{eq} \\ &= \frac{1}{2}\sin^2 2\theta \chi_z W_d^{eq}\end{aligned}$$

The spectrum of the probe beam then shows a clear signal at the Rabi frequency, showing that the Field$_z$ does indeed interact strongly with the permanent dipole moment. Notice that the line's weight is proportional to the dressed state population difference. This means that there will be no signal (to the lowest order) with an on resonance Field$_x$ ($\delta_x = 0$). This is in line with intuition, since the on-resonance case will equilibrate the dressed state populations, quenching any net absorption in the final results. Note that the maximum signal size will be when $\delta_x = \chi_x$, balancing the strength of the interaction of the probe beam with the dressed states, $\sin 2\theta\chi_z$ with the resultant population difference W_d^{eq}. Also, because the size of the Rabi transition is proportional to W_d^{eq}, in the case where $\delta_x < 0$ (i.e. when the driving field is on the high side of the transition), $W_d^{eq} > 0$ and so the transition is emissive. On the other hand, when $\delta_x > 0$, the Rabi transition is absorptive.

The motivation then of this thesis is to examine this new transition. Previously, the transition was recognized, but only used to measure the Rabi frequency in NMR experiments, using the transition as shown above [56]-[58]. This thesis intends to take this analysis further, and study the implications of treating this transition as a whole new TLA system in its own right. This new TLA has several advantages, including tunable characteristics (transition size, dipole moment etc.). Also, inhomogeneous broadening is considerably dampened in the transition. To see this, note that resonantly driving a inhomogeneously broadened line (linewidth Δ) will produce an 'average' Rabi transition of (assuming the high power case where $\chi \gg \Delta$)

$$\begin{aligned}\Omega &= \sqrt{\chi^2 + \Delta^2} \\ &\simeq \chi\left(1 + \frac{1}{2}\frac{\Delta^2}{\chi^2}\right)\end{aligned}$$

so the approximate inhomogeneous broadening of the new line is

$$\Delta_{rabi} \simeq \frac{1}{2}\left(\frac{\Delta}{\chi}\right)\Delta$$

The Rabi transition will then provide perhaps a "more perfect" TLA that can be examined. Also, as will be seen, the dynamics of a doubly driven system can be examined in a theoretically tractable manner, leading to an intuitive generalisation of the dressed states, the so called doubly dressed states. This idea can even be expanded to the higher orders to include triply dressed, quadruply dressed and so on states. These higher order interactions provide a plethora of new interactions, both in the regime of the original transition, and in the regime of the Rabi transition. Chapters 2,3 will examine the theoretical basis of this transition, as well as the results for the driven Rabi transition. Chapter 4 will then present the experimental results and compare them to theory.

1.6 The Experimental System

To understand the experiment, it is necessary to understand two distinct areas - the N-V centre (Nitrogen Vacancy centre) in diamond (the system that will be examined) and the Raman Heterodyne technique (the detection method). The N-V centre in diamond provides a convenient system to study, where impurities in the diamond allow the examination of a system that very closely approximates the TLA. This TLA can be excited with radio-frequency (RF) fields (both $\hat{x}$ polarised and $\hat{z}$ polarised) and probed with another, weak, RF field. The detection method used to examine the spectrum is the well known Raman Heterodyne method, where optical frequencies 'beat' with the applied RF fields to present the final spectrum for analysis.

1.6.1 N-V Centre in Diamond

As mentioned, the N-V centre in diamond provides a convenient substrate for examination. The N-V centre in diamond is formed in type Ib diamonds when a naturally occurring substitutional nitrogen (substituted for one of the carbon atoms in the lattice) traps a carbon-vacancy at one of its nearest neighbour sites [61],[62]. This causes four dangling bonds with each of the neighbouring carbon atoms (three of them) and the nitrogen atom. Each carbon broken bond

has a single electron associated with it, while the broken bond with nitrogen has two floating electrons. Thus, five electrons are involved. It is well known, however [64]-[71] that the orbital ground state (the ^{3}A state) is a spin triplet so it would seem there is an even number of electrons involved. This was generally explained by assuming that the centre will trap another electron. There has been some controversy over this theory [73]-[75], however, what is known is that ESR (Electron Spin Resonance) studies of the ground state NV-Centre demonstrate a spin triplet system, two levels of which form the main TLA examined in this thesis.

Also, due to the symmetry of the system, there are in fact four equivalent orientations (axes of symmetry) for the N-V Centre. The centre has trigonal symmetry of point group C_{3v} where the C_3 principle axis lies along the N-V axis. When a static magnetic field is applied along one of the symmetry axes, the other three centres are magnetically equivalent and this aligned symmetry axis of the N-V centre is then considered to make up the nearly-ideal TLA which is examined in this thesis. This TLA then occurs at RF frequencies, and only the observation of the centre needs to be examined.

The N-V Centre also exhibits optical, as well as RF, resonances. The centre can be excited with optical frequencies, where the first excited state is centered at $\sim$ 638 nm, and measurements [76]-[78] demonstrate that the ground and excited states are describable in the representation A and E respectively. The ^3A to ^3E transition is the key (optical) transition that is exploited as the detection method for this thesis - the Raman Heterodyne detection technique. The ^3E transition has a lifetime of 13 ns [79] and an inhomogeneous linewidth of $\sim$ 800 GHz (the large broadening is due to large variations in crystal strain).

To summarise to date, the NV centre's ground state is a spin one system, which is used to generate a TLA which is accessible at RF frequencies, and the transitions are observed using the optical transition with the excited state of the N-V centre. Examining the ground state sublevels in more detail, the ^3A state is split by crystal field interactions into a singlet state ($m_s = 0$) and a degenerate doublet ($m_s = \pm 1$) separated by 2.88 GHz. If a static magnetic field is applied along the N-V centre axis, it lifts the degeneracy between the $m_s = \pm 1$ sublevels. As the power is increased, the $m_s = -1$ approaches the $m_s = 0$ state. As they approach each other, they repel each other due to hyperfine interactions between them (plus any misalignment in the static field) and they form an anti-crossing. The anti-crossing (see fig 1-10) allows for a

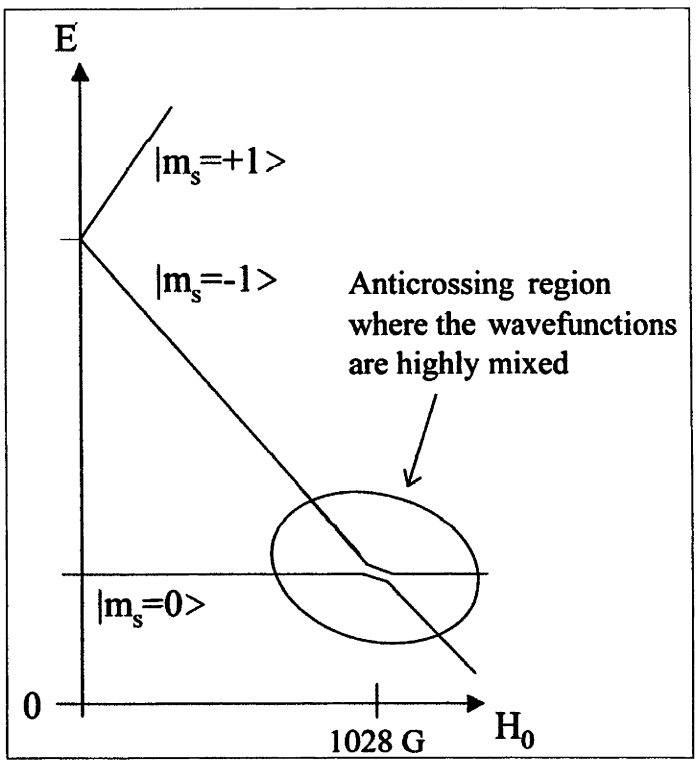

Figure 1-10: The basic energy level scheme associated with the N-V Centre ^3A ground state. The state field H_0 is applied along the symmetry axis which causes mixing between the levels at the anti-crossing region.

high level of mixing between the levels, which greatly enhances the level of interaction available to the system. The mixtures of the states lead to two quantum wavefunctions ψ_{-1} and ψ_0 which are mixtures of the spin states $|0\rangle, |-1\rangle$

$$\begin{aligned} |\psi_0\rangle &= a|0\rangle + b|-1\rangle \\ |\psi_{-1}\rangle &= -a|-1\rangle + b|0\rangle \end{aligned}$$

Note that the admixture constants, a and b, obey the relation $|a| > |b|$ [61]. The transitions between these states form the major TLA which is examined. The transition frequency in experimental situations is between 50 MHz and 100 MHz, depending on the strength of the applied static magnetic field.

The situation is complicated somewhat by the nuclear spin hyperfine levels in the $|m_s = -1\rangle$ and $|m_s = 0\rangle$ states, shown in fig 1-11. One of the areas that needs to be examined is the complication due to the extra levels that are associated with the TLA (in effect 3 sublevels). Transitions between the hyperfine levels between the wavefunctions above form the so called EPR (Electronic Paramagnetic Resonance) transitions, and between the nuclear spin substates within each wavefunction form the TLA called the NMR subsystem. Hence, the system examined actually consists of two regimes, the EPR ($\sim$70 MHz transition) and the NMR regime ($\sim$5 MHz). The bulk of the data taken in this thesis is taken in the EPR regime, in which higher Rabi frequencies are obtainable making it possible to observe the transition which is the object of this study. The EPR transition studied then has hyperfine structure associated with the following significant transitions (with their relative energies)

$$\begin{aligned} |0,0\rangle &\leftrightarrow |-1,0\rangle \qquad E = 0.0\ MHz \\ |0,-1\rangle &\leftrightarrow |-1,-1\rangle \qquad E = 2.4\ MHz \\ |0,1\rangle &\leftrightarrow |-1,1\rangle \qquad E = -1.8\ MHz \end{aligned}$$

showing that the EPR transition will show a triplet structure. In experimental situations, the dominant $|0,1\rangle \leftrightarrow |-1,1\rangle$ transition typically has a resonance frequency of 70 MHz, so the other two transitions have frequencies around 71.8 MHz and 74.2 MHz. In fact, due to state mixing near anticrossing, there are other (much weaker) transitions, but these are not considered to be significant in this thesis. The relative strengths of these transitions varies with the distance of the static field from anti-crossing, and the calculation of the line weights is not important here and is presented elsewhere [61]. As will be discussed in chapter 4, it is actually the $|0,1\rangle \leftrightarrow |-1,1\rangle$ that is singled out for study. The effects of the other two transitions are cancelled out by focusing any driving field between the other two peaks (i.e.. the detuning is $\sim$-3 MHz). The two other transitions are near resonance and are therefore saturated and produce very small signals, as well as being approximately equal and opposite in sign - therefore quenching each other's signal. Now that the transitions are understood, the detection method needs to be examined, the well known Raman Heterodyne system.

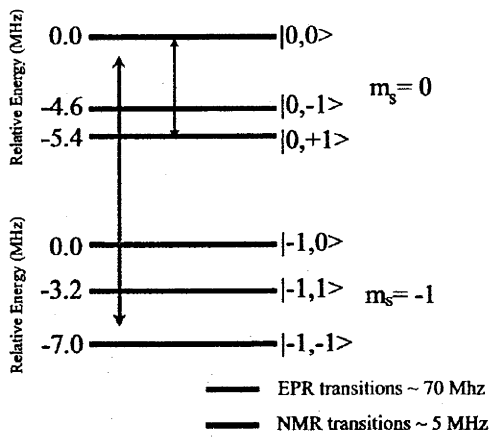

Figure 1-11: The energy level scheme for the experimental system. EPR transitions are between the $m_s = 0$ and the $m_s = -1$ electron spin states. Each of these states is a further nuclear spin triplet, and this hyperfine structure is shown here, with the energy levels separating them. This gives rise to two experimental regimes, the EPR and NMR regime (shown in colour code).

1.6.2 Raman Heterodyne Detection

The Raman Heterodyne Detection technique is a very sensitive detection technique that allows the experimenter to directly access the absorption and dispersion spectra for a system (in this case the NV - Centre driven by RF fields). It relies on the coherence of the system that is produced by the RF fields, and then optical frequency detection methods are used to observe the coherence (in both the cw and transient regimes). It is a well known detection method [61], and nothing will be added to the literature by a lengthy exposition here, so only a brief introduction will be presented here.

The technique was first reported by Mlynek *et al.* [80], and has since been used for detecting NMR (Nuclear Magnetic Resonance) and EPR (Electron Paramagnetic Resonance). Raman Heterodyne detection, as mentioned, does not give the populations of the levels, but instead allows direct observation of the coherences. Referring to Fig 1-12, the Raman Heterodyne technique is used in the case where the RF transition in question is coupled to a third level via the optical frequency laser (frequency ω_L) while being driven coherently by a RF field (frequency ω_{rf}).

The laser drives the $|1\rangle \leftrightarrow |3\rangle$ transition, while the RF field couples $|1\rangle \leftrightarrow |2\rangle$. This results

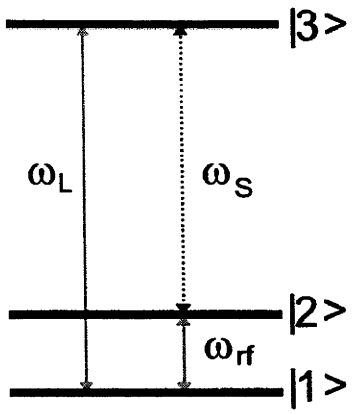

Figure 1-12: The energy level scheme for the Raman Heterodyne detection scheme. An RF field excites the $|1\rangle \leftrightarrow |2\rangle$ transition (the experimentally interesting one) and a laser excites the $|1\rangle \leftrightarrow |3\rangle$ transition.

in coherence between levels $|2\rangle \leftrightarrow |3\rangle$ which produces a Stokes Raman signal E_s at frequency $\omega_S = \omega_{32}$. This stimulated Raman signal beats with the incident laser frequency to produce a beat frequency of ω_{rf}, and it is this beat signal which is detected by a photodiode. For the particular case of the N-V Centre, the NMR and EPR centres are both magnetically allowed (the $|1\rangle \leftrightarrow |2\rangle$ transition) and transitions between the hyperfine levels of the ^3A and ^3E states provide the optical transitions that are allowed, to enable the Raman Heterodyne procedure to be used [82].

It has been shown previously [81] that the resultant intensity of the beat signal I_s for optically thin samples is given by

$$I_s \propto (\mathrm{Re}\,\langle\rho_{21}\rangle \cos\omega_{rf}t + \mathrm{Im}\,\langle\rho_{21}\rangle \sin\omega_{rf}t)$$

where the angular brackets around the ρ_{21} denote an average over optical and RF inhomogeneities. Note the coherences here are the slowly varying parts with respect to ω_{rf}. Clearly, the intensity of the signal is made of an in-phase and an out-of-phase component. These can be separately observed using phase sensitive RF detection equipment.

1.6.3 Experimental Configuration

The experimental schematic is shown in Fig 1-13. The N-V Centre was provided by a sample diamond crystal measuring approximately 1 mm^3. The sample was mounted in a pair of RF coils (made in house) that were mounted at right angles to each other. The coils and sample were then mounted in an Oxford Instruments 3T helium exchange gas cryostat (including a superconducting magnet). The superconducting magnet provided the static magnetic field to lift the degeneracy of the spin ± 1 states (see Fig 1-10). The sample was mounted in such a way that it could be rotated with respect to the applied magnetic field, allowing the experimenter to achieve an optimum signal strength by aligning the crystal's [111] direction.

The Raman Heterodyne detection technique employs an optical probe with a wavelength of around 638 nm (the colour transition in the N-V Centre). The probe is produced by a coherent CR599-21 cw single mode dye laser (power ~few mW), which was pumped by a Spectra Physics Stabilite 2016 cw Argon Ion laser (power ~4W). The probe beam was focused on the N-V Centre sample, and the output Raman beat signal was detected on a New Focus 1801 DC-125 MHz photodiode.

The RF fields were then applied to either of the two coils. One coil would generate any $\hat{x}$ polarised fields, the other $\hat{z}$ polarised fields. These fields were generated by various RF power supplies with powers ranging from -70 dBm to +2dBm. So, in the instance most used in this experiment, there would be an $\hat{x}$ polarised pump field at the EPR transition, a $\hat{z}$ polarised pump field at the Rabi transition, and a weak $\hat{x}$ or $\hat{z}$ polarised probe field, resulting in three RF power supplies. The probe field power supply originated from the spectrum analyser, the Hewlett Packard 4396A Network/Spectrum Analyser. The signals were summed and then passed through the coils, before being dumped onto a 50 Ω load.

The output is then the beat signal of the RF fields and the optical probe coming from the dye laser. The spectrum analyser then allows for easy collection of the data, and it is also possible to perform phase sensitive detection, so the absorption and dispersion of the probe spectrum can be extracted. The results were saved to PC, and further analysis was performed using SigmaPlot or IDL (interactive data language). Now that the experimental setup is well understood, it is time to move on to the theoretical underpinnings of the Rabi transition. In Chapter 2, the Dressed State formalism will be extended using the Doubly Dressed States to

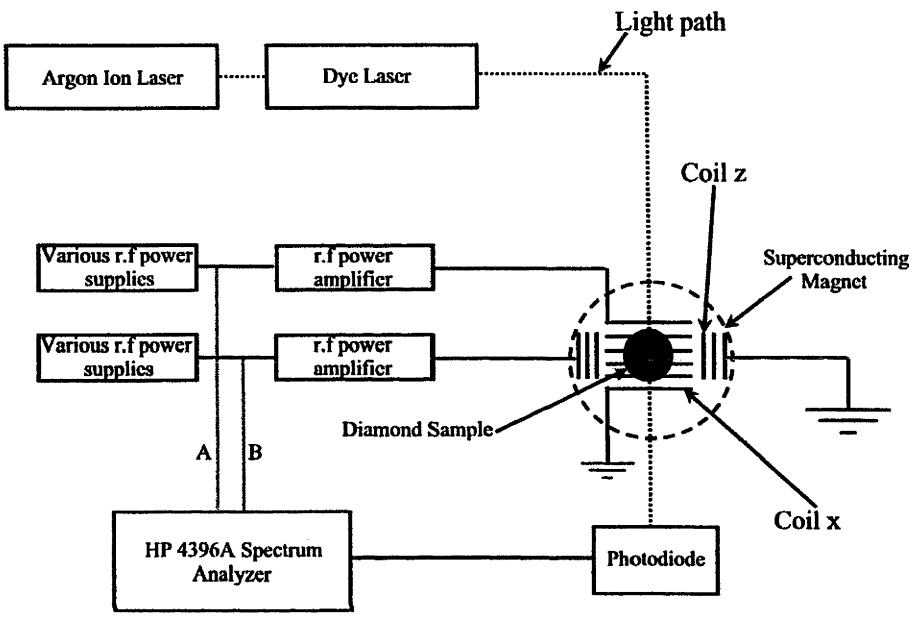

Figure 1-13: The schematic of the experimental setup. Details can be found in the text. (A) refers to the case where the probe field is $\hat{x}$ polarised, and (B) the case where the probe is $\hat{z}$ polarised.

solve for the dynamics of the Rabi transition.

1.7 Summary

In this introduction, the basic TLA theory was presented, encompassing both the semiclassical and quantum-mechanical theoretical frameworks. The geometrical presentation of the Bloch equations was developed, and this representation was used to demonstrate the existence of the Rabi transition. It was further shown that this transition arose when an $\hat{x}$ polarised field interacted with the basic TLA, and the transition was amenable to study by a second $\hat{z}$ polarised field (assuming the system had a permanent dipole moment). The semiclassical dressed states were used to derive the basic Rabi transition's spectrum when probed by a weak $\hat{z}$ polarised field, showing that its strength was directly proportional with the population difference in the dressed states. The Rabi transition established, the experimental system was then presented. The TLA studied is a transition between EPR spin states within the ground state in the N-V centre in diamond, and the detection method is the Raman Heterodyne method. In the following chapter, the fully quantum mechanical doubly dressed state formalism is carefully developed, and is applied to explain the emergence of the Rabi transition.

Chapter 2

Doubly Dressed State Formalism

In the introduction, the concept of the Rabi transition was introduced. Here, transitions between the doubly dressed state doublets become allowed if the system has a permanent dipole moment, and the second field is polarised along the same axis as the TLA. These ideas are developed more fully in this chapter, where the analytical results of using the doubly dressed state formalism are presented, showing the effects on the spectroscopy of the driven TLA when a $\hat{z}$ polarised pump field is applied. Doubly driven systems have been extensively studied theoretically [17]-[31], but there are limited experimental studies and these all involve two near resonant fields. They include several studies examining the strong pump, strong probe situation [32]-[38], resonance fluorescence [45],[46], and the Autler-Townes probe absorption spectrum [47]-[50]. This formalism then uses the theory of the doubly dressed states [51] and [52], used with varying success in the traditionally doubly driven systems, and it is found that the formalism is a very natural one to examine the Rabi transition with high accuracy. The key point is that the dipole moment of the TLA can always be resolved into components parrallel to and perpendicular with axis of the TLA. The application of two driving fields polarised parallel with these two components (the $\hat{x}$ and $\hat{z}$ polarised pump fields) then many of the rather difficulties with the solution of the equations in the traditional scenario can be avoided because of the symmetry of the situation.

2.1 Notation

The following shorthand and notation is used extensively throughout the thesis for ease of presentation

Field$_x$: refers to an $\hat{x}$ polarised pump field

Field$_z$: refers to a $\hat{z}$ polarised pump field

Probe$_x$: refers to an $\hat{x}$ polarised probe field

Probe$_z$: refers to a $\hat{z}$ polarised probe field

2.2 The "atom+2 fields" Hamiltonian

The system consists of two energy levels $|g\rangle$ and $|e\rangle$ of energies 0 and $\hbar\omega_0$ respectively, coupled to an $\hat{x}$ polarised magnetic field of frequency ω_x and a $\hat{z}$ polarised field of frequency ω_z. The Hamiltonian for the system is then given by

$$\mathcal{H} = \mathcal{H}_0 + \mathcal{H}_x + \mathcal{H}_z \tag{2.1}$$

where the parts of the Hamiltonian characterize the non-interacting TLA $\mathcal{H}_0$, the interaction with the near resonant $\hat{x}$ polarised field under the RWA $\mathcal{H}_x$ (as introduced in chapter 1), and the interaction with a low frequency $\hat{z}$ polarised field $\mathcal{H}_z$ where the system has a permanent dipole moment associated with the upper state.

$$\begin{aligned}
\mathcal{H}_0 &= \hbar\omega_0 |e\rangle\langle e| \\
\mathcal{H}_x &= \hbar\omega_x \left(a^\dagger a + \frac{1}{2}\right) + \hbar g \left(|e\rangle\langle g| a + |g\rangle\langle e| a^\dagger\right) \\
\mathcal{H}_z &= \hbar\omega_z \left(b^\dagger b + \frac{1}{2}\right) + \hbar k |e\rangle\langle e| \left(b + b^\dagger\right)
\end{aligned}$$

where a(b) and a† ($b^\dagger$) are the annihilation and creation operators for the $\hat{x}(\hat{z})$ polarised field respectively and g(k) characterises the interaction strength of the TLA with the $\hat{x}(\hat{z})$ polarised field. If $|n\rangle$ denotes the number state eigenstates of $a^\dagger a$ (i.e. Field$_x$) and $|m\rangle$ denotes the number state eigenstates of $b^\dagger b$ (i.e. Field$_z$) then the above operators can be written

$$
\begin{aligned}
a &= \sum_{n=1}^{\infty} \sqrt{n} \left|n-1\right\rangle \left\langle n\right| \qquad a^{\dagger} = \sum_{n=1}^{\infty} \sqrt{n} \left|n\right\rangle \left\langle n-1\right| \\
b &= \sum_{m=1}^{\infty} \sqrt{m} \left|m-1\right\rangle \left\langle m\right| \qquad b^{\dagger} = \sum_{m=1}^{\infty} \sqrt{m} \left|m-1\right\rangle \left\langle m\right|
\end{aligned}
$$

This defines the *bare* state system as the combination of the bare atom basis ($\left|e\right\rangle, \left|g\right\rangle$) and the number state basis for the fields, for example

$$
\left|e,n,m\right\rangle = \left|e\right\rangle \otimes \left|n\right\rangle \otimes \left|m\right\rangle
$$

The above Hamiltonians can be examined in more detail.

2.3 Dressed states - dealing with the first pump field

Starting with the case where only Field_x is actually interacting with the system, (i.e. only consider the Hamiltonian $\mathcal{H}_1 = \mathcal{H}_0 + \mathcal{H}_x$) the Hamiltonian can be written in terms of the above basis as

$$
\begin{aligned}
\mathcal{H}_1 &= \mathcal{H}_0 + \mathcal{H}_x \\
&= \hbar\omega_0 \hat{S}_e + \hbar\omega_x \left(n + \frac{1}{2}\right) \hat{I} \\
&\quad + \hbar g \sum_{n=1}^{\infty} \sqrt{n} \left(\hat{S}_+^n + \hat{S}_-^n\right)
\end{aligned}
$$

where the identity operator $\hat{\text{I}}$ and the 'spin' operator $\hat{S}_e$ are defined as

$$
\begin{aligned}
\hat{I} &= \sum_{n=0}^{\infty} \left(\left|g,n\right\rangle \left\langle g,n\right| + \left|e,n\right\rangle \left\langle e,n\right|\right) = \sum_{n=0}^{\infty} \left(\hat{S}_g^n + \hat{S}_e^n\right) \\
\hat{S}_e &= \sum_{n=0}^{\infty} \left|e,n\right\rangle \left\langle e,n\right| \\
\hat{S}_e^n &= \left|e,n\right\rangle \left\langle e,n\right| \qquad \hat{S}_g^n = \left|g,n\right\rangle \left\langle g,n\right|
\end{aligned}
$$

$$\hat{S}_+^n = |e,n-1\rangle\langle g,n| \qquad \hat{S}_-^n = |g,n\rangle\langle e,n-1|$$

In all of the cases considered in the following, strong pump fields are considered (i.e. $n, m \gg 1$) so the terms in the above Hamiltonian associated with the $n = 0$ case can be disregarded. The Hamiltonian $\mathcal{H}_1$ is therefore separated into an infinite ladder of manifolds, with each manifold referring to the energy level doublet associated with the nearly degenerate levels $|e,n-1\rangle, |g,n\rangle$.

$$\begin{aligned}
\mathcal{H}_1 &= \sum_{n=1}^{\infty} \mathcal{H}_1^n \\
\mathcal{H}_1^n &= \hbar\left(\omega_0 + \omega_x\left(n - \frac{1}{2}\right)\right)\hat{S}_e^{n-1} + \hbar\omega_x\left(n + \frac{1}{2}\right)\hat{S}_g^n \\
&\quad + \hbar g\sqrt{n}\left(\hat{S}_+^n + \hat{S}_-^n\right)
\end{aligned} \tag{2.4a}$$

These equations can be written in matrix form

$$\mathcal{H}_1^n = \hbar\left(\frac{1}{2}\omega_0 + n\omega_x\right)\begin{pmatrix} 1 & 0 \\ 0 & 1 \end{pmatrix} - \frac{\hbar}{2}\begin{pmatrix} \delta_x & \chi_x^n \\ \chi_x^n & -\delta_x \end{pmatrix} \tag{2.5}$$

where the detuning $\delta_x = \omega_0 - \omega_x$ and the Rabi frequency associated with Field$_x$ $\chi_x^n = -2g\sqrt{n}$ have been defined. Here the basis is taken to be

$$|g,n\rangle = \begin{pmatrix} 1 \\ 0 \end{pmatrix} \qquad |e,n-1\rangle = \begin{pmatrix} 0 \\ 1 \end{pmatrix}$$

The second matrix is diagonalised with a simple transformation to the *dressed states basis*

$$\begin{aligned}
|1,n\rangle &= \cos\theta_n |e,n-1\rangle + \sin\theta_n |g,n\rangle \\
|2,n\rangle &= -\sin\theta_n |e,n-1\rangle + \cos\theta_n |g,n\rangle
\end{aligned}$$

where the following definitions have been made;

$$\cos 2\theta_n = -\frac{\delta_x}{\Omega_n^x} \qquad \sin 2\theta_n = \frac{\chi_n}{\Omega_n^x} \qquad (0 < 2\theta_n < \pi)$$

where the generalised Rabi frequency $(\Omega_x^n)^2 = \delta_x^2 + (\chi_x^n)^2$. Under this transformation, equation (2.5) becomes (where $\mathcal{H}'$ refers to the Hamiltonian transformed into the dressed state basis)

$$\mathcal{H}_1^{n\prime} = \hbar\left(\frac{1}{2}\omega_0 + n\omega_x\right)\begin{pmatrix} 1 & 0 \\ 0 & 1 \end{pmatrix} + \frac{\hbar}{2}\Omega_x^n \begin{pmatrix} -1 & 0 \\ 0 & 1 \end{pmatrix}$$

or in operator form

$$\mathcal{H}_1^{n\prime} = \hbar\left(\frac{1}{2}\omega_0 + n\omega_x\right)\tilde{I}^n + \frac{\hbar}{2}\Omega_x^n \tilde{S}_z^n$$

where the operators are defined as

$$\begin{aligned} \tilde{I}^n &= |1,n\rangle\langle 1,n| + |2,n\rangle\langle 2,n| \\ \tilde{S}_z^n &= -|1,n\rangle\langle 1,n| + |2,n\rangle\langle 2,n| \end{aligned}$$

The Hamiltonian, when diagonalised, produces an infinite ladder of energy level doublets, with the energy level splitting between each doublet given by ω_x and the intra-doublet splitting given by the generalised Rabi frequency Ω_x^n. In the strong field case $n \gg 1$, and the Rabi frequency $\chi_x^n = -2g\sqrt{n}$ varies only by very little between the various (high) values of n. Therefore, the Rabi frequency can be considered to be fixed ($\chi_x^n \approx \chi_x$) for the physically relevant energy levels, which simplifies the picture. Now the energy level doublets are separated by ω_x, but the intra-doublet spacing is given by the fixed value Ω_x which is *independent* of n. A schematic representation of this is shown in fig 2-1.

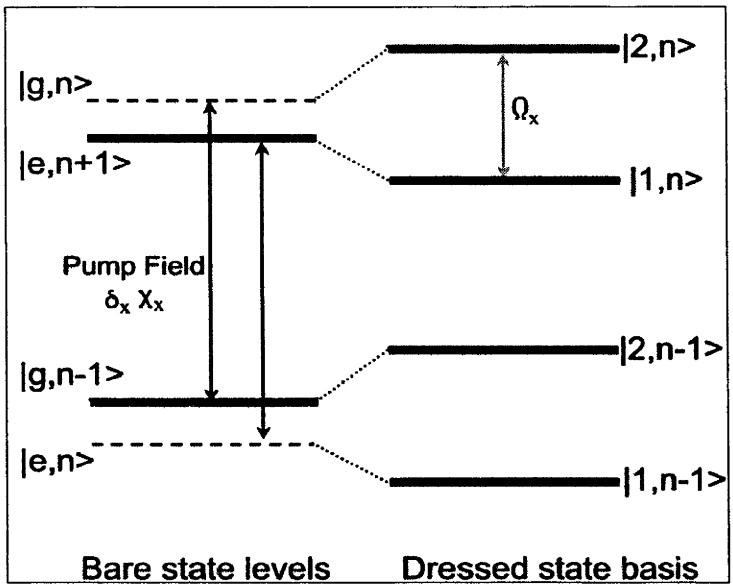

Figure 2-1: The energy level scheme for the singly driven TLA. On the left, the bare state transitions are driven by a field of frequency ω_x, detuning δ_x and Rabi frequency χ_x.

2.4 Doubly dressed states - dealing with the second pump field

Section 2.3 demonstrated how the dressed states diagonalised the Hamiltonian associated with a single field interacting with the two level system. In the case of a second, $\hat{z}$ polarised field interacting with a system with a permanent dipole moment this formalism is elegantly extended. To begin with, extending the notation to include the number states of Field$_z$

$$|e, n, m\rangle = |e, n\rangle \otimes |m\rangle$$

and examining the interaction term of the Hamiltonian (2.1) $\mathcal{H}_z$

$$\begin{aligned}
\mathcal{H}_z &= \hbar k \, |e\rangle \langle e| \left(b + b^\dagger\right) \\
&= \hbar k \sum_{m=1,n=1}^{\infty} \sqrt{m} \, |e, n-1, m-1\rangle \langle e, n-1, m| \\
&\quad + \hbar k \sum_{m=1,n=1}^{\infty} \sqrt{m} \, |e, n-1, m\rangle \langle e, n-1, m-1|
\end{aligned}$$

To understand this interaction, it is convenient to transform it into the dressed state basis

$$\begin{aligned}\mathcal{H}_z^D &= \hbar k \sum_{m=1,n=1}^{\infty} \sqrt{m}\left(\cos\theta_n \left|1,n,m-1\right\rangle - \sin\theta_n \left|2,n,m-1\right\rangle\right) \\ &\quad \times \left(\cos\theta_n \left\langle 1,n,m\right| - \sin\theta_n \left\langle 2,n,m\right|\right) \\ &\quad + \hbar k \sum_{m=1,n=1}^{\infty} \sqrt{m}\left(\cos\theta_n \left|1,n,m\right\rangle - \sin\theta_n \left|2,n,m\right\rangle\right) \\ &\quad \times \left(\cos\theta_n \left\langle 1,n,m-1\right| - \sin\theta_n \left\langle 2,n,m-1\right|\right) \\ &= \mathcal{H}_z^{D,r} + \mathcal{H}_z^{D,ar} + \mathcal{H}_z^{D,rr}\end{aligned}$$

where the three subcomponents are

$$\mathcal{H}_z^{D,r} = -\hbar k \sum_{n,m} \sqrt{m}\cos\theta_n \sin\theta_n \left(\left|2,n,m-1\right\rangle\left\langle 1,n,m\right| + \left|1,n,m\right\rangle\left\langle 2,n,m-1\right|\right) \quad (2.8a)$$

$$\mathcal{H}_z^{D,ar} = -\hbar k \sum_{n,m} \sqrt{m}\cos\theta_n \sin\theta_n \left(\left|2,n,m\right\rangle\left\langle 1,n,m-1\right| + \left|1,n,m-1\right\rangle\left\langle 2,n,m\right|\right) \quad (2.8b)$$

$$\begin{aligned}\mathcal{H}_z^{D,rr} &= \hbar k \sum_{n,m} \sqrt{m}\cos^2\theta_n \left(\left|1,n,m-1\right\rangle\left\langle 1,n,m\right| + \left|1,n,m\right\rangle\left\langle 1,n,m-1\right|\right) \\ &\quad + \hbar k \sum_{n,m} \sqrt{m}\sin^2\theta_n \left(\left|2,n,m\right\rangle\left\langle 2,n,m-1\right| + \left|2,n,m-1\right\rangle\left\langle 2,n,m\right|\right) \quad (2.8c)\end{aligned}$$

It is useful at this point to discuss the physical interpretation of these terms. The first term $\mathcal{H}_z^{D,r}$ represents transitions between the dressed states $|2,n\rangle$ and $|1,n\rangle$ with a concurrent loss or gain of a photon from Field$_z$. The transition frequency between the states $|2,n\rangle$ and $|1,n\rangle$ (i.e. within the doublets of the dressed state basis) is given by the generalised Rabi frequency Ω_x. So for the case where Field$_z$ is nearly resonant with this transition, the so called *Rabi transition*, $\mathcal{H}_z^{D,r}$ represents the resonant interaction where, for instance, the system is raised from the $|1,n\rangle$ to the $|2,n\rangle$ state with a concurrent loss of a photon from Field$_z$. As can be seen, the form of this interaction is completely analogous to equation (2.4*a*) which describes the interaction of Field$_x$ with the bare states. It is clear then that the basic physical interpretation of the permanent dipole moment interaction is similar to that of the normal dipole moment interaction, except that the Field$_z$ interacts with the *dressed states* rather than the bare states. It is obvious then that the Rabi transition only arises in response to an initial pump Field$_x$

though the Zeeman effect can be seen as the natural limit of this process as $\chi_x \to 0$.

The next part of the interaction Hamiltonian, $\mathcal{H}_z^{D,ar}$, is responsible for *anti-resonant* interactions. These anti-resonant terms describe interactions such as $|1,n\rangle \to |2,n\rangle$ coupled with a interaction $|m-1\rangle \to |m\rangle$ which clearly do not conserve energy. The terms are equivalent to the types of terms that appear in the standard driven two level atom which are discarded when taking the rotating wave approximation. Likewise, these terms in this expression can be discarded if Ω_x is large and the detuning of Field$_z$ (δ_z) is also not large. The second condition also applies to the more traditional RWA, but the second condition (which is already assumed above anyway) is important as Ω_x determines the transition frequency of the Rabi transition. Clearly, the smaller this transition frequency, the less valid the RWA becomes.

The last terms $\mathcal{H}_z^{D,rr}$ describe a higher order interaction of the Field$_z$ with the Rabi transition. To understand this, consider $\mathcal{H}_z^{D,rr}$ rewritten in the following form

$$\mathcal{H}_z^{D,rr} = \hbar k \sum_{n=1}^{\infty} \left(\cos^2\theta_n |1,n\rangle\langle 1,n| + \sin^2\theta_n |2,n\rangle\langle 2,n|\right)\left(b+b^\dagger\right)$$

which now looks like the standard interaction of a $\hat{z}$ polarised field with a system with a permanent dipole moment. Whereas in the bare state, only the excited state $|e\rangle$ had a permanent dipole moment associated with it, in this case it is clear that both the excited state $|2,N\rangle$ and the "ground" state $|1,N\rangle$ have permanent dipole moments associated with them. This difference does not affect the essential physics of the situation. Clearly then, this terms refers to the interaction of Field$_z$ with the second order Rabi transition generated by the interaction of Field$_z$ with the Rabi transition. This transition can be dubbed the *Rabi of the Rabi* (refered to as Rabi^2) and it will have a transition frequency related to the detuning of Field$_z$ from the Rabi transition δ_z and the Rabi frequency of Field$_z$ $\chi_z^{n,m}$ which, by analogy between equations (2.4*a*) and (??) is given by

$$\chi_z^{n,m} = 2k\sqrt{m}\cos\theta_n \sin\theta_n$$

and therefore the Rabi of the Rabi has a transition frequency given $\Omega_z^{n,m}$

$$(\Omega_z^{n,m})^2 = \delta_z^2 + (\chi_z^{n,m})^2$$

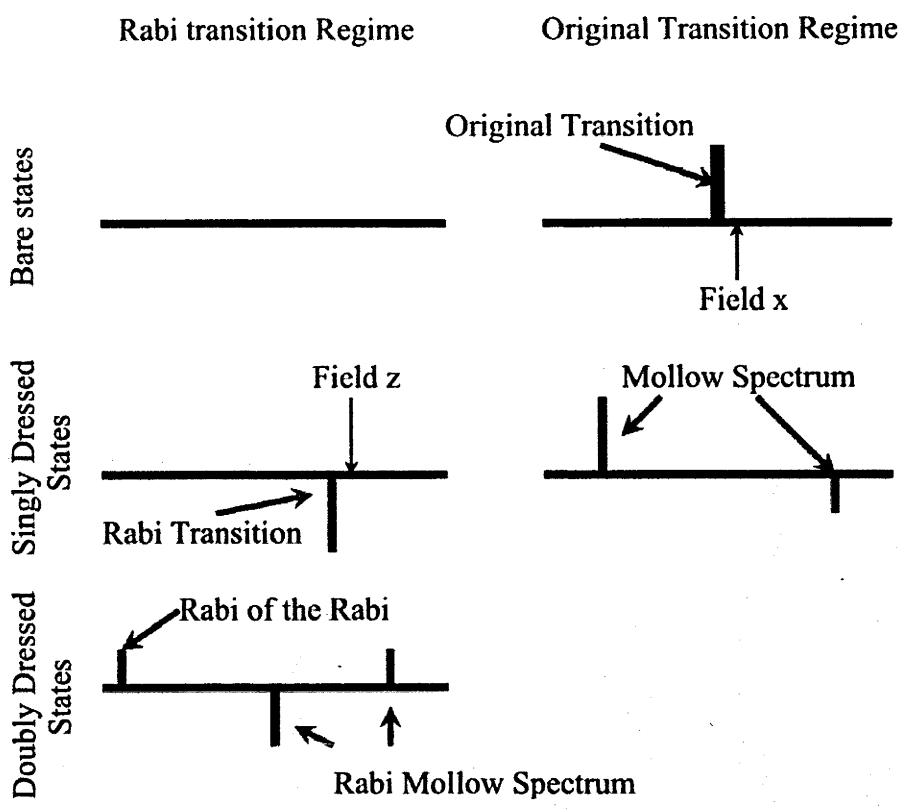

Figure 2-2: A schematic showing the emergence of the Rabi of the Rabi transition. The original transition is driven by Field$_x$ which gives rise to the standard Mollow spectrum plus the (emissive in this case) Rabi transition. A Field$_z$ drives the Rabi transition, which leads to a Mollow spectrum around the Rabi transition, and the emergence of its own 'Rabi' transition, the so called Rabi of the Rabi.

In Fig 2-2 a schematic pictures demonstrates how driving the Rabi transition gives rise to the Rabi of the Rabi (Rabi^2).The original driven transition causes the emergence of the Rabi transition between the singly dressed states. This transition, when driven, gives rise to the doubly dressed states, and a new transition at the *intra-doublet* separation frequency, the Rabi of the Rabi transition.

In most experimental cases, $\Omega_z^{n,m} \ll \omega_z$, meaning that the Field$_z$ is well detuned from this higher order resonance, and so its effect is assumed negligible. This assumption is clearly going to be erroneous in two cases. Firstly, when the power of Field$_z$ is such that $\chi_z^{n,m} \sim \Omega_x^n$ so that Field$_z$ is nearly resonant with Rabi^2 the interaction will be sizeable in nature and cannot be ignored. Secondly, there is the case where δ_z is large enough that Field$_z$ is nearly resonant with

Rabi[2] again. The results of experiments such as these will be discussed in Chapter 4.

Assuming then the conditions $1 \ll m \ll n$, the final result for the expansion of the full Hamiltonian in the singly dressed state basis is given by

$$\mathcal{H} = \sum_{n,m=1}^{\infty} \mathcal{H}^{n,m}$$

where the components of this Hamiltonian are

$$\begin{aligned} \mathcal{H}^{n,m} &= \hbar\left(\frac{1}{2}\omega_0 + n\omega_x + \omega_z\left(m+\frac{1}{2}\right) - \frac{1}{2}\Omega_x^n\right)\tilde{\sigma}_1 \\ &\quad +\hbar\left(\frac{1}{2}\omega_0 + n\omega_x + \omega_z\left(m-\frac{1}{2}\right) + \frac{1}{2}\Omega_x^n\right)\tilde{\sigma}_2 \\ &\quad -\hbar k\sqrt{m}\cos\theta_n \sin\theta_n\left(\tilde{\sigma}_- + \tilde{\sigma}_+\right) \end{aligned}$$

with the definitions for the dressed state "spin" operators

$$\begin{aligned} \tilde{\sigma}_1 &= |1,n,m\rangle\langle 1,n,m| \qquad \tilde{\sigma}_2 = |2,n,m-1\rangle\langle 2,n,m-1| \\ \tilde{\sigma}_+ + \tilde{\sigma}_- &= |2,n,m-1\rangle\langle 1,n,m| + |1,n,m\rangle\langle 2,n,m-1| \end{aligned}$$

Each one of these manifolds can be viewed in matrix form

$$\begin{aligned} \mathcal{H}^{n,m} &= \hbar\left(\frac{1}{2}\omega_0 + n\omega_x + m\omega_z\right)\begin{pmatrix} 1 & 0 \\ 0 & 1 \end{pmatrix} \\ &\quad -\frac{\hbar}{2}\begin{pmatrix} \delta_z & \chi_z^{n,m} \\ \chi_z^{n,m} & -\delta_z \end{pmatrix} \end{aligned}$$

with the basis states given by

$$|1,n,m\rangle = \begin{pmatrix} 1 \\ 0 \end{pmatrix} \qquad |2,n,m-1\rangle = \begin{pmatrix} 0 \\ 1 \end{pmatrix}$$

This is again easily diagonalised by transforming to the *Doubly Dressed states.*

$$\begin{aligned} |\alpha, n, m\rangle &= \cos\phi_{n,m}\,|2, n, m-1\rangle + \sin\phi_{n,m}\,|1, n, m\rangle \\ |\beta, n, m\rangle &= -\sin\phi_{n,m}\,|2, n, m-1\rangle + \cos\phi_{n,m}\,|1, n, m\rangle \end{aligned}$$

where the angles are defined as (where $\delta_z = \Omega_x - \omega_z$ is the Field$_z$ detuning)

$$\cos 2\phi_{n,m} = -\frac{\delta_z}{\Omega_z^{n,m}} \qquad \sin 2\phi_{n,m} = \frac{\chi_z^{n,m}}{\Omega_z^{n,m}}$$

giving for the final result

$$\begin{aligned} \mathcal{H}^{n,m} &= \hbar\left(\frac{1}{2}\omega_0 + n\omega_x + m\omega_z\right)\begin{pmatrix} 1 & 0 \\ 0 & 1 \end{pmatrix} \\ &\quad + \frac{\hbar\Omega_z^{n,m}}{2}\begin{pmatrix} -1 & 0 \\ 0 & 1 \end{pmatrix} \end{aligned}$$

or assuming that there is no n, m dependency (i.e. $n, m \gg 1$) in the parameters (that is, Field$_x$ and Field$_z$ are of high power)

$$\begin{aligned} \mathcal{H}^{n,m} &= \hbar\left(\omega_x\left(n + \frac{1}{2}\right) + \frac{1}{2}\delta_x + m\omega_z\right)\begin{pmatrix} 1 & 0 \\ 0 & 1 \end{pmatrix} \\ &\quad + \frac{\hbar\Omega_z}{2}\begin{pmatrix} -1 & 0 \\ 0 & 1 \end{pmatrix} \end{aligned}$$

In summary, the bare states interact with Field$_x$ which then results in the singly dressed states (as eigenstates of the "atom + 1 field" Hamiltonian). As long as the system has a permanent dipole moment, these dressed states may then interact with Field$_z$ with transition frequency given by the Rabi frequency Ω_x. This interaction, when included in the Hamiltonian with the non-resonant terms discarded, produces the doubly dressed states. Just as the dressed

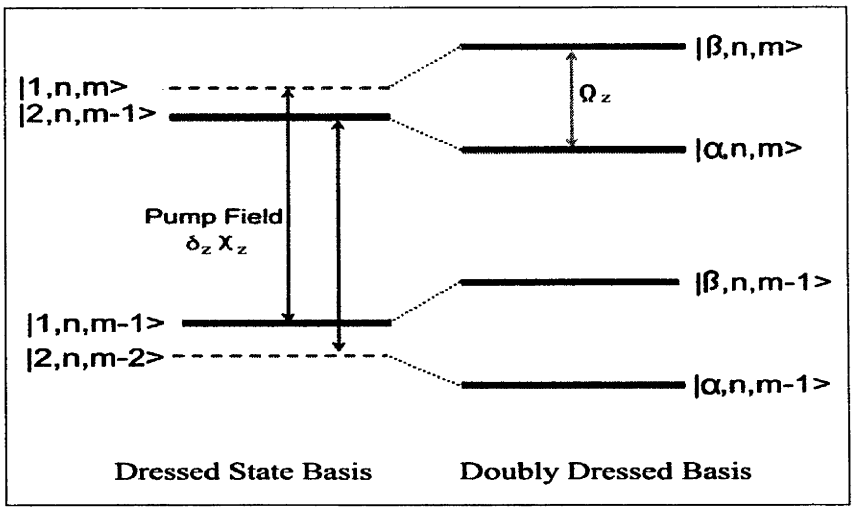

Figure 2-3: Doubly dressed state energy level diagram. The dressed state basis is further split by the application of the $\hat{z}$ polarised field (of detuning δ_z and Rabi frequency χ_z) to the Rabi transition.

states form an infinite ladder of energy level doublets, so the double dressed states also form a "lattice" of doublets. Each doublet is uniquely identified by the field strengths n, m and is centered about the energy $\hbar\left(\frac{1}{2}\omega_0 + n\omega_x + m\omega_z\right)$, while the intra-doublet spacing is given by $\hbar\Omega_z$. A representative diagram of this is shown in fig 2-3.

The doubly dressed states are traditionally used to study doubly driven systems, however their utility is often limited in the standard doubly driven systems. They usually require that more stringent conditions are met for them to be useful. Here, however, because of the orthogonal nature of the driving field polarizations, it is possible to use the doubly driven formalism to generate a more broadly useful set of solutions, which are acceptable for a wide range of experimentally viable parameters.

2.5 The Master Equation

In the previous section, the Hamiltonian describing the doubly driven system was diagonalised by using the doubly dressed states formalism. To proceed further, the effects of relaxation must be incorporated into the system, allowing spectroscopic results to be obtained and compared with experiment. To include relaxation terms, the standard approach is to examine the Master

equation which gives the equations of motion for the density matrix ρ under conditions of spontaneous emission from the excited to the ground state [9]-[12],[63].

The Master equation is given by

$$\dot{\rho} = -i\left[\mathcal{H}, \rho\right] - \frac{\Gamma}{2}\left(S_+ S_- \rho + \rho S_+ S_-\right) + \Gamma S_- \rho S_+ \tag{2.10}$$

where $S_+ = |e,n,m\rangle\langle g,n,m|$ and $S_- = |g,n,m\rangle\langle e,n,m|$ are the standard spin raising and lowering operators. The Master equation, it should be noted, deals with a system that allows $\hat{\mathrm{x}}$ polarised spontaneous emission, but disregards the spontaneous emission terms that would arise from $\hat{\mathrm{z}}$ polarised emission due to the permanent dipole moment. The interaction between the atom and the reservoir that leads to this Master equation only include the *off-diagonal* dipole coupling terms (for example, proportional to $|e\rangle\langle g|$) rather than the on-diagonal coupling terms that would lead to spontaneous emission at the Rabi transition.

However, since the frequency of the transition over which these sorts of emissions occur is given by Ω_x which is in all cases studied here much less than the bare state transition frequency ω_0, any spontaneous emission terms would be dominated by the contribution due to the $\hat{\mathrm{x}}$ polarised transitions. This is readily apparent when examining the Weisskopf-Wigner spontaneous emission decay rate

$$\Gamma = \frac{1}{4\pi\epsilon_0}\frac{4\omega^3 |\mu|^2}{3\hbar c^3}$$

where μ is the dipole moment and ω is the frequency of the spontaneous emission. So, in the case where the dipole moments μ_x and μ_z are of the same order, and $\omega_0 \gg \Omega_x$ it is clear that the rate of $\hat{\mathrm{x}}$ polarised decay Γ_x will strongly dominate over the rate of $\hat{\mathrm{z}}$ polarised decay Γ_z due to the ω^3 dependence of the emission rate.

There are two approaches to solving equation (2.10). The first approach, not adopted here, is to write the equation out in the bare state basis, which results in simple terms for the relaxation results, and attempt to solve it that way. However, the Hamiltonian tends to be complicated in this basis, and the solution is often not analytically reducible. However, if the Master equation is written in the double dressed state basis [9], the Hamiltonian is diagonalised, making those terms trivial. Several crucial assumptions about the relaxation of the system can then be made,

and an analytical solution is possible.

As a first step, the operators S_+ are written in the doubly dressed state basis.

$$\begin{aligned} S_+ &= \sum_{n,m,n',m'} |e,n,m\rangle \langle g,n',m'| \\ &= \sum_{n,m,i,j} \sum_{x=-1}^{1} \Gamma_{ij}^{x} |i,n,m\rangle \langle j,n-1,m+x| \end{aligned} \tag{2.11}$$

where the i,j indices indicate either α or β, and Γ_{ij}^{x} gives the matrix elements of S_+ in the doubly dressed states basis.

The following table outlines the particular values of the matrix elements

Matrix Element	**Rate**
$\Gamma_{\alpha\alpha}^{-1}$	$-\frac{1}{2}\sin 2\phi \sin^2\theta$
$\Gamma_{\alpha\alpha}^{0}$	$-\frac{1}{2}\cos 2\phi \sin 2\theta$
$\Gamma_{\alpha\alpha}^{1}$	$\frac{1}{2}\sin 2\phi \cos^2\theta$
$\Gamma_{\alpha\beta}^{-1}$	$-\sin^2\theta \cos^2\phi$
$\Gamma_{\alpha\beta}^{0}$	$\frac{1}{2}\sin 2\theta \sin 2\phi$
$\Gamma_{\alpha\beta}^{1}$	$-\cos^2\theta \sin^2\phi$
$\Gamma_{\beta\alpha}^{-1}$	$\sin^2\theta \sin^2\phi$
$\Gamma_{\beta\alpha}^{0}$	$\frac{1}{2}\sin 2\theta \sin 2\phi$
$\Gamma_{\beta\alpha}^{1}$	$\cos^2\theta \cos^2\phi$
$\Gamma_{\beta\beta}^{-1}$	$\frac{1}{2}\sin 2\phi \sin^2\theta$
$\Gamma_{\beta\beta}^{0}$	$\frac{1}{2}\cos 2\phi \sin 2\theta$
$\Gamma_{\beta\beta}^{1}$	$-\frac{1}{2}\sin 2\phi \cos^2\theta$

These matrix elements can then be used to calculate the elements of the Master equation, which can then be solved by making specific assumptions. These solutions then readily yield the spectra of absorption, fluorescence and Autler-Townes style experiments.

2.5.1 The Doubly Dressed state populations

To begin with, the following notation for the matrix elements of the density matrix ρ is employed;

$$\rho_{i,n,m}^{i',n',m'} = \langle i',n',m' | \rho | i,n,m \rangle$$

where $i, i' = \alpha$ or β. Returning to the Master equation (2.10), recall that the Hamiltonian $\mathcal{H}$ is diagonalised in the doubly dressed state basis. The Master equation for the populations is calculated by sandwiching the equation between the appropriate states

$$\frac{d}{dt}\rho_{i,n,m}^{i,n,m} = \langle i,n,m | \left(-\frac{\Gamma}{2} \left(S_+ S_- \rho + \rho S_+ S_- \right) + \Gamma S_- \rho S_+ \right) | i,n,m \rangle$$

where the commutator $[\mathcal{H},\rho]$ vanishes as the Hamiltonian has been diagonalised. In general, this equation results in a complex infinite series of equations, where the evolution of the populations is coupled via the relaxation terms to coherences and so on. To proceed, the next step is to take the *secular approximation*, whereby the population terms and coherence terms are decoupled. This is because the coherence between two states of energies E_a and E_b always rotate at $\exp\left(i\hbar\left(E_b - E_a\right)t\right)$, but the populations have no such terms. If all of the energy levels are well separated (i.e. any energy differences $\Delta E \gg$ any of the linewidths) then it is assumed that all of the coherences evolve approximately independently, and the populations also evolve independently of the coherences. In practice, this implies that the natural linewidth of the original transition, Γ obeys the following condition

$$\Gamma \ll \Omega_z \ll \Omega_x \ll \omega_0$$

or, in spectroscopic terms, all of the resonances are well separated. Under these conditions, the population equations of motion reduce to

$$\frac{d}{dt}\rho_{i,n,m}^{i,n,m} = -\Gamma \langle i,n,m | S_+ S_- | i,n,m \rangle \rho_{i,n,m}^{i,n,m}$$

$$= -\Gamma \sum_j \sum_{x=-1}^{1} \left(\Gamma_{ij}^x\right)^2 \rho_{i,n,m}^{i,n,m} + \Gamma \sum_j \sum_{x=-1}^{1} \left(\Gamma_{ji}^x\right)^2 \rho_{j,n-1,m+x}^{j,n-1,m+x} \tag{2.12}$$

The next important assumption is tied to the assumption of earlier that $n, m \gg 1$. This condition allows the observation that there should be very little variation between the doublets in the dressed and doubly dressed states basis, that is that $\chi^{n,m}$ does not depend on n, m. This is extended here to the populations, where it is assumed that $\rho_{j,n-1,m+x}^{j,n-1,m+x} \simeq \rho_{j,n,m}^{j,n,m}$, i.e. that the population difference between corresponding energy levels (for example $|1,n,m\rangle$ and $|1,n-1,m+1\rangle$) in neighbouring doublets is negligible. In terms of the familiar singly dressed states, the condition of strong fields leads to the approximate equality of the populations in the $|1,n\rangle$ state and the $|1,n-1\rangle$ state. Note, however, that there might be considerable difference between the populations in $|2,n,m\rangle$ and $|1,n-1,m\rangle$ for instance. This assumption is only valid when applied to corresponding energy levels.

Applying this important assumption to equation (2.12) the final rate equations for the populations are arrived at.

$$\frac{d}{dt}\rho_{i,n,m}^{i,n,m} = -\Gamma \sum_j \sum_{x=-1}^{1} \left(\Gamma_{ij}^x\right)^2 \rho_{i,n,m}^{i,n,m} + \Gamma \sum_j \sum_{x=-1}^{1} \left(\Gamma_{ji}^x\right)^2 \rho_{j,n,m}^{j,n,m}$$

Taking the trace of these equations over the field numbers n, m and defining the reduced density matrices

$$\sigma_{ij}^{xy} = \sum_{n,m} \rho_{i,n,m}^{j,n+x,m+y}$$

so that the populations become

$$P_i = \sigma_{ii}^{00}$$

The rate equations then become simply

$$\frac{dP_\alpha}{dt} = -\Gamma_{\alpha\to\beta} P_\alpha + \Gamma_{\beta\to\alpha} P_\beta \tag{2.13}$$

$$\frac{dP_\beta}{dt} = -\Gamma_{\beta\to\alpha}P_\beta + \Gamma_{\alpha\to\beta}P_\alpha$$

The rates of population transfer are then given by

$$\Gamma_{\alpha\to\beta} = \Gamma \sum_{x=-1}^{1} \left(\Gamma^x_{\alpha\beta}\right)^2 \qquad \Gamma_{\beta\to\alpha} = \Gamma \sum_{x=-1}^{1} \left(\Gamma^x_{\beta\alpha}\right)^2$$

The rate equations (2.13) are easily solved to find the steady state populations $P^{st}_{\alpha/\beta}$ of the doubly dressed states

$$\begin{aligned} P^{st}_\alpha &= \frac{\Gamma_{\beta\to\alpha}}{\Gamma_{\beta\to\alpha}+\Gamma_{\alpha\to\beta}} \\ P^{st}_\beta &= \frac{\Gamma_{\alpha\to\beta}}{\Gamma_{\beta\to\alpha}+\Gamma_{\alpha\to\beta}} \end{aligned}$$

and the transient solutions are

$$P_i(\tau) = P^{st}_i + \left(P_i(0) - P^{st}_i\right) e^{-\Gamma_{pop}\tau}$$

where the populations relaxation rate $\Gamma_{pop} = \Gamma_{\beta\to\alpha}+\Gamma_{\alpha\to\beta}$. The parameters can be expanded

$$\begin{aligned} \Gamma_{\alpha\to\beta} &= \left(\sin^2\theta\cos^2\phi\right)^2 + \left(\cos^2\theta\sin^2\phi\right)^2 + \left(\frac{1}{2}\sin 2\theta\sin 2\phi\right)^2 \\ \Gamma_{\beta\to\alpha} &= \left(\sin^2\theta\sin^2\phi\right)^2 + \left(\cos^2\theta\cos^2\phi\right)^2 + \left(\frac{1}{2}\sin 2\theta\sin 2\phi\right)^2 \end{aligned}$$

It should be noted that in the case when Field$_x$ is on resonance (i.e. $\cos\theta = \sin\theta$) then the two rates become equal so that

$$P^{st}_\alpha = P^{st}_\beta = \frac{1}{2}$$

independent of the detuning and Rabi frequency of Field$_z$. This can be understood by examining the populations of the singly dressed states when Field$_x$ is on resonance. In this case

the populations of the singly dressed states are equal. Hence, the interaction of Field$_z$ with the Rabi transition becomes equivalent to a field driving a transition with zero initial population difference. This raises the important point that the Rabi transition *cannot be directly observed* when the Field$_x$ is on resonance. However, as will be seen, the interaction of Field$_z$ with the resonance still occurs, and will have an impact on the Mollow spectrum of the original transition.

If Field$_x$ is off resonance, but Field$_z$ is on resonance, then likewise the populations of the doubly dressed states are equal, which is completely analogous to the one field singly dressed atom case.

2.5.2 Doubly Dressed State Coherences

The next equations to solve from the Master equation are the equations of motion for the coherences. Again, the secular approximation is employed to decouple any coherences that correspond to different transition frequencies. It is convenient to break up the coherences into two broad categories which will be useful for the calculation of spectral features in the future. The first case includes coherences that have degenerate frequencies, producing rate equations very similar to those produced for the populations. The second case generates equations for the coherences for which no degenerate frequencies with other coherences exist.

Coherences of type $\rho_{i,n,m}^{i,n+z,m+v}$

Since the coherences $\rho_{\alpha,n,m}^{\alpha,n+z,m+v}$ and $\rho_{\beta,n,m}^{\beta,n+z,m+v}$ revolve at the same frequency, they cannot be decoupled in the master equations when taking the secular approximation. The Master equation for the evolution of these coherences is therefore given by

$$\begin{aligned}\frac{d}{dt}\rho_{i,n,m}^{i,n+z,m+v} &= \left[-i\left(z\omega_x + v\omega_z\right) - \Gamma\sum_{y=-1}^{1}\left(\Gamma_{il}^{y}\right)^2\right]\rho_{i,n,m}^{i,n+z,m+v} \\ &\quad +\Gamma\sum_{y=-1}^{1}\left(\Gamma_{li}^{y}\right)^2\rho_{l,n,m}^{l,n+z,m+v}\end{aligned}$$

where $l = \alpha, \beta$ when $i = \beta, \alpha$. Performing the trace over the field variables, the equations reduce to the rate equations

$$\begin{aligned}\frac{d}{dt}\sigma_{\alpha\alpha}^{zv} &= \left[-i\left(z\omega_x + v\omega_z\right) - \Gamma_{\alpha\to\beta}\right]\sigma_{\alpha\alpha}^{zv} + \Gamma_{\beta\to\alpha}\sigma_{\beta\beta}^{zv} \\ \frac{d}{dt}\sigma_{\beta\beta}^{zv} &= \left[-i\left(z\omega_x + v\omega_z\right) - \Gamma_{\beta\to\alpha}\right]\sigma_{\beta\beta}^{zv} + \Gamma_{\alpha\to\beta}\sigma_{\alpha\alpha}^{zv}\end{aligned}$$

which, aside from the free evolution terms, are entirely analogous to the population rate equations(2.13) . The solution of these equations is given by

$$\sigma_{ii}^{zv}(\tau) = \left(P_i^{st} - \left(P_i^{st} - \sigma_{ii}^{zv}(\tau)\right)e^{-\Gamma_{pop}\tau}\right)e^{-i(z\omega_z + v\omega_z)\tau} \tag{2.17}$$

showing their relation to the population solutions, with a free evolution component.

Coherences of type $\rho_{\alpha\beta}^{zv}$

Finally, coherences of the type $\rho_{\alpha\beta}^{zv}$ are solved for. These coherences, by the secular approximation, can be decoupled from all other coherences and populations, resulting in the equations of motion

$$\begin{aligned}\frac{d}{dt}\rho_{\alpha,n,m}^{\beta,n+z,m+v} &= \left(-i\left(\Omega_z + z\omega_x + v\omega_z\right) - \Gamma_{coh}\right)\rho_{\alpha,n,m}^{\beta,n+z,m+v} \\ \frac{d}{dt}\rho_{\beta,n,m}^{\alpha,n+z,m+v} &= \left(-i\left(-\Omega_z + z\omega_x + v\omega_z\right) - \Gamma_{coh}\right)\rho_{\beta,n,m}^{\alpha,n+z,m+v}\end{aligned}$$

or in reduced density matrix terms

$$\frac{d}{dt}\sigma_{\beta\alpha}^{zv} = \left(-i\left(\Omega_z + z\omega_x + v\omega_z\right) - \Gamma_{coh}\right)\sigma_{\beta\alpha}^{zv} \tag{2.19a}$$

$$\frac{d}{dt}\sigma_{\alpha\beta}^{zv} = \left(-i\left(-\Omega_z + z\omega_x + v\omega_z\right) - \Gamma_{coh}\right)\sigma_{\alpha\beta}^{zv} \tag{2.19b}$$

where the coherence decay rate Γ_{coh} is

$$\begin{aligned}\Gamma_{coh} &= \frac{\Gamma}{2}\sum_{k=\alpha,\beta}\sum_{y=-1}^{1}\left(\left(\Gamma^{y}_{\beta k}\right)^{2}+\left(\Gamma^{y}_{\alpha k}\right)^{2}\right)-\Gamma\sum_{y=-1}^{1}\Gamma^{y}_{\beta\beta}\Gamma^{y}_{\alpha\alpha} \\ &= \frac{1}{2}\Gamma_{pop}+2\Gamma\sum_{y=-1}^{1}\left(\Gamma^{y}_{\alpha\alpha}\right)^{2}\end{aligned}$$

where the fact that $\Gamma^{y}_{\beta\beta} = -\Gamma^{y}_{\alpha\alpha}$ has been used to simplify the expression. The overall solutions for the coherences of this type are then given by

$$\begin{aligned}\sigma^{zv}_{\alpha\beta}(\tau) &= \sigma^{zv}_{\alpha\beta}(0)\exp\left(\left(-i\left(-\Omega_z+z\omega_x+v\omega_z\right)-\Gamma_{coh}\right)\tau\right) \\ \sigma^{zv}_{\beta\alpha}(\tau) &= \sigma^{zv}_{\beta\alpha}(0)\exp\left(\left(-i\left(\Omega_z+z\omega_x+v\omega_z\right)-\Gamma_{coh}\right)\tau\right)\end{aligned}$$

All that remains is to now use these results to obtain the various spectra for the different types of spectroscopic measurements.

2.6 Calculation of Spectra

2.6.1 Fluorescence Spectra

Calculation of spectral components

The calculation of Fluorescence spectra is a well established procedure. In the experiment, the emitted light from the sample excited by the coherent radiation is collected. The resultant emission intensity spectrum is required, which is given by the following expression

$$\Im(\omega) = \frac{\Gamma}{\pi}\,\mathrm{Re}\int_0^\infty \langle S_+(\tau)\,S_-(0)\rangle\, e^{i\omega\tau}d\tau \tag{2.21}$$

As previously, this expression actually calculates the $\hat{\mathrm{x}}$ polarised emission only. However, since the effects of $\hat{\mathrm{z}}$ polarised relaxation were ignored, the $\hat{\mathrm{x}}$ polarised emission spectrum provides the more valuable and accurate information.

In the previous section, the solutions for the equations of motion for the various components of the S_+ operator were found, and these solutions are employed to evaluate equation (2.21). In order to do so, it is important to apply the *quantum regression theorem* which shows that

the expectation value of the operator $\langle S_+(\tau) S_-(0)\rangle$ obeys the same equations of motion as the expectation value of the operator $\langle S_+(\tau)\rangle$. Examining the spectral distribution of $\langle S_+(\tau)\rangle$ (and referring to equation (2.11))

$$\begin{aligned}\langle S_+(\tau)\rangle &= \left\langle \sum_{n,m,i,j}\sum_{y=-1}^{1} \Gamma_{ij}^{y} |i,n,m\rangle \langle j,n-1,m+y| \right\rangle \\ &= \sum_{i,j}\sum_{y=-1}^{1} \Gamma_{ij}^{y}\sigma_{ji}^{-1y} \\ &= \sum_{i,j}\sum_{y=-1}^{1} \left\langle S_+^{i,j,y}\right\rangle \end{aligned} \tag{2.22a}$$

The definition has been made

$$\begin{aligned}\left\langle S_+^{i,j,y}\right\rangle &= \Gamma_{ij}^{y}\sigma_{ji}^{-1y} \\ \sigma_{ji}^{-1y} &= \langle |i,n,m\rangle \langle j,n-1,m+y|\rangle\end{aligned}$$

The Master equation generates the equations of motion for the coherences from equation (2.19*a*) for instance,

$$\frac{d}{dt}\left\langle S_+^{\alpha,\beta,y}\right\rangle = \left(-i\left(\Omega_z - \omega_x + y\omega_z\right) - \Gamma_{coh}\right)\left\langle S_+^{\alpha,\beta,y}\right\rangle$$

By the quantum regression theorem then the equations of motion for the component of the $\langle S_+(\tau) S_-(0)\rangle$ expectation value becomes

$$\frac{d}{dt}\left\langle S_+^{\alpha,\beta,y}(\tau) S_-(0)\right\rangle = \left(-i\left(\Omega_z - \omega_x + y\omega_z\right) - \Gamma_{coh}\right)\left\langle S_+^{\alpha,\beta,y}(\tau) S_-(0)\right\rangle \tag{2.23}$$

where the expansion

$$\langle S_+(\tau) S_-(0)\rangle = \sum_{i,j}\sum_{y=-1}^{1}\left\langle S_+^{i,j,y}(\tau) S_-(0)\right\rangle$$

has been made in much the same manner as equation (2.22*a*). Likewise

$$\frac{d}{dt}\left\langle S_{+}^{\beta,\alpha,y}(\tau)\,S_{-}(0)\right\rangle = \left(-i\left(-\Omega_z-\omega_x+y\omega_z\right)-\Gamma_{coh}\right)\left\langle S_{+}^{\beta,\alpha,y}(\tau)\,S_{-}(0)\right\rangle \tag{2.24}$$

The solutions of these two equations of motion are

$$\begin{aligned}\left\langle S_{+}^{\alpha,\beta,y}(\tau)\,S_{-}(0)\right\rangle &= \left\langle S_{+}^{\alpha,\beta,y}(0)\,S_{-}(0)\right\rangle \exp\left(-i\left(\Omega_z-\omega_x+y\omega_z\right)-\Gamma_{coh}\right)\tau \\ \left\langle S_{+}^{\beta,\alpha,y}(\tau)\,S_{-}(0)\right\rangle &= \left\langle S_{+}^{\beta,\alpha,y}(0)\,S_{-}(0)\right\rangle \exp\left(-i\left(-\Omega_z-\omega_x+y\omega_z\right)-\Gamma_{coh}\right)\tau\end{aligned}$$

For the other components of the $\langle S_{+}(\tau)\,S_{-}(0)\rangle$ operator

$$\begin{aligned}\frac{d}{dt}\left\langle S_{+}^{i,i,y}(\tau)\,S_{-}(0)\right\rangle &= \left(-i\left(-\omega_x+y\omega_z\right)-\Gamma_{l\to i}\right)\left\langle S_{+}^{i,i,y}(\tau)\,S_{-}(0)\right\rangle \\ &\quad -\Gamma_{i\to l}\left\langle S_{+}^{l,l,y}(\tau)\,S_{-}(0)\right\rangle\end{aligned} \tag{2.25}$$

where $i=\alpha/\beta$ and $l=\beta/\alpha$, and the fact that $\Gamma_{ii}^{y}=-\Gamma_{ll}^{y}$ is employed. To write down the final solution of this equation and equations (2.23, 2.24) it is necessary to evaluate the initial condition terms. Here, it is assumed that the system has reached its steady state before the spectroscopic measurements are begun. The expression for these terms is given by

$$\left\langle S_{+}^{i,j,y}(0)\,S_{-}(0)\right\rangle = \sum_{I,Y}\Gamma_{ij}^{y}\Gamma_{Ij}^{Y}\left(\sigma_{Ii}^{0,y-Y}\right)_{ss}$$

In the steady state limit, it is clear from the equations (2.17, 2.19*b*, 2.19*a*) for terms like $\sigma_{Ii}^{0,Y}$, that only in the case where $i=I$ would there exist steady state limits, and also only in the case where $y-Y=0$ would the steady state limits not average out to zero (since the steady state solution has rotating terms for the case where $y-Y\neq 0$). This means that these initial conditions reduce to expressions that depend upon the steady state populations of the doubly dressed states;

$$\left\langle S_+^{i,j,y}(0)\, S_-(0)\right\rangle = \left(\Gamma_{ij}^y\right)^2 P_i^{st}$$

Thus, the solutions to equations (2.23, 2.24) are given by

$$\begin{aligned}
\left\langle S_+^{\alpha,\beta,y}(\tau)\, S_-(0)\right\rangle &= \left(\Gamma_{\alpha\beta}^y\right)^2 P_\alpha^{st} \exp\left(-i\left(\Omega_z - \omega_x + y\omega_z\right) - \Gamma_{coh}\right)\tau \\
\left\langle S_+^{\beta,\alpha,y}(\tau)\, S_-(0)\right\rangle &= \left(\Gamma_{\beta\alpha}^y\right)^2 P_\beta^{st} \exp\left(-i\left(-\Omega_z - \omega_x + y\omega_z\right) - \Gamma_{coh}\right)\tau
\end{aligned}$$

leaving only equation (2.25) to be solved. Upon transforming to the rotating frame

$$\left\langle S_+^{i,i,y}(\tau)\, S_-(0)\right\rangle = \eta_i \exp\left(-i\left(-\omega_x + y\omega_z\right)\tau\right)$$

the equations can be written in matrix form

$$\frac{d}{d\tau}\begin{pmatrix}\eta_\alpha \\ \eta_\beta\end{pmatrix} = -A\begin{pmatrix}\eta_\alpha \\ \eta_\beta\end{pmatrix}$$

where

$$A = \begin{pmatrix}\Gamma_{\alpha\to\beta} & \Gamma_{\beta\to\alpha} \\ \Gamma_{\alpha\to\beta} & \Gamma_{\beta\to\alpha}\end{pmatrix}$$

Matrix A has eigenvalues $0, \Gamma_{pop} = \Gamma_{\alpha\to\beta} + \Gamma_{\beta\to\alpha}$. This means that the following relation holds true

$$\left\langle\left[S_+^{\alpha,\alpha,y}(\tau) + S_+^{\beta,\beta,y}(\tau)\right] S_-(0)\right\rangle = \left(a + be^{-\Gamma_{pop}\tau}\right)\exp\left(-i\left(-\omega_x + y\omega_z\right)\tau\right) \tag{2.27}$$

which leads to the following limits: In the $\tau \to 0$ limit (again assuming the system has reached the steady state)

$$\begin{aligned} a+b &= \left\langle \left[S_+^{\alpha,\beta,y}(0) + S_+^{\beta,\alpha,y}(0) \right] S_-(0) \right\rangle \\ &= \left(\Gamma_{\alpha\alpha}^y\right)^2 P_\alpha^{st} + \left(\Gamma_{\beta\beta}^y\right)^2 P_\beta^{st} \\ &= \left(\Gamma_{\alpha\alpha}^y\right)^2 \left(P_\alpha^{st} + P_\beta^{st}\right) \\ &= \left(\Gamma_{\alpha\alpha}^x\right)^2 \end{aligned}$$

and in the $\tau \to \infty$ limit, where it is assumed that the operators become decoupled

$$a \exp\left(-i\left(-\omega_x + y\omega_z\right)\tau\right) = \left\langle \left[S_+^{\alpha,\alpha,y}(\tau) + S_+^{\beta,\beta,y}(\tau) \right] \right\rangle_{st} \langle S_-(0) \rangle_{st}$$

Using the fact that

$$\begin{aligned} \left\langle S_+^{i,i,y}(\tau) \right\rangle_{st} &= \Gamma_{ii}^y \left(\sigma_{ii}^{-1y}\right)_{st} \\ &= \Gamma_{ii}^y P_i^{st} \exp\left(-i\left(-\omega_x + y\omega_z\right)\tau\right) \end{aligned}$$

an expression for a can be derived

$$a = \langle S_-(0) \rangle_{st} \Gamma_{\beta\beta}^y \left(P_\beta^{st} - P_\alpha^{st}\right)$$

It only remains to evaluate $\langle S_-(0) \rangle_{st}$. Here, the secular approximation is again applied, so that only the terms that rotate at the same frequency as $\left\langle S_+^{i,i,y}(\tau) \right\rangle_{st}$ are kept. This leads to the following expression

$$\begin{aligned} \langle S_-(0) \rangle_{st} &= \sum_{i,j} \sum_{y=-1}^{1} \Gamma_{ij}^y \left(\sigma_{ij}^{-1y}\right)^{st} \\ &= \Gamma_{\beta\beta}^y \left(P_\beta^{st} - P_\alpha^{st}\right) \end{aligned}$$

and the overall coefficients in the equation (2.27) are then given by

$$
\begin{aligned}
a &= \left(\Gamma^{y}_{\beta\beta}\right)^{2}\left(P^{st}_{\beta}-P^{st}_{\alpha}\right)^{2} \\
b &= \left(\Gamma^{y}_{\beta\beta}\right)^{2}\left(1-\left(P^{st}_{\beta}-P^{st}_{\alpha}\right)^{2}\right)
\end{aligned}
$$

All of the relevant terms in the expansion of $\langle S_{+}(\tau)\, S_{-}(0)\rangle$ have now been evaluated, and it only remains to produce the final expression for the Fluorescence spectrum.

The Fluorescence Spectrum

The integrand in equation (2.21) has been evaluated, so it is simple to write down the final result

$$
\begin{aligned}
\Im(\omega) &= \frac{\Gamma}{\pi}\sum_{i,j}\sum_{y=-1}^{1}\mathrm{Re}\int_{0}^{\infty}\left\langle S_{+}^{i,j,y}(\tau)\, S_{-}(0)\right\rangle e^{i\omega\tau}d\tau \\
&= \frac{\Gamma}{\pi}\sum_{y=-1}^{1}\mathrm{Re}\int_{0}^{\infty}\left\langle S_{+}^{\alpha,\beta,y}(\tau)\, S_{-}(0)\right\rangle e^{i\omega\tau}d\tau \\
&\quad +\frac{\Gamma}{\pi}\sum_{y=-1}^{1}\mathrm{Re}\int_{0}^{\infty}\left\langle S_{+}^{\beta,\alpha,y}(\tau)\, S_{-}(0)\right\rangle e^{i\omega\tau}d\tau \\
&\quad +\frac{\Gamma}{\pi}\sum_{y=-1}^{1}\mathrm{Re}\int_{0}^{\infty}\left\langle \left[S_{+}^{\alpha,\alpha,y}(\tau)+S_{+}^{\beta,\beta,y}(\tau)\right] S_{-}(0)\right\rangle e^{i\omega\tau}d\tau
\end{aligned}
$$

Using the expression of earlier on, we evaluate the individual components of the spectrum, for example

$$
\begin{aligned}
&\frac{\Gamma}{\pi}\sum_{y=-1}^{1}\mathrm{Re}\int_{0}^{\infty}\left\langle S_{+}^{\alpha,\beta,y}(\tau)\, S_{-}(0)\right\rangle e^{i\omega\tau}d\tau \\
&= \sum_{y=-1}^{1}\frac{\Gamma}{\pi}\left(\Gamma^{y}_{\alpha\beta}\right)^{2}P^{st}_{\alpha}\frac{\Gamma_{coh}}{\left(\omega-\omega_{x}+\Omega_{z}+y\omega_{z}\right)^{2}+\Gamma_{coh}}
\end{aligned}
\tag{2.30}
$$

and

$$\begin{aligned}
&\frac{\Gamma}{\pi}\sum_{y=-1}^{1}\mathrm{Re}\int_0^\infty\left\langle S_+^{\beta,\alpha,y}(\tau)\,S_-(0)\right\rangle e^{i\omega\tau}d\tau \\
&= \sum_{y=-1}^{1}\frac{\Gamma}{\pi}\left(\Gamma_{\beta\alpha}^{y}\right)^2 P_\beta^{st}\frac{\Gamma_{coh}}{\left(\omega-\omega_x-\Omega_z+y\omega_z\right)^2+\Gamma_{coh}}
\end{aligned} \tag{2.31}$$

and finally

$$\begin{aligned}
&\frac{\Gamma}{\pi}\sum_{y=-1}^{1}\mathrm{Re}\int_0^\infty\left\langle\left[S_+^{\alpha,\alpha,y}(\tau)+S_+^{\beta,\beta,y}(\tau)\right]S_-(0)\right\rangle e^{i\omega\tau}d\tau \\
&= \Gamma\sum_{y=-1}^{1}\left(\Gamma_{\beta\beta}^{y}\right)^2\left(P_\beta^{st}-P_\alpha^{st}\right)^2\delta\left(\omega-\omega_x+y\omega_z\right) \\
&+\frac{\Gamma}{\pi}\sum_{y=-1}^{1}\left(\Gamma_{\beta\beta}^{y}\right)^2\left(1-\left(P_\beta^{st}-P_\alpha^{st}\right)^2\right)\frac{\Gamma_{pop}}{\left(\omega-\omega_x+y\omega_z\right)^2+\Gamma_{pop}}
\end{aligned} \tag{2.32}$$

giving for the overall spectrum

$$\begin{aligned}
\Im(\omega) &= \frac{\Gamma}{\pi}\sum_{y=-1}^{1}\left(\Gamma_{\alpha\beta}^{y}\right)^2 P_\alpha^{st}L_A^{\Gamma_{coh}}\left(\omega-\omega_x+\Omega_z+y\omega_z\right) \\
&+\frac{\Gamma}{\pi}\sum_{y=-1}^{1}\left(\Gamma_{\beta\alpha}^{y}\right)^2 P_\beta^{st}L_A^{\Gamma_{coh}}\left(\omega-\omega_x-\Omega_z+y\omega_z\right) \\
&+\frac{\Gamma}{\pi}\sum_{y=-1}^{1}\left(\Gamma_{\beta\beta}^{y}\right)^2\left(1-\left(P_\beta^{st}-P_\alpha^{st}\right)^2\right)L_A^{\Gamma pop}\left(\omega-\omega_x+y\omega_z\right) \\
&+\Gamma\sum_{y=-1}^{1}\left(\Gamma_{\beta\beta}^{y}\right)^2\left(P_\beta^{st}-P_\alpha^{st}\right)^2\delta\left(\omega-\omega_x+y\omega_z\right)
\end{aligned}$$

with the expanded definition of the Lorentzian to allow for different linewidths

$$L_A^{\Gamma_i}(\alpha)=\frac{\Gamma_i}{\alpha^2+\Gamma_i^2}$$

The spectrum therefore consists of nine Lorentzians (the incoherent part) and the coherent

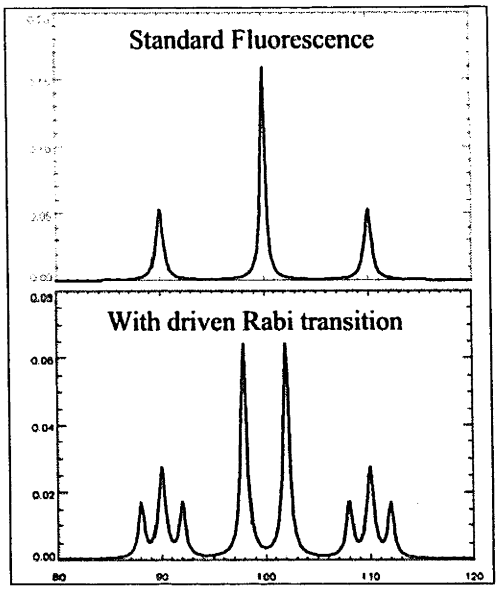

Figure 2-4: The incoherent part of the on-resonance Fluorescence spectrum. Firstly, the standard driven TLA is presented, with $\chi_x = 10$ MHz. In the second plot, Field$_z$ is applied on resonance to the Rabi transition, with $\chi_z = 2$ MHz.

part associated with the delta function in equation (2.32). Four resonances appear at the frequencies $\omega = \omega_x \pm \omega_z \pm \Omega_z$, two at $\omega = \omega_x \pm \Omega_z$, two at $\omega = \omega_x \pm \omega_z$ and finally one resonance at $\omega = \omega_x$. The weights of the lines are seen to be simple products of the dressed state populations and the transition rates as given earlier. For example, to calculate the weight of the Lorentzian that appears at $\omega = \omega_x + \omega_z + \Omega_z$, which refers to emission from the state $|\beta, n, m\rangle$ to the state $|\alpha, n-1, m-1\rangle$, one simply uses the population in state $|\beta, n, m\rangle$, given by P_β^{st}, and the rate of the relaxation, given by $\Gamma_{\beta\alpha}^{-1}$, the weight then being given by $\left(\Gamma_{\beta\alpha}^{-1}\right)^2 P_\beta^{st}$. The on-resonance case is presented in fig 2-4. The only surprise is the suppression of the central peak, which is due to the fact that the relaxation rate $\Gamma_{\beta\beta}^0$ goes to zero when the fields are on resonance. As mentioned before, the Fluorescence spectra are presented here for completeness, however they are not the focus of this thesis since the experimental system gathers absorption, not fluorescence data, and the full theoretical analysis of this is performed in chapter 3.

This simple procedure, well known in the singly dressed atom case, easily extends then to the doubly dressed atom case. This symmetry enables the use of the doubly dressed states, which are useful over a broad range of experimental parameters, and provide analytical solutions for

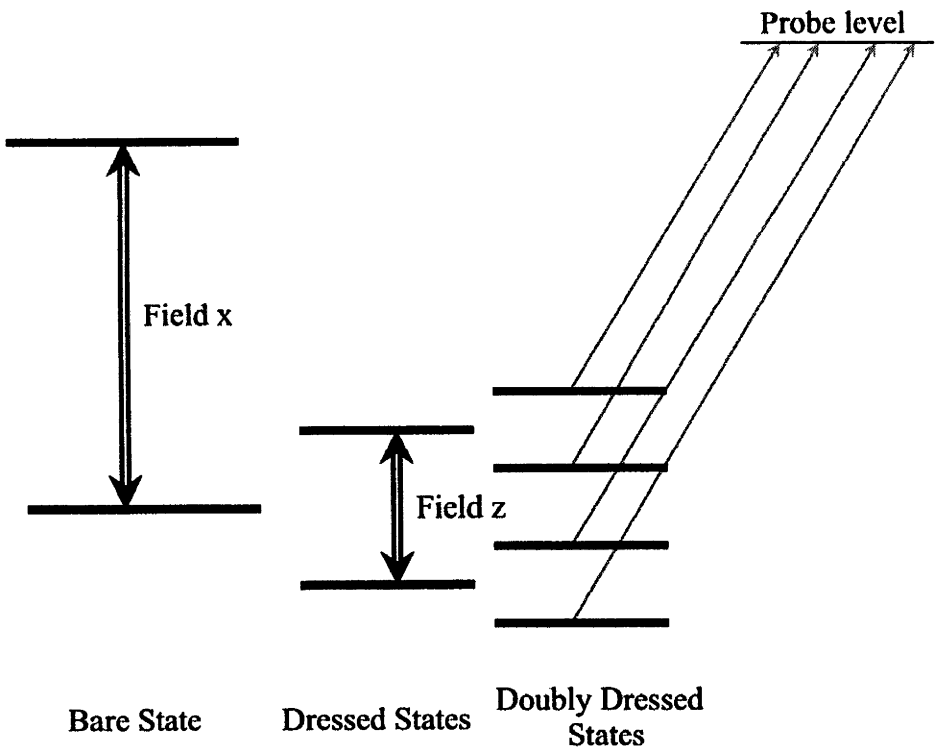

Figure 2-5: The schematic of the Autler-Townes spectrum. The doubly dressed states are probed to a third, weakly interacting level, leading to four resonances.

the spectroscopic features of the doubly driven two level atom.

2.6.2 Autler-Townes Spectra

Like fluorescence spectra, the Autler-Townes spectrum is also very easily calculated. The Autler-Townes spectrum arises when the two level atom is probed to a third level. The third level is assumed to be far enough away that the pump fields don't couple either the ground or the excited level to the probe level. The configuration is shown in Fig 2-5.

The spectrum is easy to calculate. Assuming that the probe fields couple the $|g, n, m\rangle$ level to the third level $|3\rangle$, clearly then, the doubly driven system, when probed to the third level, will exhibit a four peak structure, as the traditional Autler-Townes doublet is split again by Field$_z$. The weight of each line is proportional to the product of the steady state population in the doubly dressed state P_i^{ss} multiplied by the projection of the doubly dressed state basis onto

the bare state i.e. $|\langle i, n', m'|g, n, m\rangle|^2$ where $i = \alpha/\beta$ denotes the doubly dressed states. The following table shows the weights of the lines, as well as their frequencies (assuming that the third level is separated from the ground state by frequency ω_{g3} and the probe beam frequency is given by ω_p).

Coupled Levels	Peak Frequency	Weight
$\|\beta, n, m\rangle \rightarrow \|3\rangle$	$\omega_p = \omega_{g3} - \frac{1}{2}\Omega_x - \frac{1}{2}\Omega_z$	$P_\beta^{ss} (\sin\phi\cos\theta)^2$
$\|\alpha, n, m\rangle \rightarrow \|3\rangle$	$\omega_p = \omega_{g3} - \frac{1}{2}\Omega_x + \frac{1}{2}\Omega_z$	$P_\alpha^{ss} (\cos\phi\cos\theta)^2$
$\|\beta, n, m-1\rangle \rightarrow \|3\rangle$	$\omega_p = \omega_{g3} + \frac{1}{2}\Omega_x - \frac{1}{2}\Omega_z$	$P_\beta^{ss} (\cos\phi\sin\theta)^2$
$\|\alpha, n, m-1\rangle \rightarrow \|3\rangle$	$\omega_p = \omega_{g3} + \frac{1}{2}\Omega_x + \frac{1}{2}\Omega_z$	$P_\alpha^{ss} (\sin\phi\sin\theta)^2$

The widths of the lines are given by the sum of the natural linewidth of the level 3 and the width of level $|i, n, m\rangle$. The spectra of the singly and doubly driven on-resonance case is shown in Figure 2-6.

The Autler-Townes spectrum provides the simplest and most easily understood example of the calculations that are possible using the doubly dressed state basis. Finally, the last of the common spectroscopic techniques is examined, and the results for the absorption spectrum are discussed.

2.6.3 The probe absorption spectrum

In this situation, a probe beam is scanned over the same transition as the one the pump fields are driving. In this case, the fluorescence calculation is readily generalised to include absorption as well as stimulated emission, and the overall probe absorption spectrum is then given by the difference between the two. At least a qualitative understanding of the system is clear just from observing the population differences in the doubly dressed states. For example, if the probe is coupling the $|\beta, n, m\rangle$ state and the $|\alpha, n, m-1\rangle$ state, and $P_\beta^{ss} > P_\alpha^{ss}$ then the overall absorptive pattern will be emissive for that transition. To calculate the weights of the various spectral lines, one needs to calculate the following;

$$\Im(\omega) = \frac{\Gamma}{\pi} \mathrm{Re} \int_0^\infty \langle [S_+(\tau), S_-(0)] \rangle e^{i\omega\tau} d\tau \tag{2.34}$$

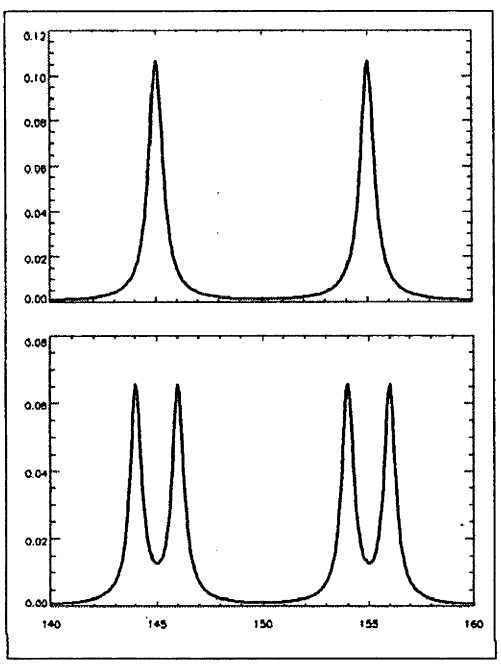

Figure 2-6: The Autler-Townes spectrum (top) in the singly driven case where Field_x is applied on resonance to a transition with $\chi_x = 10$ MHz. The probe beam level is chosen to be (rather arbitrarily) at 150 MHz. In the second case (bottom), Field_z is applied on resonance with the Rabi transition, with $\chi_z = 2$ MHz. Note the graph scales are different, so the doubly driven signal is considerably smaller than the singly driven spectrum.

The first term of the commutator within the integrand in equation (2.34) is calculated above, and the second term (the pure absorption term) can be calculated in exactly the same way. Therefore only the overall results are shown here. The analysis leads to a series of Lorentzians, again with very simple interpretation. For instance, the line at $\omega_x + \omega_z + \Omega_z$ corresponds to transitions between the $|\beta, n, m\rangle$ and $|\alpha, n-1, m-1\rangle$ states, where the weight of the line is simply given by $\left(\Gamma_{\beta\alpha}^{-1}\right)^2 (P_\beta - P_\alpha)$, the product of the relaxation rate and difference in population between the populations. To summarise, the Lorentzians and their weights are shown on the following table.

Lorentzian $(\gamma = -1, 0, 1)$	**Weight**
$L^{\Gamma_{coh}}(\omega - \omega_x + \Omega_z + \gamma\omega_z)$	$\frac{\Gamma}{\pi}\left(\Gamma_{\alpha\beta}^{\gamma}\right)^2\left(P_\alpha^{st} - P_\beta^{st}\right)$
$L^{\Gamma_{coh}}(\omega - \omega_x - \Omega_z + \gamma\omega_z)$	$\frac{\Gamma}{\pi}\left(\Gamma_{\beta\alpha}^{\gamma}\right)^2\left(P_\beta^{st} - P_\alpha^{st}\right)$

The absorption spectrum is very straightforward in this approximation. Note that in the case of the pump fields being on resonance, the spectrum reduces to zero. It is well known [3]-[4] that in the standard Mollow spectrum, this is also the case - however when the theory is studied more carefully, there is a weak on-resonance signal. This is certainly also the case here, and the next chapter will deal with the semi-classical theory, which is more exact (though in some ways less intuitive) than the above analysis. More discussion of the absorption spectrum will therefore be held over until the following chapter, though it is apparent here that the basic dynamics are simply understood in terms of the population differences between the doubly dressed levels, and the coherences between the levels, in a manner that is completely analogous to the standard Cohen-Tannoudji analysis applied to the singly driven TLA. In fact, this essential symmetry between the 'bare TLA + Field$_x$' interaction and the 'Dressed TLA (Rabi transition) + Field$_z$' interaction form the central idea of this thesis, and the level to which the symmetry holds highlights the interesting dynamics of this doubly driven TLA.

2.7 Summary

In this chapter, the basic process for solving the dynamics of the Rabi transition was carefully presented. The analysis proceeds in three basic steps

1. Interaction of Field$_x$ with the bare TLA is handled by transforming to the *dressed state basis*

2. Apply the RWA to Field$_z$. Field$_z$ is then seen as driving transitions between the dressed state levels, with transition frequency Ω_x.

3. This interaction of Field$_z$ with the dressed states is then handled by transforming to the doubly dressed states, which naturally diagonalises the 'driven TLA + Field$_z$' Hamiltonian.

During this process, it is noted that the interaction of Field$_z$ with the Rabi transition also generates its own 'Rabi transition', the so called Rabi of the Rabi. Field$_z$ also interacts with this transition, but in many cases this interaction can be ignored. Chapter 3 discusses these higher level interactions, and the effect that they have on the dynamics of the system, as well as providing the semi-classical analogue of the above calculation.

Chapter 3

Semiclassical Regime

Chapter 3 outlined the first calculation that was performed to model the physical system of a two level atom interacting with two pump fields, one $\hat{\mathbf{x}}$ polarised (that is, parallel to μ_{eg}), and the second $\hat{\mathbf{z}}$ polarised (parallel to μ_{ee}). The calculation introduced the doubly dressed states, which provide an elegant and intuitive mechanism for diagonalising the Hamiltonian. The spectroscopic results were generated from this, showing the chief features in the Fluorescence, Autler-Townes and probe beam absorption cases.

However, some relatively stringent approximations had to be made along the way. In particular, the secular approximation was required to proceed with the solution. As is well known, the on-resonance probe absorption spectrum for the singly driven system does indeed show a marginal signal, but this is not evident in the previous analysis. Clearly, an analysis with a broader applicability is required. This chapter shows the results of employing the dressed states to solve for the same situation, but in the semiclassical regime, where the atom is modelled quantum mechanically, and the fields are classical [13]-[15].

In order to proceed with the calculation, it is necessary to make several approximations. The first is that the rates of transverse and longitudinal relaxation (Γ and γ respectively) are equal. This ensures that a transformation to the dressed state frame does not introduce off diagonal relaxation terms. The second major approximation is the rotating wave approximation, related to the one taken in chapter 2.

3.1 The equations of motion

Consider a two level atom coupled to one $\hat{\mathbf{x}}$ polarised *classical* field,

$$\overrightarrow{E}_x = \hat{x} E_x \cos\omega_x t$$

and one $\hat{\mathbf{z}}$ polarised field

$$\overrightarrow{E}_z = \hat{z} E_z \cos\omega_z t$$

These fields are inserted into the Hamiltonian for the dipole interaction in matrix form

$$\begin{aligned} H &= -\overrightarrow{\mu} \cdot \left(\overrightarrow{E}_x + \overrightarrow{E}_z \right) \\ &= \hbar \begin{pmatrix} 0 & \chi_x \\ \chi_x & 0 \end{pmatrix} \cos\omega_x t + \hbar \begin{pmatrix} 0 & 0 \\ 0 & 2\chi_z \end{pmatrix} \cos\omega_z t \end{aligned}$$

where the Rabi frequencies χ_x and χ_z have been defined as

$$\begin{aligned} \chi_x &= -\frac{\mu_x E_x}{\hbar} \\ \chi_z &= -\frac{\mu_z E_z}{2\hbar} \end{aligned}$$

and it is again assumed that the excited level $|e\rangle$ has a permanent dipole moment, and the ground state $|g\rangle$ has none. Therefore $\hat{\mu}_z = \mu_z |e\rangle\langle e|$ and $\hat{\mu}_x = \mu_x \left(|e\rangle\langle g| + |g\rangle\langle e| \right)$. Using this equation with the Liouville equation for the density matrix equations of motion

$$\dot{\rho} = -\frac{i}{\hbar} [H, \rho]$$

and the individual components of the density matrix are obtained

$$\begin{aligned}
\dot{\rho}_{ge} &= 2i\chi_z \cos\omega_z t \rho_{ge} - i\chi_x \cos\omega_x t \left(\rho_{ee} - \rho_{gg}\right) \\
\dot{\rho}_{gg} &= -i\chi_x \cos\omega_x t \left(\rho_{eg} - \rho_{ge}\right) \\
\dot{\rho}_{ee} &= i\chi_x \cos\omega_x t \left(\rho_{eg} - \rho_{ge}\right)
\end{aligned}$$

where the fourth equation is left out as $\rho_{eg} = \rho_{ge}^{\star}$. Next terms for the two level atom $H_0 = \hbar\omega_0 |e\rangle \langle e|$ as well as the standard phenomenological relaxation terms are added. Furthermore, defining the population difference $W = \rho_{ee} - \rho_{gg}$, these equations become

$$\begin{aligned}
\dot{\rho}_{ge} &= \left\{i\left(\omega_0 + 2\chi_z \cos\omega_z t\right) - \Gamma\right\} \rho_{ge} - i\chi_x \cos\omega_x t W \\
\dot{W} &= 2i\chi_x \cos\omega_x t \left(\rho_{eg} - \rho_{ge}\right) - \Gamma\left(W - W^{eq}\right)
\end{aligned}$$

where the isotropic phenomenological relaxation rate Γ has been included. Finally, the transformation to the rotating frame is performed;

$$\begin{aligned}
\rho_{ge} &= \tilde{\rho}_{ge} e^{i\omega_x t} \\
\rho_{eg} &= \tilde{\rho}_{eg} e^{-i\omega_x t}
\end{aligned}$$

and the standard rotating wave approximation is taken by dropping all of the anti-resonant rapidly rotating terms. This leads to the final form of the Bloch equations which arise from the doubly driven system, as shown in chapter 1,

$$\frac{d}{dt}\tilde{\rho}_{ge} = \left\{i\left(\delta_x + 2\chi_z \cos\omega_z t\right) - \Gamma\right\} \tilde{\rho}_{ge} - i\frac{\chi_x}{2} W \tag{3.5a}$$

$$\dot{W} = i\chi_x \left(\tilde{\rho}_{eg} - \tilde{\rho}_{ge}\right) - \Gamma\left(W - W^{eq}\right) \tag{3.5b}$$

where the detuning $\delta_x = \omega_0 - \omega_x$. This equation describes the dynamics of the doubly driven system. To solve it, the doubly dressed states are once again needed, but this time they

are the semiclassical doubly dressed states. These arise in an entirely analogous fashion to the fully quantum mechanical ones, as shown in the introduction.

3.2 The semiclassical dressed states

To solve equations $(3.5a, 3.5b)$ it is firstly necessary to transform the equations into the semi-classical singly dressed state basis

$$\begin{aligned} |1\rangle &= \cos\theta\,|g\rangle - \sin\theta\,|e\rangle \\ |2\rangle &= \sin\theta\,|g\rangle + \cos\theta\,|e\rangle \end{aligned}$$

where the angles are defined as

$$\cos 2\theta = \frac{\delta_x}{\Omega_x} \qquad \sin 2\theta = \frac{\chi_x}{\Omega_x}$$

and the generalised Rabi frequency $\Omega_x^2 = \delta_x^2 + \chi_x^2$ is defined. This basis is the semi-classical analogue of the fully quantum mechanical dressed states which were employed in the previous chapter. In this basis, equations $(3.5a, 3.5b)$ become

$$\dot{\rho}_{12} = i\left(\Omega_x + 2\chi_z'' \cos\omega_z t - \Gamma\right)\rho_{12} - i\chi_z' \cos\omega_z t W_d - \rho_{12}^{eq} \tag{3.7a}$$

$$\dot{W}_d = 2i\chi_z' \cos\omega_z t\,(\rho_{21} - \rho_{12}) - \Gamma\left(W_d - W_d^{eq}\right) \tag{3.7b}$$

where the definitions have been made

$$\begin{aligned} W_d &= \rho_{22} - \rho_{11} \\ \rho_{12}^{eq} &= \frac{1}{2}\Gamma \sin 2\theta W^{eq} = \frac{\chi_x \Gamma W^{eq}}{2\Omega_x} \\ W_d^{eq} &= \cos 2\theta W^{eq} = \frac{\delta_x}{\Omega_x} W^{eq} \end{aligned}$$

$$\chi_z' = -\sin 2\theta \chi_z = -\frac{\chi_x}{\Omega_x}\chi_z$$
$$\chi_z'' = \cos 2\theta \chi_z = \frac{\delta_x}{\Omega_x}\chi_z$$

Clearly, these equations have much in common with the standard Bloch equations. This demonstrates the effective symmetry that underlies the system, as explained in the introductory remarks using the graphical representation of the Rabi transition. In fact, the only substantial difference is that now the equations involve an equilibrium coherence ρ_{12}^{eq}. It is clear then what the physical interpretation of equations $(3.7a, 3.7b)$ is. Field$_x$ interacts with the two level system, "generating" the Rabi transition. Field$_z$ interacts with the Rabi transition with a transition frequency given by Ω_x. Furthermore, the time dependent term proportional to $\chi_z'' \cos\omega_z t$ in equation $(3.7a)$ shows that Field$_z$ will also interact with the Rabi of the Rabi, generating a series of higher order interactions (see section 3.5.2). In the dressed state basis, part of Field$_z$ interacts with the Rabi transition (term proportional to χ_z'), and part of the field interacts with the Rabi of the Rabi (term proportional to χ_z''). This equation describes the dynamics of the Rabi transition, and it is clear that as was seen in Chapter 2, the Rabi transition is entirely analogous to the standard bare transition. The Rabi transition has an off diagonal magnetic dipole interaction with a field that is polarised at right angles to it. This leads to the χ_z' term. The χ_z'' term arises from the fact that in the off-resonant case (i.e. when the Field$_x$ is off resonant: $\delta_x \neq 0$), there is a component of the Field$_z$ that still lies parallel to the axis of the Rabi transition.

To see this, examine the classical magnetic dipole (recalling that it is entirely analogous to the semiclassical 'Bloch' vector). In the classical dipole treatment, a static magnetic field is defined to lie along the $\hat{\mathbf{z}}$ axis which defines the axis of the system. The magnetic dipole will precess about the static field with frequency given by ω_0, the Larmor frequency. This is equivalent to the bare state transition frequency ω_0. If a field rotating about $\hat{\mathbf{z}}$ at frequency ω_1 and strength χ is applied, a transformation to the frame rotating with frequency ω_1 is then required to remove the time dependence of the rotating field. In the rotating frame, the static magnetic field now has a Larmor frequency of $\delta = \omega_0 - \omega_1$. So in this rotating frame, we now have a new static field, given by $\delta\hat{\mathbf{z}} + \chi\hat{\mathbf{x}}$. The magnetic dipole (Bloch Vector) now precesses about this new, static field with a frequency given by the generalised Rabi frequency $\Omega = \sqrt{\chi^2 + \delta^2}$.

If a $\hat{\mathbf{z}}$ polarised field of frequency $\omega_z \approx \Omega$ is applied to the system , then it is unaffected by the transformation to the rotating frame. In the rotating frame, we see that the linearly polarised $\hat{\mathbf{z}}$ field is actually composed of two, oppositely rotating circularly polarised fields. One of these fields is nearly resonant with the precession frequency of the dipole in this frame and the other is anti-resonant. It is the antiresonant component that can now be discarded, which is the rotating wave approximation. Now, the origin of the Rabi transition, and the origin of the higher order terms, is clear. Since any non-zero δ will ensure that the Bloch vector $\delta\hat{\mathbf{z}}+\chi\hat{\mathbf{x}}$ is not perfectly at right angles to the $\hat{\mathbf{z}}$ axis, then only a component of the $\hat{\mathbf{z}}$ polarised field actually drives the Rabi transition, since only a component of the field ($\chi_z \cos 2\theta$) is actually orthogonal to the axis of the Bloch vector. This component is the one at right angles to the Bloch vector. The remaining component of the $\hat{\mathbf{z}}$ field is actually parallel to the Bloch vector, and plays a role in higher order interactions, by driving the Rabi of the Rabi transition that is generated by the interaction of the perpendicular component of the $\hat{\mathbf{z}}$ field. These higher order interactions will be examined in section 3.5.2.

To proceed analytically from this point, two approximations must be applied which are entirely analogous to those made in chapter 2. Firstly, it is assumed that ω_z is sufficiently large that it is possible to transform these equations to the rotating frame and then take the rotating wave approximation in exactly the same fashion as shown earlier. Transforming to the rotating frame

$$\begin{aligned} \rho_{12} &= \tilde{\rho}_{12} e^{i\omega_z t} \\ \rho_{21} &= \tilde{\rho}_{21} e^{-i\omega_z t} \end{aligned}$$

the equations of motion become (after the RWA has been applied)

$$\frac{d}{dt}\tilde{\rho}_{12} = i\left(\delta_z + 2\chi_z'' \cos\omega_z t - \Gamma\right)\tilde{\rho}_{12} - i\frac{\chi_z'}{2} W_d - \rho_{12}^{eq} e^{-i\omega_z t} \tag{3.9a}$$

$$\dot{W}_d = i\chi_z'\left(\tilde{\rho}_{21} - \tilde{\rho}_{12}\right) - \Gamma\left(W_d - W_d^{eq}\right) \tag{3.9b}$$

where the detuning $\delta_z = \Omega_x - \omega_z$ has been defined. This approximation is taken under the

assumption that the system is

(i) strongly driven. This allows for a large Rabi frequency Ω_x.

(ii) that ω_z is on or near the Rabi resonance.

Therefore, since $\omega_z \approx \Omega_x$ and Ω_x is sufficiently large, the rotating wave approximation is valid in this new frame. In the experimental system studied in this work, Rabi frequencies are typically of order 5-10 MHz in size, which certainly validates the taking of the rotating wave approximation, considering the initial Larmor frequency $\omega \approx 70$ MHz. The effects of not taking the rotating wave approximation will be examined in section 3.5.1.

To proceed from this point, it is assumed that ω_z is nearly resonant with the Rabi transition, and that $\chi_z \ll \Omega_x$. This implies that ω_z will be very far detuned from the Rabi of the Rabi transition, and so this higher order term will have only a negligible impact on the results. When $\delta_z \ll \chi_z \ll \Omega_x$ then we have a number of results. Firstly $\chi_z'' \ll \chi_z'$. This comes about because the interaction of Field$_z$ with the Rabi transition is proportional to χ_z', and the interaction with the Rabi of the Rabi is proportional to χ_z''. Physically, since the Rabi transition is at Ω_x, and Field$_z$ is nearly resonant with this, we expect a Rabi of the Rabi to be generated with at $\simeq \chi_z$. Field$_z$ is well detuned from this new interaction, so the interaction of Field$_z$ with the Rabi of the Rabi can be ignored. This time dependent term proportional to χ_z'' is therefore neglected, and the final form of these equations may be arrived at

$$\frac{d}{dt}\tilde{\rho}_{12} = i\left(\delta_z - \Gamma\right)\tilde{\rho}_{12} - i\frac{\chi_z'}{2}W_d - \rho_{12}^{eq}e^{-i\omega_z t} \tag{3.10a}$$

$$\dot{W}_d = i\chi_z'\left(\tilde{\rho}_{21} - \tilde{\rho}_{12}\right) - \Gamma\left(W_d - W_d^{eq}\right) \tag{3.10b}$$

These equations then describe the interaction of Field$_z$ with the Rabi transition, which was generated by the application of Field$_x$ to the original transition. To solve these equations, it is necessary to employ the *semiclassical* doubly dressed states, defined in a manner entirely analogous to the definition seen in chapter 2;

$$|\alpha\rangle = \cos\phi\,|1\rangle - \sin\phi\,|2\rangle$$

$$|\beta\rangle = \sin\phi\,|1\rangle + \cos\phi\,|2\rangle$$

where

$$\cos 2\phi = \frac{\delta_z}{\Omega_z} \qquad \sin 2\phi = \frac{\chi_z'}{\Omega_z}$$

and the new generalised Rabi frequency $\Omega_z^2 = \delta_z^2 + (\chi_z')^2$ is defined. This basis, which was introduced in the case of the fully quantum mechanical equations in the previous chapter, was derived from the essential symmetry of equations $(3.10a, 3.10b)$ with equations $(3.5a, 3.5b)$ for the standard Bloch equations. When the equations of motion are transformed into this basis, the following equations result;

$$\dot{\rho}_{\alpha\beta} = (i\Omega_z - \Gamma)\,\rho_{\alpha\beta} - \rho_{\alpha\beta}^{eq} - \left(P_- e^{-i\omega_z t} - P_+ e^{i\omega_z t}\right) \tag{3.12a}$$

$$\dot{W}_{dd} = -\Gamma\left(W_{dd} - W_{dd}^{eq}\right) + w^r\left(e^{i\omega_z t} + e^{-i\omega_z t}\right) \tag{3.12b}$$

with the following definitions

$$\begin{aligned}
W_{dd} &= \rho_{\beta\beta} - \rho_{\alpha\alpha} \\
\rho_{\alpha\beta}^{eq} &= \frac{1}{2}\Gamma \sin 2\phi W_d^{eq} = \frac{\chi_z' \Gamma W_d^{eq}}{2\Omega_z} \\
W_{dd}^{eq} &= \cos 2\phi W_d^{eq} = \frac{\delta_z}{\Omega_z} W_d^{eq} \\
P_- &= \frac{\rho_{12}^{eq}}{2}\left(1 - \frac{\delta_z}{\Omega_z}\right) = \rho_{12}^{eq}\cos^2\phi \\
P_+ &= \frac{\rho_{12}^{eq}}{2}\left(1 - \frac{\delta_z}{\Omega_z}\right) = \rho_{12}^{eq}\sin^2\phi \\
w^r &= -\rho_{12}^{eq}\frac{\chi_z'}{\Omega_z} = -\sin 2\phi \rho_{12}^{eq}
\end{aligned}$$

To reiterate, these equations describe the dynamics of the TLA which is driven by two classical fields. Field$_x$ drives the original TLA atom transition which will then produce an $\hat{\mathbf{x}}$ polarised transition at the Rabi frequency of the original field Ω_x. A second, $\hat{z}$ polarised field can

now be applied to this new transition. Now examine the general properties of these equations. Equations $(3.12a, 3.12a)$ are easily solved for the steady state limit, giving for the coherences as $t \rightarrow \infty$

$$\rho_{\alpha\beta}^{ss} = \rho_{\alpha\beta}^{0} + \rho_{\alpha\beta}^{-1} e^{-i\omega_z t} + \rho_{\alpha\beta}^{1} e^{i\omega_z t} \tag{3.14}$$

where the components are given by

$$\begin{aligned} \rho_{\alpha\beta}^{0} &= -\rho_{\alpha\beta}^{eq} L(-\Omega_z) \\ \rho_{\alpha\beta}^{-1} &= -P_{-} L(-\omega_z - \Omega_z) \\ \rho_{\alpha\beta}^{1} &= P_{+} L(\omega_z - \Omega_z) \end{aligned}$$

Now the steady state population terms are examined

$$W_{dd}^{ss} = w^0 + w^{-1} e^{-i\omega_z t} + w^1 e^{i\omega_z t} \tag{3.16}$$

where

$$\begin{aligned} w^0 &= W_{dd}^{eq} \\ w^1 &= w^r L(\omega_z) \\ w^{-1} &= w^r L(-\omega_z) \end{aligned}$$

Clearly then, the population dynamics consist of a steady state component W_{dd}^{eq} and a rotating component, due to the steady state coherence set up by the first pump field (i.e. $\propto \rho_{12}^{eq}$). The population in the doubly dressed states undergoes Rabi flopping, with frequency given by ω_z, with an in phase component proportional to $\cos\omega_z t$ given by

$$-2\rho_{12}^{eq} \frac{\chi_z'}{\Omega_z} L_A(\omega_z)$$

and a component out of phase (i.e. proportional to $\sin\omega_z t$) given by

$$-2\rho_{12}^{eq}\frac{\chi_z'}{\Omega_z}L_D\left(\omega_z\right)$$

This contrasts with the standard singly driven system (i.e. $\chi_z = 0$) which only has a steady state population term, and does not include this population flopping. This is because the standard driven system does not have a steady state coherence term to drive population flopping. To compare the singly and doubly driven systems, examine equations $(3.7a, 3.7b)$ without the second pump field (which is simply the singly driven system).

$$\begin{aligned}\dot{\rho}_{12} &= \left(i\Omega_x - \Gamma\right)\rho_{12} - \rho_{12}^{eq} \\ \dot{W}_d &= -\Gamma\left(W_d - W_d^{eq}\right)\end{aligned}$$

which has steady state solution

$$\begin{aligned}\rho_{12}^{ss} &= -\rho_{12}^{eq}L\left(-\Omega_x\right) \\ W_d^{ss} &= W_d^{eq}\end{aligned}$$

It is obvious then the clear differences between the doubly driven and the singly driven solutions, in particular the lack of oscillating components in the solution. Now, it is easy to compare the steady state population values in the singly and doubly driven scenarios. Firstly, in the singly driven case, the steady state populations of the singly dressed states are

$$\begin{aligned}P_1^{st} &= \frac{1}{2}\left(1 - W_d^{eq}\right) = \frac{1}{2}\left(1 - \frac{\delta_x}{\Omega_x}W^{eq}\right) \\ P_2^{st} &= \frac{1}{2}\left(1 + \frac{\delta_x}{\Omega_x}W^{eq}\right)\end{aligned}$$

and for the doubly driven case the steady state populations of the doubly dressed states are

$$P_\alpha^{st} = \frac{1}{2}\left(1 - W_{dd}^{eq}\right) = \frac{1}{2}\left(1 - \frac{\delta_z}{\Omega_z}\frac{\delta_x}{\Omega_x}W^{eq}\right) = \frac{1}{2}\left(1 - \frac{\delta_z}{\Omega_z}W_d^{eq}\right)$$
$$P_\beta^{st} = \frac{1}{2}\left(1 + \frac{\delta_z}{\Omega_z}\frac{\delta_x}{\Omega_x}W^{eq}\right) = \frac{1}{2}\left(1 + \frac{\delta_z}{\Omega_z}W_d^{eq}\right)$$

Recalling that W_d^{eq} is the steady state population difference between the singly dressed states, it is clear that their forms are analogous, and equally clear that in the case where $\delta_x = 0$ then $P_\alpha^{st} = P_\beta^{st}$ regardless of the detuning of Field$_z$ as was demonstrated in Chapter 2. This is because if the first field is on resonance, then the singly dressed states have equal populations, and when the second pump field is applied, it is equivalent to driving a two level system (in this case, the Rabi transition) with no initial population difference. It is therefore no surprise that the net effect is to have equal doubly dressed state populations.

So far, it is obvious that the interaction of Field$_z$ with the Rabi transition is fundamentally very similar to a normal pump field driving a traditional two level system. It has however several advantages. Firstly, there is the obvious advantage that this is a doubly driven system which allows an analytical solution. From an experimental point of view, the Rabi transition is of interest because it allows better results than the bare system in many cases (see Chapter 1). Finally, the Rabi transition provides a two level atom to explore, but one with many tunable characteristics, like transition frequency, dipole moment and so on.

Now that the doubly driven dynamics are known, it is now possible to derive the the probe absorption spectrum. It is also possible to derive the fluorescence spectrum, but since the main experimental thrust in the thesis is the probe absorption spectra, the fully quantum mechanical calculation for fluorescence has been performed in chapter 2 only. Here, the analysis is restricted to only the probe beam absorption spectra.

The first thing to understand before undertaking this calculation is that there are two separate regions that can be probed. An $\hat{\mathbf{x}}$ polarised probe beam, which drives transitions between the $|g\rangle$ state and the $|e\rangle$ state (the bare states), can examine the effect that doubly driving the system has on the probe absorption spectrum in the region about the original transition frequency ω_0. More interestingly however, as was shown in chapter 1, a $\hat{\mathbf{z}}$ polarised probe (which drives transitions between the *dressed states*) can be used to examine the Rabi

transition directly.

3.3 Probing the Rabi transition

It is possible to examine the probe absorption spectrum at the Rabi frequency in the doubly driven TLA. To perform this calculation, the doubly pumped results (Equations 3.16, 3.14) are used to calculate the solution to the first order in the probe field, Probe_z. The equations of motion for the doubly driven system, with a strong pump on the original transition, a strong pump driving the Rabi transition, and finally a weak probe in the region of the Rabi transition, are given by (in the rotating frame)

$$\begin{aligned}\frac{d}{dt}\tilde{\rho}_{ge} &= \left\{i\left(\delta_x + 2\chi_z\cos\omega_z t + 2\alpha\cos\omega_p t\right) - \Gamma\right\}\tilde{\rho}_{ge} - i\frac{\chi_x}{2}W \\ \dot{W} &= i\chi_x\left(\tilde{\rho}_{eg} - \tilde{\rho}_{ge}\right) - \Gamma\left(W - W^{eq}\right)\end{aligned}$$

where α is the (weak) probe Rabi frequency and ω_p is the probe frequency. Writing this equation out to first order in the probe power α

$$\frac{d}{dt}\tilde{\rho}_{ge}^{(1)} = \left\{i\left(\delta_x + 2\chi_z\cos\omega_z t\right) - \Gamma\right\}\tilde{\rho}_{ge}^{(1)} + 2i\alpha\cos\omega_p t\tilde{\rho}_{ge}^{(0)} - i\frac{\chi_x}{2}W^{(1)} \quad (3.22a)$$

$$\dot{W}^{(1)} = i\chi_x\left(\tilde{\rho}_{eg}^{(1)} - \tilde{\rho}_{ge}^{(1)}\right) - \Gamma W^{(1)} \quad (3.22b)$$

The equations (3.16, 3.14) are then employed as the zeroth order solution $\tilde{\rho}_{ge}^{(0)}$. To proceed, exactly the same procedure is applied. A transformation to the singly dressed basis is firstly applied, then to the rotating frame (applying the rotating wave approximation) and finally a transformation to the doubly dressed state basis is performed. Again, the higher order interactions of Field_z with the Rabi transition are ignored. The final form for equations (3.22*a*, 3.22*b*) after these transformations is given by

$$\dot{\rho}_{\alpha\beta}^{(1)} = \left(i\Omega_z - \Gamma\right)\rho_{\alpha\beta}^{(1)} + \alpha\cos\omega_p t\left(\rho_- e^{-i\omega_z t} + \rho_0 + \rho_+ e^{i\omega_z t}\right)$$

$$\begin{aligned}
\dot{\rho}^{(1)}_{\beta\alpha} &= (-i\Omega_z - \Gamma)\,\rho^{(1)}_{\alpha\beta} + \alpha\cos\omega_p t\left(\rho^{\star}_{-}e^{i\omega_z t} + \rho^{\star}_{0} + \rho^{\star}_{+}e^{-i\omega_z t}\right)\\
\dot{W}^{(1)}_{dd} &= -\Gamma W^{(1)}_{dd} + \alpha\cos\omega_p t\left(w_{-}e^{-i\omega_z t} + w_0 + w_{+}e^{i\omega_z t}\right)
\end{aligned}$$

where

$$\begin{aligned}
\rho_{-} &= i\sin 2\theta\left(\cos^2\phi W^{ss}_{dd} - \sin 2\phi\rho^{ss}_{\alpha\beta}\right)\\
\rho_{+} &= -i\sin 2\theta\left(\sin^2\phi W^{ss}_{dd} + \sin 2\phi\rho^{ss}_{\alpha\beta}\right)\\
\rho_{0} &= i\cos 2\theta\left(2\cos 2\phi\rho^{ss}_{\alpha\beta} + \sin 2\phi W^{ss}_{dd}\right)
\end{aligned}$$

and

$$\begin{aligned}
w_0 &= -2i\sin 2\phi\cos 2\theta\left(\rho^{ss}_{\beta\alpha} - \rho^{ss}_{\alpha\beta}\right)\\
w_{-} &= 2i\sin 2\theta\left(\rho^{ss}_{\alpha\beta}\cos^2\phi - \rho^{ss}_{\beta\alpha}\sin^2\phi\right)\\
w_{+} &= 2i\sin 2\theta\left(\rho^{ss}_{\alpha\beta}\sin^2\phi - \rho^{ss}_{\beta\alpha}\cos^2\phi\right)
\end{aligned}$$

recalling that these terms (e.g. ρ_{-}) are all time varying as well since they are all functions of the zeroth order solutions $\rho^{ss}_{\alpha\beta}$, $\rho^{ss}_{\beta\alpha}$ and W^{ss}_{dd}, given in Equations 3.14 and 3.16. That is, they can all be written in the form (for instance)

$$\rho_{-} = \sum_{k=-1}^{1}\rho^{k}_{-}e^{ik\omega_z t}$$

and so the final form for the solutions of the above equations would then be

$$\begin{aligned}
\rho^{(1)}_{\alpha\beta} &= \sum_{k=-1}^{1}\rho^{k,l}_{\alpha\beta}L\left(k\omega_z + l\omega_p - \Omega_z\right)\exp\left(ik\omega_z t\right)\exp\left(il\omega_p t\right)\\
\rho^{(1)}_{\beta\alpha} &= \sum_{k=-1}^{1}\rho^{k,l}_{\beta\alpha}L\left(k\omega_z + l\omega_p + \Omega_z\right)\exp\left(ik\omega_z t\right)\exp\left(il\omega_p t\right)
\end{aligned}$$

$$W_{dd}^{(1)} = \sum_{k=-1}^{1} w^{k,l} L\left(k\omega_z + l\omega_p\right) \exp\left(ik\omega_z t\right) \exp\left(il\omega_p t\right)$$

where

$$\begin{aligned}
\rho_{\alpha\beta}^{k,l} &= \frac{1}{2}\alpha\left(\rho_{-}^{k+1} + \rho_{0}^{k} + \rho_{+}^{k-1}\right) \\
\rho_{\beta\alpha}^{k,l} &= \left(\rho_{\alpha\beta}^{-k,-l}\right)^{\star} \\
w^{k,l} &= \frac{1}{2}\alpha\left(w_{-}^{k+1} + w_{0}^{k} + w_{+}^{k-1}\right)
\end{aligned}$$

Only the portion of the solution that is relevant to the probe absorption spectrum is presented. Therefore, only the bare state population terms need to be examined. These need to be written out in terms of the doubly dressed state solutions

$$\begin{aligned}
W^{0,1} = & -\sin 2\theta\left(\cos^2\phi\rho_{\alpha\beta}^{-1,1}L_{-1,1}^{-} - \sin^2\phi\rho_{\beta\alpha}^{-1,1}L_{-1,1}^{+} + \frac{1}{2}\sin 2\phi w^{-1,1}L_{-1,1}\right) \\
& -\sin 2\theta\left(-\sin^2\phi\rho_{\alpha\beta}^{1,1}L_{1,1}^{-} + \cos^2\phi\rho_{\beta\alpha}^{1,1}L_{1,1}^{+} + \frac{1}{2}\sin 2\phi w^{1,1}L_{1,1}\right) \\
& +\cos 2\theta\left(-2\cos\phi\sin\phi\left(\rho_{\alpha\beta}^{0,1}L_{0,1}^{-} + \rho_{\beta\alpha}^{0,1}L_{0,1}^{+}\right) + \sin 2\phi w^{0,1}L_{0,1}\right)
\end{aligned}$$

with the definitions for notational convenience

$$\begin{aligned}
L_{x,y}^{-} &= L\left(x\omega_z + y\omega_p - \Omega_z\right) \\
L_{x,y}^{+} &= L\left(x\omega_z + y\omega_p + \Omega_z\right) \\
L_{x,y} &= L\left(x\omega_z + y\omega_p\right)
\end{aligned}$$

The solution is then a series of nine Lorentzians, with linewidths Γ, and weights given in the following table:

Lorentzian	Weight
$L(\omega_p - \omega_z - \Omega_z)$	$-\sin 2\theta \cos^2 \phi \rho_{\alpha\beta}^{-1,1}$
$L(\omega_p - \omega_z + \Omega_z)$	$\sin 2\theta \sin^2 \phi \rho_{\beta\alpha}^{-1,1}$
$L(\omega_p - \omega_z)$	$-\frac{1}{2} \sin 2\theta \sin 2\phi w^{-1,1}$
$L(\omega_p + \omega_z - \Omega_z)$	$\sin 2\theta \sin^2 \phi \rho_{\alpha\beta}^{1,1}$
$L(\omega_p + \omega_z + \Omega_z)$	$-\sin 2\theta \cos^2 \phi \rho_{\beta\alpha}^{1,1}$
$L(\omega_p + \omega_z)$	$-\frac{1}{2} \sin 2\theta \sin 2\phi w^{1,1}$
$L(\omega_p - \Omega_z)$	$-\cos 2\theta \sin 2\phi \rho_{\alpha\beta}^{0,1}$
$L(\omega_p + \Omega_z)$	$-\cos 2\theta \sin 2\phi \rho_{\beta\alpha}^{0,1}$
$L(\omega_p)$	$\cos 2\theta \cos 2\phi w^{0,1}$

Clearly then, the Rabi transition is split by the applied field, resulting in a Mollow type spectrum, with peaks at $\omega_z, \omega_z \pm \Omega_z$. Note also that the Rabi of the Rabi transition $L(\omega_p - \Omega_z)$ is present, and is probed by Probe$_z$ also. The interaction of the pump Field$_z$ with this transition was ignored in the analysis, however the transition itself still appears since the probe beam, of course, interacts with it also.

Further, notice that there is also a peak at $\omega_p = 0$. This is not surprising, since when the probe beam approaches 0 frequency, it will behave in the same way that a static field behaves on the bare state (i.e.. it will change, slightly, the original transition frequency ω_0). This Lorentzian is to be expected, but will not be of much interest here.

The full form of these weights (which are quite complicated) are given in the Appendix. To further understand the dynamics of the situation, several simplifying approximations can be made under some particular circumstances, listed below.

3.3.1 Field$_x$ on resonance case

Previously, it was seen that driving the initial transition on-resonance (i.e. $\delta_x = 0$) quenched the Rabi resonance, since the populations in the upper and lower dressed states equalised. It is to be expected then that driving this "hidden" transition would not produce any probe absorption spectra around the Rabi transition. This is indeed the case. Noting that $\rho_{\alpha\beta}^{eq}, W_{dd}^{eq}, \rho_0, w_0 = 0$

in this limit, then all of the weights of the above Lorentzians reduce to zero, as expected. The Rabi transition behaves like a TLA with a steady state population difference of zero and the net absorption of the probe beam is zero.

3.3.2 Field$_z$ on resonance case

Examining this circumstance ($\delta_z = 0$), the results in tabular format are

Lorentzian	Weight
$L(\omega_p - \omega_z - \Omega_z)$	$\alpha' \left(\tilde{\rho}^{eq}_{\alpha\beta} L(-\Omega_z) - \tilde{\rho}^{eq}_{12} L(-\Omega_x)\right)$
$L(\omega_p - \omega_z + \Omega_z)$	$\alpha' \left(\tilde{\rho}^{eq}_{\alpha\beta} L(\Omega_z) - \tilde{\rho}^{eq}_{12} L(-\Omega_x)\right)$
$L(\omega_p - \omega_z)$	$\alpha' \left(2\tilde{\rho}^{eq}_{\alpha\beta} L_A(\Omega_z) - \tilde{\rho}^{eq}_{12} (L(-\Omega_x + \Omega_z) + L(-\Omega_x - \Omega_z))\right)$
$L(\omega_p - \Omega_z)$	$-\alpha' \tilde{\rho}^{eq}_{12} (-2iL_D(\Omega_x) + L(\Omega_x - \Omega_z) - L(-\Omega_x - \Omega_z))$
$L(\omega_p)$	0

where the results have been defined in terms of the dressed state and doubly dressed state equilibrium coherences ρ^{eq}_{12} and $\rho^{eq}_{\alpha\beta}$. Also the following definitions have been employed;

$$\begin{aligned} \alpha' &= \frac{1}{4} i\alpha \sin 2\theta, \tilde{\rho}^{eq}_{12} \\ \tilde{\rho}^{eq}_{12} &= \cos 2\theta \rho^{eq}_{12} \\ \tilde{\rho}^{eq}_{\alpha\beta} &= \sin 2\theta \rho^{eq}_{\alpha\beta} \end{aligned}$$

A typical example is shown in figure 3-1. This demonstrates some of the surprising differences between the split Rabi case and the standard Mollow spectrum. Firstly, notice that the sidebands at $\omega_z \pm \Omega_z$ are asymmetric because of the term $\cos 2\theta \rho^{eq}_{12} L(-\Omega_x)$, whereas in the standard Mollow case these are symmetric peaks. This highlights a difference between the two systems. In the Mollow case, the bare TLA that is driven has no equilibrium coherence (only an equilibrium population) - however in the Rabi case Field$_z$ acts on a system with an equilibrium coherence, notated ρ^{eq}_{12}. Furthermore, the Rabi of the Rabi transition, produced in entirely analogous fashion to the Rabi transition, is visible despite the fact that the doubly dressed state populations are equalized. Recall that the Rabi transition is not visible in the case where

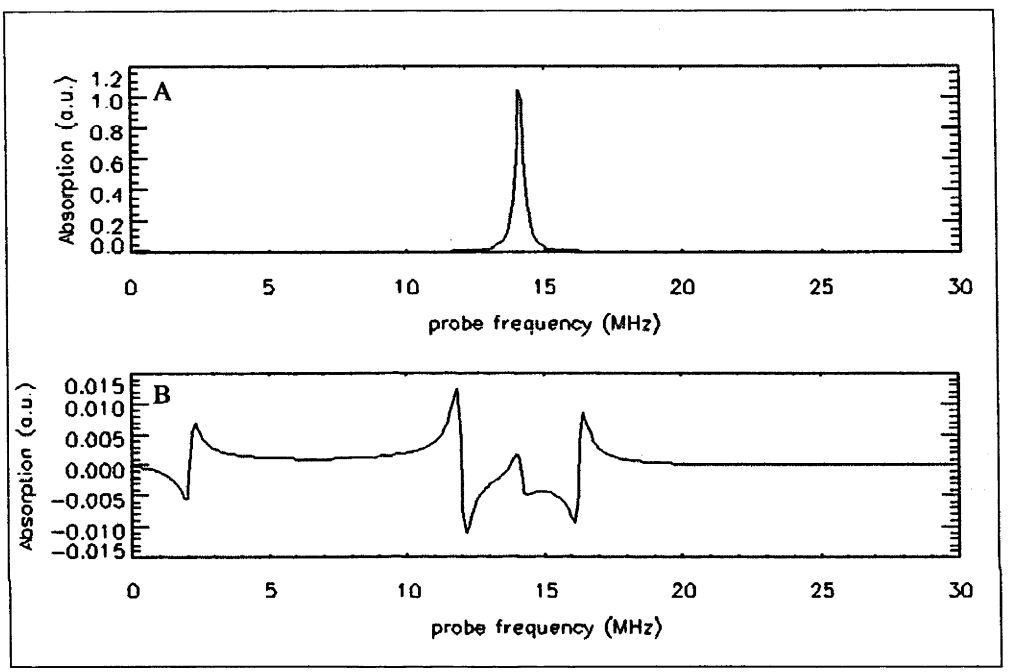

Figure 3-1: the Rabi transition with δ_x=10 MHz, χ_x=10 MHz which is then driven on resonance by Field$_z$ where χ_z=3 MHz. (A) is the undriven Rabi transition, (B) is the driven case.

Field$_x$ is on resonance, since the populations in the singly dressed states are equalized.

These features deserve extra attention. The standard Mollow situation sees a TLA driven by Field$_x$. Two observations relevant to these discussions are that;

1. the basic (undressed) TLA has an equilibrium population difference W^{eq}
2. the basic TLA *has no* equilibrium coherence (i.e. $\rho_{ge}^{eq} = 0$)

Now, once the TLA has been dressed by Field$_x$, then a new TLA is produced, with resonance centred at the Rabi frequency. Making analogous observations about this system,

1. the dressed 'Rabi' TLA (call it TLA$_R$) has an equilibrium population difference given by $W_d^{eq} = \cos 2\theta W^{eq}$
2. TLA$_R$ now has an equilibrium coherence $\rho_{12}^{eq} = -\frac{1}{2}\sin 2\theta \Gamma W^{eq}$

This is the key difference between the standard Mollow and the TLA$_R$ systems. Notice that the surprising features in the above spectrum, the asymmetry in the sidebands and the appearance of the Rabi of the Rabi transition, are both features proportional to ρ_{12}^{eq}. The equilibrium coherence in TLA$_R$ clearly allows for new interactions that manifest themselves as these features after transforming to the doubly dressed states. In fact, if ρ_{12}^{eq} is imagined to equal zero, then the analogue of the original Mollow spectrum is recovered. To see this, compare the results of the standard on resonance Mollow spectrum;

Mollow Lorentzian	**Weight**
$L(\omega_p - \omega_x - \Omega_x)$	$\frac{1}{4}i\alpha\rho_{12}^{eq}L(-\Omega_x)$
$L(\omega_p - \omega_x + \Omega_x)$	$\frac{1}{4}i\alpha\rho_{12}^{eq}L(\Omega_x)$
$L(\omega_p - \omega_x)$	$i\frac{1}{2}\alpha\rho_{12}^{eq}L_A(\Omega_x)$

with the results from above with the only change being that ρ_{12}^{eq} is set to zero, and $\sin 2\theta = 1$ (the on resonance Mollow case);

Rabi Lorentzian	Weight
$L(\omega_p - \omega_z - \Omega_z)$	$\frac{1}{4} i\alpha\rho^{eq}_{\alpha\beta} L(-\Omega_z)$
$L(\omega_p - \omega_z + \Omega_z)$	$\frac{1}{4} i\alpha\rho^{eq}_{\alpha\beta} L(\Omega_z)$
$L(\omega_p - \omega_z)$	$i\frac{1}{2}\alpha\rho^{eq}_{\alpha\beta} L_A(\Omega_z)$
$L(\omega_p - \Omega_z)$	0
$L(\omega_p)$	0

Clearly this demonstrates that it is indeed equilibrium coherence in TLA_R that is the cause of the extra interactions that give rise to the modified spectrum. The interactions come from the mixing of the singly dressed atom states caused by this coherence, which allows weak interactions not demonstrated in the basic Mollow case. Examine the peak centered at $\omega_p = \omega_z + \Omega_z$ which, borrowing the notation of the fully quantum mechanical case for the sake of clarity, is equivalent to the transitions between $|2, n, m\rangle$ and $|1, n, m-1\rangle$. Note that the 'anomalous' interaction giving rise to the asymmetry in the sidebands is proportional to $L(-\Omega_x)$. Examining the case of well separated peaks (i.e. $\omega_z \gg \Omega_z \gg \Gamma$) it is possible to approximate this

$$L(-\Omega_x) \simeq -iL_D(-\Omega_x) \sim i\frac{1}{\Omega_x}$$

whereas the 'normal' (Mollow-like) term is proportional to

$$L(-\Omega_z) \sim i\frac{1}{\Omega_z}$$

and so it is expected that the 'anomalous' term is significantly smaller than the normal one. To reiterate, the normal term is due to mixing between the doubly dressed states, attributable to the doubly dressed state steady state coherence $\rho^{eq}_{\alpha\beta}$. This mixing occurs in the standard Mollow spectrum. However, TLA_R, conceptually analogous to the bare state transition in the standard Mollow circumstance, displays an equilibrium coherence of ρ^{eq}_{12}. This introduces the asymmetry since there are *unequal* populations in the singly dressed states. If the original

Field$_x$ were on resonance, then all of the $cos2\theta\rho_{12}^{eq}$ terms disappear (as indeed does the entire spectrum) which effectively removes the asymmetry.

3.3.3 High Power Case

When probing the undriven Rabi transition with a weak probe, the spectrum was considerably simplified if the high power limit (similar to the secular approximation in the previous chapter) was taken. In this limit, $\omega_z \gg \Omega_z \gg \Gamma$. The limit assumes that the Lorentzians are well separated. This is still a useful limit to take in this case to at least get some sense of the off resonance dynamics. Note that this approximation is only taken for the off resonance case. As before, note that in the high power limit the zeroth order solutions become

$$\begin{aligned}
\rho_{\alpha\beta}^{0} &= -\rho_{\alpha\beta}^{eq} L\left(-\Omega_z\right) \approx -i\rho_{\alpha\beta}^{eq} L_D\left(\Omega_z\right) \\
\rho_{\alpha\beta}^{-1} &= -P_{-} L\left(-\omega_z - \Omega_z\right) \approx -iP_{-} L_D\left(\omega_z\right) \\
\rho_{\alpha\beta}^{1} &= P_{+} L\left(\omega_z - \Omega_z\right) \approx -iP_{+} L_D\left(\omega_z\right)
\end{aligned}$$

and for the population terms

$$\begin{aligned}
w^{0} &= W_{dd}^{eq} \\
w^{1} &= w^{+} L\left(\omega_z\right) \approx -iw^{+} L_D\left(\omega_z\right) \\
w^{-1} &= w^{+} L\left(-\omega_z\right) \approx iw^{+} L_D\left(\omega_z\right)
\end{aligned}$$

Noting that in general $\rho_{\alpha\beta}^{0} L_D\left(\Omega_z\right) \ll W_{dd}^{eq}$ as $\rho_{\alpha\beta}^{0} L_D\left(\Omega_z\right) \propto \frac{\Gamma}{\Omega_z}$, then looking at one of the terms as an example

$$\begin{aligned}
\rho_{-}^{0} &= i \sin 2\theta \left(\cos^2\phi W_{dd}^{eq} + i \sin 2\phi \rho_{\alpha\beta}^{eq} L_2\left(\Omega_z\right)\right) \\
&\approx i \sin 2\theta \cos^2\phi W_{dd}^{eq}
\end{aligned}$$

and

$$\rho_{-}^{-1} = -\sin 2\theta L_D(\omega_z)\left(\cos^2\phi w^{+} + \sin 2\phi P_{-}\right)$$

As $\rho_{-}^{-1} \propto L_D(\omega_z)$, a small number, then $\rho_{-}^{0} \gg \rho_{-}^{-1}$. This sort of argument, when used with the remainder of the terms, considerably simplifies the weights of the Lorentzians. The new weights (for the experimental peaks i.e. $\omega_p > 0$) are then given in the table below;

Lorentzian	**Weight**
$L(\omega_p - \omega_z - \Omega_z)$	$-i\alpha\Delta W_{dd}^{eq}\cos^4\phi$
$L(\omega_p - \omega_z + \Omega_z)$	$i\alpha\Delta W_{dd}^{eq}\sin^4\phi$
$L(\omega_p - \omega_z)$	$\frac{1}{2}\alpha\sin^2 2\theta\Delta'\rho_{\alpha\beta}^{eq}L_D(\Omega_z)$
$L(\omega_p - \Omega_z)$	$-\frac{1}{2}i\alpha\cos^2 2\theta\sin^2 2\phi W_{dd}^{eq}$
$L(\omega_p)$	$-2\alpha\cos^2 2\theta\Delta'\rho_{\alpha\beta}^{eq}L_D(\Omega_z)$

where

$$\begin{aligned}\Delta &= \frac{1}{2}\sin^2 2\theta \\ \Delta' &= \cos 2\phi \sin 2\phi\end{aligned}$$

The absorption and dispersion are given as

$$\begin{aligned}A &= Abs \propto \Im W^{0,1} \\ D &= Disp \propto \Re W^{0,1}\end{aligned}$$

In interpreting these results, it is useful to bear in mind the simple rule that *if the weight of the Lorentzian is real, then the absorption spectrum will be dispersive in nature*, since the absorption spectrum is proportional to the imaginary part of a general Lorentzian (of form $L(x) = L_A(x) - iL_D(x)$) times a real weight. Looking at the experimental peaks

Peak	Absorption
$\omega_p = \omega_z + \Omega_z$	$-\alpha\Delta \cos^4\phi W_{dd}^{eq} L_A(\omega_p - \omega_z - \Omega_z)$
$\omega_p = \omega_z - \Omega_z$	$\alpha\Delta \sin^4\phi W_{dd}^{eq} L_A(\omega_p - \omega_z + \Omega_z)$
$\omega_p = \omega_z$	$-\frac{1}{2}\alpha \sin^2 2\theta\Delta' L_D(\Omega_z)\rho_{\alpha\beta}^{eq} L_D(\omega_p - \omega_z)$
$\omega_p = \Omega_z$	$-\frac{1}{2}\alpha \cos^2 2\theta \sin^2 2\phi W_{dd}^{eq} L_A(\omega_p - \Omega_z)$
$\omega_p = 0$	$2\alpha \cos^2 2\theta\Delta' L_D(\Omega_z)\rho_{\alpha\beta}^{eq} L_D(\omega_p)$

and for the dispersion spectrum

Peak	Dispersion
$\omega_p = \omega_z + \Omega_z$	$-\alpha\Delta \cos^4\phi W_{dd}^{eq} L_D(\omega_p - \omega_z - \Omega_z)$
$\omega_p = \omega_z - \Omega_z$	$\alpha\Delta \sin^4\phi W_{dd}^{eq} L_D(\omega_p - \omega_z + \Omega_z)$
$\omega_p = \omega_z$	$\frac{1}{2}\alpha \sin^2 2\theta\Delta' L_D(\Omega_z)\rho_{\alpha\beta}^{eq} L_A(\omega_p - \omega_z)$
$\omega_p = \Omega_z$	$-\frac{1}{2}\alpha \cos^2 2\theta \sin^2 2\phi W_{dd}^{eq} L_D(\omega_p - \Omega_z)$
$\omega_p = 0$	$-2\alpha \cos^2 2\theta\Delta'\rho_{\alpha\beta}^{eq} L_A(\Omega_z) L_A(\omega_p)$

There are four major peaks (as well as a minor one at $\omega_p = 0$), centred at the Rabi of the Rabi ($\omega_p = \Omega_z$), at the driving frequency ($\omega_p = \omega_z$) and at two Mollow-like sidebands ($\omega_p = \omega_z \pm \Omega_z$). Looking at the general form of these weights, it is obvious that the peak at $\omega_p = \omega_z$ is very much smaller than the other peaks, since it is proportional to $L_D(\Omega_z)$. The signs of the Mollow sidebands are worth examining because $\Delta \propto W_{dd}^{eq} = \cos 2\theta \cos 2\phi W^{eq}$, these obviously have opposite sign always, just as in the case for the standard Mollow spectrum. Further, if Field$_x$ is negatively detuned (i.e. $\delta_x < 0$), then there is more population in the $|2\rangle$ singly dressed state (the higher energy state): there is a *population inversion* in the dressed states. When a weak probe examines the Rabi transition, then it will be *emissive* in nature. If Field$_z$ is then applied, and is negatively detuned, $\delta_z < 0$, then the situation is reversed (since in this Rabi transition, the steady state population is now positive), and there will be more population in the doubly dressed $|\alpha\rangle$ state. It is expected in this case then, that the transition from $|\beta\rangle$ to $|\alpha\rangle$, characterised by the Mollow peak at $\omega_p = \omega_z + \Omega_z$, will be absorptive in

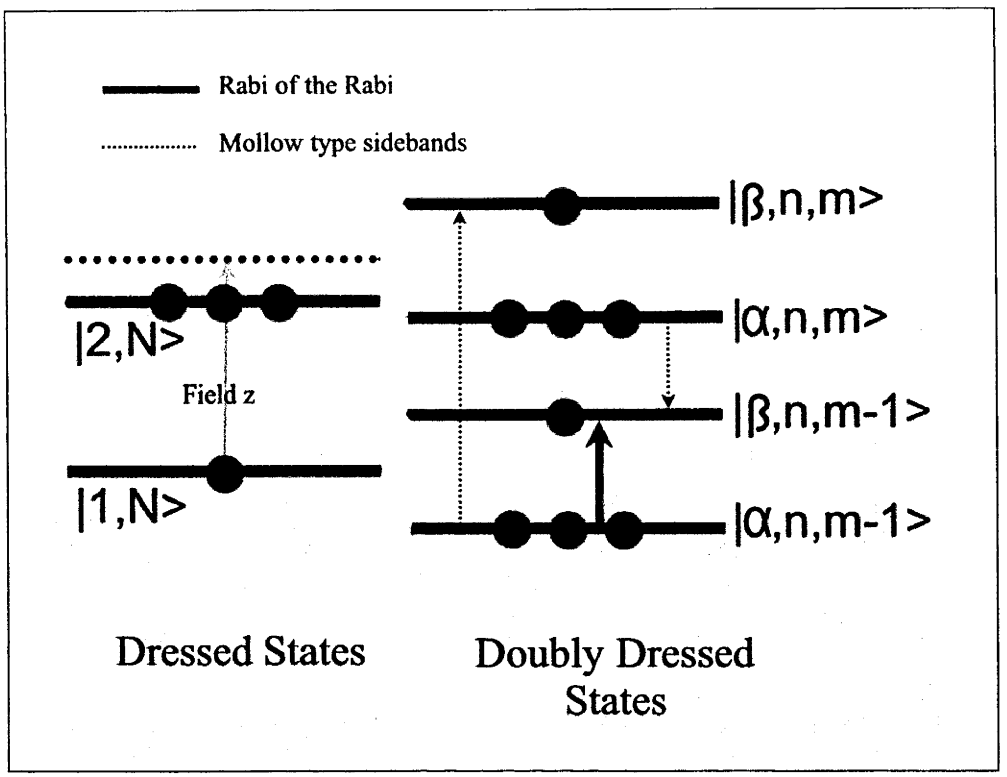

Figure 3-2: The energy level scheme where Field_x and Field_z are both negatively detuned. The circles represent the populations in the levels, and the transitions for the major peaks are shown, with the arrows indicating whether the transition is absorptive (up) or emissive (down) in nature. The fully quantum mechanical notation is used here for pedagogical clarity.

nature, which is indeed the case ($W_{dd}^{eq} < 0$). It would also be expected that the Rabi of the Rabi transition would likewise be absorptive, which again holds true. It can be seen that these peak positions and signs follow from a very simple analysis, and the resultant behaviour in this simplified case is exactly as predicted (see Fig 3-2)

It is worthwhile, once again, comparing these results to those of the standard Mollow spectrum in the high power limit. The Mollow spectrum has the following form in the high power limit (recalling that W_d^{eq} is the steady state singly dressed state population difference):

Lorentzian	Weight
$L(\delta_p - \Omega_x)$	$-i\frac{\alpha}{2}\cos^4\theta W_d^{eq}$
$L(\delta_p + \Omega_x)$	$i\frac{\alpha}{2}\sin^4\theta W_d^{eq}$
$L(\delta_p)$	$\frac{1}{2}\alpha\sin 2\theta\cos 2\theta\rho_{12}^{eq}L_D(\Omega_x)$

which is clearly entirely analogous to the above results. It is plain then that the split Rabi spectrum behaves in an entirely analogous fashion with the standard Mollow spectrum, and can be understood in the same terms. The only differences, then, are the transition at the Rabi of the Rabi, and the transition at 0 frequency. In these broad terms, as allowed in this high power approximation, the split Rabi spectrum behaves in exactly the same fashion as the standard Mollow spectrum. Note that as part of this approximation, the terms that are proportional to the 'anomalous' ρ_{12}^{eq} have all been dropped. These terms will change the situation somewhat, but since they are all proportional to $L(\omega_z)$ then it is expected that these modifications will be slight, as in the on resonance case mentioned above. Some examples of the interactions are shown in figure (3-3)

3.4 Probing the original transition

As seen above, the Rabi transition can be seen to undergo a Mollow split like any normal driven TLA, with the Rabi of the Rabi transition emerging, and so on. It is also, of course, possible to delve into the other regime, the probe absorption spectrum at the original transition, the doubly driven Mollow spectrum. The Bloch equations with the Probe$_x$ included are as follows

$$\begin{aligned}\frac{d}{dt}\tilde{\rho}_{ge} &= \{i(\delta_x + 2\chi_z\cos\omega_z t) - \Gamma\}\tilde{\rho}_{ge} - i\frac{\chi_x}{2}W - i\frac{\alpha}{2}We^{i\delta_p t}\\ \dot{W} &= i\chi_x(\tilde{\rho}_{eg} - \tilde{\rho}_{ge}) - i\alpha\left(\tilde{\rho}_{eg}e^{i\delta_p t} - \tilde{\rho}_{ge}e^{-i\delta_p t}\right) - \Gamma(W - W^{eq})\end{aligned}$$

where the probe field detuning δ_p is given by

$$\delta_p = \omega_p - \omega_x$$

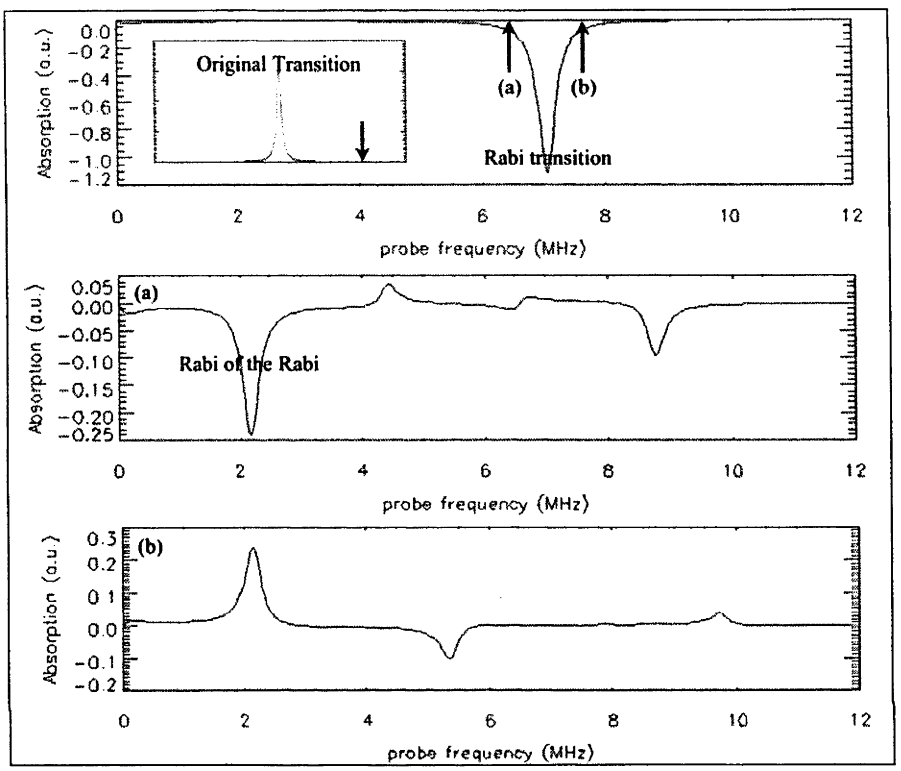

Figure 3-3: Off resonance driving of the Rabi transition. Initial (bare) state transition is shown in the inset, with an arrow indicating the position of Field$_x$ ($\delta_x = -5$ MHz, $\chi_x = 5$ MHz). Rabi transition is then emissive under these circumstances. The arrows show the position of Field$_z$ ($\delta_z = \pm 0.5$ MHz, $\chi_z = 3$ MHz) in the bottom graphs (a) and (b). Note that graph (b) shows the spectrum discussed in the energy level diagram shown above. Note that the Rabi of the Rabi is at $\Omega_z = \sqrt{\delta_z^2 + (\sin 2\theta \chi_z)^2}$ hence it appears to be lower than 3 MHz.

The procedure is exactly the same as above so only the results are shown. The final equations of motion of the coherence in the doubly dressed state basis are given by

$$\frac{d}{dt}\rho_{\alpha\beta}^{(1)} = \left(i\Omega_z - \Gamma\right)\rho_{\alpha\beta}^{(1)} + \sum_{k,l=-1}^{1} \gamma_{k,l} e^{ik\delta_p t} e^{i\omega_z t}$$

where

$$\begin{aligned}
\gamma_{-1,-1} &= -i\frac{\alpha}{2}\sin^2\theta A \\
\gamma_{-1,0} &= i\frac{\alpha}{2}\sin 2\theta C \\
\gamma_{-1,1} &= i\frac{\alpha}{2}\cos^2\theta B \\
\gamma_{1,-1} &= i\frac{\alpha}{2}\cos^2\theta A \\
\gamma_{1,0} &= i\frac{\alpha}{2}\sin 2\theta C \\
\gamma_{1,1} &= -i\frac{\alpha}{2}\sin^2\theta B \\
\gamma_{0,x} &= 0 \qquad x = -1, 0, 1
\end{aligned}$$

where

$$\begin{aligned}
A &= \sin 2\phi\rho_{\alpha\beta}^{ss} - \cos^2\phi W_{dd}^{ss} \\
B &= \sin 2\phi\rho_{\alpha\beta}^{ss} + \sin^2\phi W_{dd}^{ss} \\
C &= \cos 2\phi\rho_{\alpha\beta}^{ss} + \frac{1}{2}\sin 2\phi W_{dd}^{ss}
\end{aligned}$$

Now for the population terms

$$\dot{W}_{dd}^{(1)} = -\Gamma W_{dd}^{(1)} + \sum \mu_{k,l} e^{ik\delta_p t} e^{il\omega_z t}$$

where

$$
\begin{aligned}
\mu_{-1,-1} &= -i\alpha \sin^2\theta D \\
\mu_{-1,0} &= -i\frac{\alpha}{2} \sin 2\theta \sin 2\phi E \\
\mu_{-1,1} &= -i\alpha \cos^2\theta D^\star \\
\mu_{1,-1} &= i\alpha \cos^2\theta D \\
\mu_{1,0} &= -i\frac{\alpha}{2} \sin 2\theta \sin 2\phi E \\
\mu_{1,1} &= -i\alpha \sin^2\theta D^\star
\end{aligned}
$$

where

$$
\begin{aligned}
D &= \cos^2\phi \rho^{ss}_{\beta\alpha} + \sin^2\phi \rho^{ss}_{\alpha\beta} \\
E &= \rho^{ss}_{\beta\alpha} - \rho^{ss}_{\alpha\beta}
\end{aligned}
$$

Each of the coefficients $A, B...E$ are further subdivided into 3 rotating terms since they contain the zeroth order solutions, giving for example,

$$
A^1 = \sin 2\phi \rho^1_{\alpha\beta} - \cos^2\phi w^1
$$

and each component above is broken down into (for example)

$$
\mu_{-1,0} = \mu^{-1}_{-1,0} e^{-i\omega_z t} + \mu^0_{-1,0} + \mu^1_{-1,1} e^{i\omega_z t}
$$

The final form of the equations of motion are then

$$
\begin{aligned}
\frac{d}{dt}\rho^{(1)}_{\alpha\beta} &= (i\Omega_z - \Gamma)\rho^{(1)}_{\alpha\beta} + \sum \rho^{k,l}_{\alpha\beta} e^{ik\delta_p t} e^{il\omega_z t} \\
\dot{W}^{(1)}_{dd} &= -\Gamma W^{(1)}_{dd} + \sum w^{k,l} e^{ik\delta_p t} e^{il\omega_z t}
\end{aligned}
$$

where

$$\begin{aligned}
\rho_{\alpha\beta}^{k,l} &= \gamma_{k,l-1}^{1} + \gamma_{k,l}^{0} + \gamma_{k,l+1}^{-1} \\
w^{k,l} &= \mu_{k,l-1}^{1} + \mu_{k,l}^{0} + \mu_{k,l+1}^{-1}
\end{aligned}$$

Finally, the term ρ_{ge} rotating at the probe beam detuning δ_p (the probe absorption spectrum) is,

$$\begin{aligned}
\rho_{ge}^{1,0} &= \cos^2\theta\left(\cos^2\phi\rho_{\alpha\beta}^{1,-1}L_{1,-1}^{-} - \sin^2\phi\rho_{\beta\alpha}^{1,-1}L_{1,-1}^{+} + \cos\phi\sin\phi w^{1,-1}L_{1,-1}\right) \\
&\quad - \sin^2\theta\left(-\sin^2\phi\rho_{\alpha\beta}^{1,1}L_{1,1}^{-} + \cos^2\phi\rho_{\beta\alpha}^{1,1}L_{1,1}^{+} + \cos\phi\sin\phi w^{1,1}L_{1,1}\right) \\
&\quad + \cos\theta\sin\theta\left(-2\cos\phi\sin\phi\left(\rho_{\alpha\beta}^{1,0}L_{1,0}^{-} + \rho_{\beta\alpha}^{1,0}L_{1,0}^{+}\right) + \left(\cos^2\phi - \sin^2\phi\right)w^{1,0}L_{1,0}\right)
\end{aligned}$$

Once again with the Lorentzian notations employed

$$\begin{aligned}
L_{k,l}^{\pm} &= L\left(k\delta_p + l\omega_z \pm \Omega_z\right) \\
L_{k,l} &= L\left(k\delta_p + l\omega_z\right)
\end{aligned}$$

The result is a series of Lorentzians in the final solution for $\rho_{ge}^{1,0}$

Lorentzian	**Weight**
$L\left(\delta_p - \omega_z - \Omega_z\right)$	$\cos^2\theta\cos^2\phi\rho_{\alpha\beta}^{1,-1}$
$L\left(\delta_p - \omega_z + \Omega_z\right)$	$-\cos^2\theta\sin^2\phi\rho_{\beta\alpha}^{1,-1}$
$L\left(\delta_p - \omega_z\right)$	$\cos^2\theta\cos\phi\sin\phi w^{1,-1}$
$L\left(\delta_p + \omega_z - \Omega_z\right)$	$\sin^2\theta\sin^2\phi\rho_{\alpha\beta}^{1,1}$
$L\left(\delta_p + \omega_z + \Omega_z\right)$	$-\sin^2\theta\cos^2\phi\rho_{\beta\alpha}^{1,1}$
$L\left(\delta_p + \omega_z\right)$	$-\sin^2\theta\cos\phi\sin\phi w^{1,1}$
$L\left(\delta_p - \Omega_z\right)$	$-2\cos\theta\sin\theta\cos\phi\sin\phi\rho_{\alpha\beta}^{1,0}$
$L\left(\delta_p + \Omega_z\right)$	$-2\cos\theta\sin\theta\cos\phi\sin\phi\rho_{\beta\alpha}^{1,0}$
$L\left(\delta_p\right)$	$\cos\theta\sin\theta\left(\cos^2\phi - \sin^2\phi\right)w^{1,0}$

The original Mollow Lorentzians $L(\delta_p \pm \Omega_x)$, $L(\delta_p)$ are each split into a triplet by the action of the driving field on the Rabi transition. Once again, it is possible to examine a few specific scenarios to simplify the above coefficients, which are quite complicated (for the full form of the coefficients, see the appendix).

3.4.1 High power case (off-resonance)

To understand the general dynamics of the situation, it is possible to resort to the off resonant high power case. Explicitly then, in this case, the weights of the various Lorentzians become

Lorentzian	**Weight**
$L(\delta_p - \omega_z - \Omega_z)$	$-i\frac{\alpha}{2}\cos^4\theta\cos^4\phi W_{dd}^{eq}$
$L(\delta_p - \omega_z + \Omega_z)$	$i\frac{\alpha}{2}\cos^4\theta\sin^4\phi W_{dd}^{eq}$
$L(\delta_p - \omega_z)$	$-\frac{\alpha}{4}\sin 2\phi\cos^2\theta\rho_{12}^{eq}L_D(\omega_z)\nu$
$L(\delta_p + \omega_z - \Omega_z)$	$-i\frac{\alpha}{2}\sin^4\theta\sin^4\phi W_{dd}^{eq}$
$L(\delta_p + \omega_z + \Omega_z)$	$i\frac{\alpha}{2}\sin^4\theta\cos^4\phi W_{dd}^{eq}$
$L(\delta_p + \omega_z)$	$\frac{\alpha}{4}\sin 2\phi\sin^2\theta\rho_{12}^{eq}L_D(\omega_z)\nu'$
$L(\delta_p - \Omega_z)$	$-i\frac{\alpha}{8}\sin^2 2\theta\sin^2 2\phi W_{dd}^{eq}$
$L(\delta_p + \Omega_z)$	$i\frac{\alpha}{8}\sin^2 2\theta\sin^2 2\phi W_{dd}^{eq}$
$L(\delta_p)$	$-\frac{1}{2}\alpha\sin^2 2\theta\cos 2\phi\sin 2\phi\rho_{\alpha\beta}^{eq}L_D(\Omega_z)$

with the coefficient definitions

$$\begin{aligned}\nu &= \sin 2\theta\sin 2\phi - 2\cos^2\theta\cos 2\phi \\ \nu' &= \sin 2\theta\sin 2\phi + 2\sin^2\theta\cos 2\phi\end{aligned}$$

To gain an understanding of what is happening here, compare once again with the singly driven Mollow spectrum in the same limit

Lorentzian	Weight
$L(\delta_p - \Omega_x)$	$-i\frac{\alpha}{2}\cos^4\theta W_d^{eq}$
$L(\delta_p + \Omega_x)$	$i\frac{\alpha}{2}\sin^4\theta W_d^{eq}$
$L(\delta_p)$	$\frac{1}{2}\alpha\sin 2\theta\cos 2\theta\rho_{12}^{eq}L_D(\Omega_x)$

It is clear that, again the form of the equations are quite analogous. Consider the Mollow peak at $\delta_p = -\Omega_x$. Its weight is given by $i\frac{\alpha}{2}\sin^4\theta W_d^{eq} = W_{Mollow}W_d^{eq}$. When Field$_z$ is applied to the Rabi transition, the peak is split into 3 peaks. The new sidebands at $\delta_p = -\omega_z + \Omega_z$ and $\delta_p = -\omega_z - \Omega_z$ have weights $-W_{Mollow}\sin^4\phi W_{dd}^{eq}$ and $W_{Mollow}\cos^4\phi W_{dd}^{eq}$ respectively. There is also a (small) peak at $\delta_p = \omega_z$. So in the absorption case, the single Mollow peak of form $L_A(\delta_p + \Omega_x)$ is split into two oppositely signed absorptive type peaks of form $L_A(\delta_p + \omega_z - \Omega_z)$ and $L_A(\delta_p + \omega_z + \Omega_z)$. These transitions correspond to transitions between the quantum mechanical dressed states of $|\beta, n, m-1\rangle \rightarrow |\alpha, n-1, m\rangle$ and $|\alpha, n, m-1\rangle \rightarrow |\beta, n-1, m\rangle$ respectively (see fig 3-4). Likewise for the low frequency Mollow sideband at $\delta_p = \Omega_x$.

More interesting structure is apparent when the central (small) Mollow peak is examined. The peak at $\delta_p = 0$ also splits, but whereas in the singly driven case the central peak is very small (being due to coherent mixing between the dressed states ρ_{12}^{eq}) the two sidebands that arise from the application of Field$_z$ are significant in size. The peaks, at $\delta_p = \pm\Omega_z$ are oppositely signed and have the same weight. They are due to transitions between (again in the fully quantum mechanical case) $|\alpha, n, m\rangle \leftrightarrow |\beta, n-1, m\rangle$ states and $|\beta, n, m\rangle \leftrightarrow |\alpha, n-1, m\rangle$. There is still a small central peak due to the coherence term once again. The essentials dynamics of the situation are demonstrated in Fig 3-5

3.4.2 Field$_x$ on resonance

In this case, $\delta_x = 0$, the explicit form of the above coefficients is given by (again in the high power limit as above)

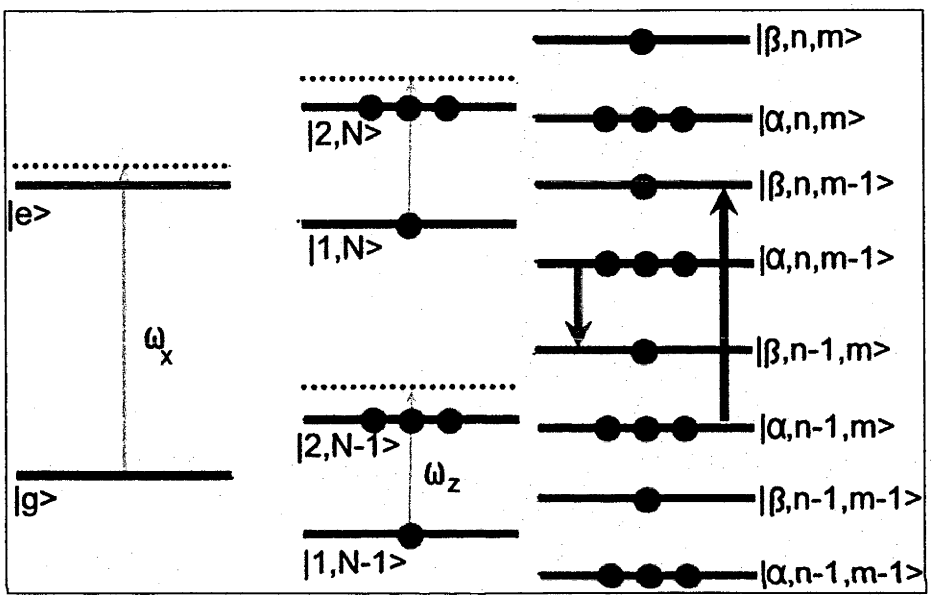

Figure 3-4: The transitions that give rise to the peaks at $L(\delta_p + \omega_z - \Omega_z)$ (blue) and $L(\delta_p + \omega_z + \Omega_z)$ (red). The populations of the levels are represented by the number of circles, the direction of the arrow specifies whether the resultant transition is absorptive (up) or emmissive (down). The quantum mechanical notation here is used for pedagogical clarity.

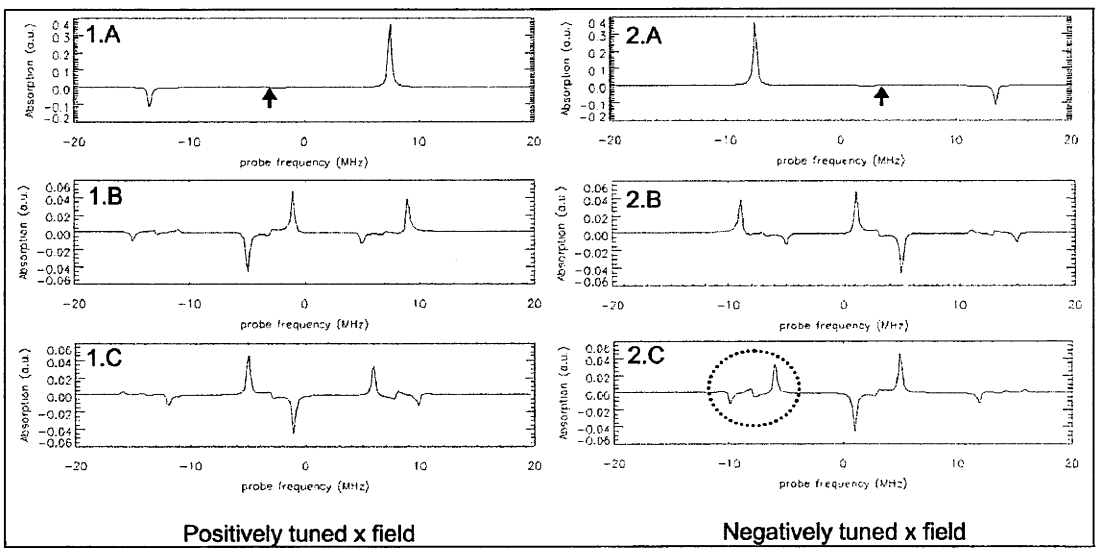

Figure 3-5: Off-resonance spectrum. On the left, the graphs show the probe absorption spectrum with a positively detuned x pump (ie. $\delta_x > 0$) and on the right Field$_x$ is negatively detuned. (1.A): no Field$_z$ - the standard Mollow spectrum with $\delta_x = 3$ MHz, $\chi_x = 10$ MHz. (1.B): Field$_z$ applied with $\delta_z = 0.5$ MHz, $\chi_z = 2$ MHz. (1.C): Field$_z$ applied with $\delta_z = -0.5$ MHz, $\chi_z = 2$ MHz. (2.A): no Field$_z$ - the standard Mollow spectrum with $\delta_x = -3$ MHz, $\chi_x = 10$ MHz. (2.B): $\delta_z = 0.5$ MHz, $\chi_z = 2$ MHz. (2.C): $\delta_z = -0.5$ MHz, $\chi_z = 2$ MHz. The arrows show where Field$_x$ has been applied, and the circled transitions energy level scheme is discussed in the above figure. Note the probe frequency is in terms of the probe beam detuning $\delta_p = \omega_p - \omega_x$

Lorentzian	Weight
$L(\delta_p - \omega_z - \Omega_z)$	$-\frac{\alpha}{4}\rho_{12}^{eq}\cos^4\phi L_D(\omega_z)$
$L(\delta_p - \omega_z + \Omega_z)$	$-\frac{\alpha}{4}\rho_{12}^{eq}\sin^4\phi L_D(\omega_z)$
$L(\delta_p - \omega_z)$	$-\frac{\alpha}{8}\sin^2 2\phi\rho_{12}^{eq}L_D(\omega_z)$
$L(\delta_p + \omega_z - \Omega_z)$	$\frac{\alpha}{4}\rho_{12}^{eq}\sin^4\phi L_D(\omega_z)$
$L(\delta_p + \omega_z + \Omega_z)$	$\frac{\alpha}{4}\rho_{12}^{eq}\cos^4\phi L_D(\omega_z)$
$L(\delta_p + \omega_z)$	$\frac{\alpha}{8}\sin^2 2\phi\rho_{12}^{eq}L_D(\omega_z)$
$L(\delta_p - \Omega_z)$	$\frac{\alpha}{8}\sin^2 2\phi\rho_{12}^{eq}\frac{\Omega_z}{\omega_z^2}$
$L(\delta_p + \Omega_z)$	$-\frac{\alpha}{8}\sin^2 2\phi\rho_{12}^{eq}\frac{\Omega_z}{\omega_z^2}$
$L(\delta_p)$	$i\frac{\alpha}{2}\rho_{12}^{eq}\cos^2 2\phi L_A(\omega_z)$

The results again show the standard Mollow spectrum breaking up into nine peaks. Figure 3-6 shows the results, with the standard on resonance Mollow spectrum generated by Field$_x$ split into a series of peaks by a positively and negatively detuned Field$_z$. Here is a clear example of the fact that, despite the fact that the Rabi resonance is not directly observable here (since the dressed state populations are equalized by an on-resonance Field$_x$), the effect of Field$_z$ on the Rabi transition is still plain when the original transition is observed.

3.4.3 Field$_z$ on resonance case

In this circumstance, again under the assumption of high power and that Field$_x$ is off-resonance, the weights of the Lorentzians become

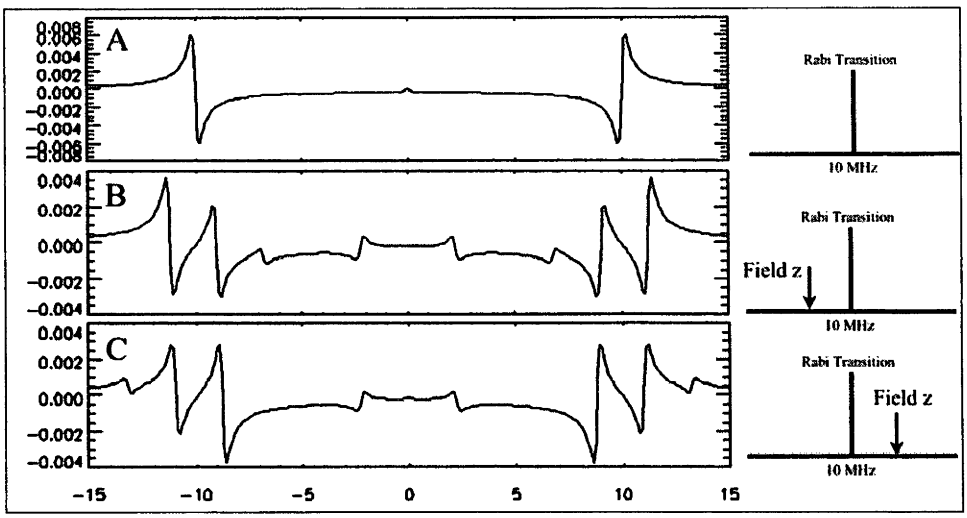

Figure 3-6: On resonance Mollow spectrum, split by the Field$_z$ being applied to either side of the Rabi transition. The arrows on the right show (pictorially) the positions of Field$_z$. (A) No Field$_z$; standard Mollow spectrum with $\delta_x = 0, \chi_x = 10$ MHz. (B) positively detuned Field$_z$: $\delta_z = 1$ MHz, $\chi_z = 2$ MHz. (C) negatively detuned Field$_z$: $\delta_z = -1$ MHz, $\chi_z = 2$ MHz. The probe frequency is in terms of the probe detuning $\delta_p = \omega_p - \omega_x$.

Lorentzian	**Weight**
$L(\delta_p - \omega_z - \Omega_z)$	$-\frac{\alpha}{4}\cos^4\theta\rho^{eq}_{\alpha\beta}L_D(\Omega_z)$
$L(\delta_p - \omega_z + \Omega_z)$	$\frac{\alpha}{4}\cos^4\theta\rho^{eq}_{\alpha\beta}L_D(\Omega_z)$
$L(\delta_p - \omega_z)$	$-i\frac{\alpha}{4}\cos^2\theta\left(-i\sin 2\theta\rho^{eq}_{12}L_D(\omega_z) - 2\cos^2\theta\rho^{eq}_{\alpha\beta}L_A(\Omega_z)\right)$
$L(\delta_p + \omega_z - \Omega_z)$	$\frac{\alpha}{4}\sin^4\theta\rho^{eq}_{\alpha\beta}L_D(\Omega_z)$
$L(\delta_p + \omega_z + \Omega_z)$	$-\frac{\alpha}{4}\sin^4\theta\rho^{eq}_{\alpha\beta}L_D(\Omega_z)$
$L(\delta_p + \omega_z)$	$i\frac{\alpha}{4}\sin^2\theta\left(-i\sin 2\theta\rho^{eq}_{12}L_D(\omega_z) - 2\sin^2\theta\rho^{eq}_{\alpha\beta}L_A(\Omega_z)\right)$
$L(\delta_p - \Omega_z)$	$\frac{\alpha}{4}\sin 2\theta\cos 2\theta\rho^{eq}_{12}L_D(\omega_z)$
$L(\delta_p + \Omega_z)$	$\frac{\alpha}{4}\sin 2\theta\cos 2\theta\rho^{eq}_{12}L_D(\omega_z)$
$L(\delta_p)$	0

Note the complication of the weights of $L(\delta_p \pm \omega_z)$, since it is not possible to (in general) say whether or not $L_D(\omega_z) \gg L_A(\Omega_z)$. In Figure 3-7, it is possible with the parameters given

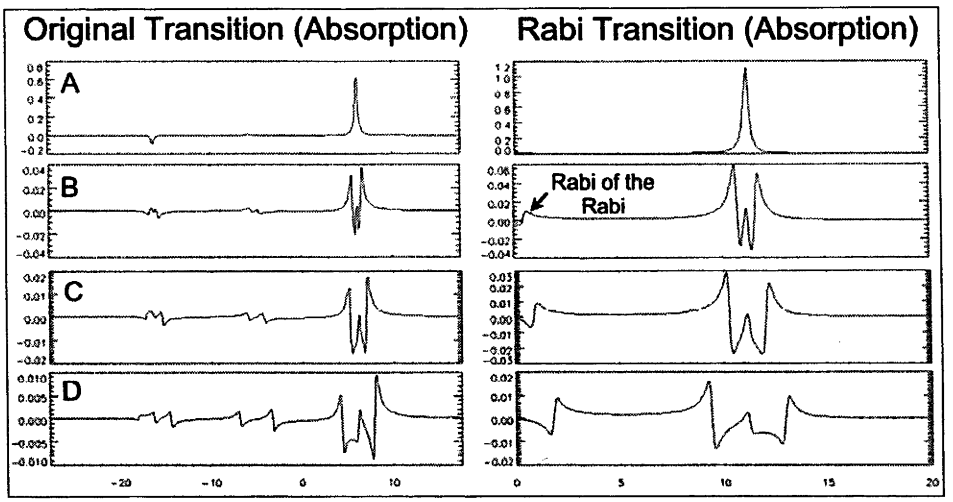

Figure 3-7: On the left, the original Mollow spectrum is shown in (A), where $\chi_x = 10$ MHz, $\delta_z = 5$ MHz. On the right, the resultant Rabi transition is also shown. The Rabi transition is then driven resonantly with powers of (B) $\chi_z = 0.5$ MHz, (C) $\chi_z = 1.0$ MHz, (D) $\chi_z = 2.0$ MHz. The results for the $\hat{x}$ probe and the $\hat{z}$ probe are shown for each power. The probe frequency is in terms of the probe detuning $\delta_p = \omega_p - \omega_x$.

to make just that approximation, and so the absorption spectrum ends up being dispersive in structure. The figure then shows the general dynamics of this situation.

3.4.4 Field$_x$ and Field$_z$ on resonance

The final situation that will be examined involves looking at the case when both driving fields are on resonance. The weights in this situation (the high power limit) reduce to

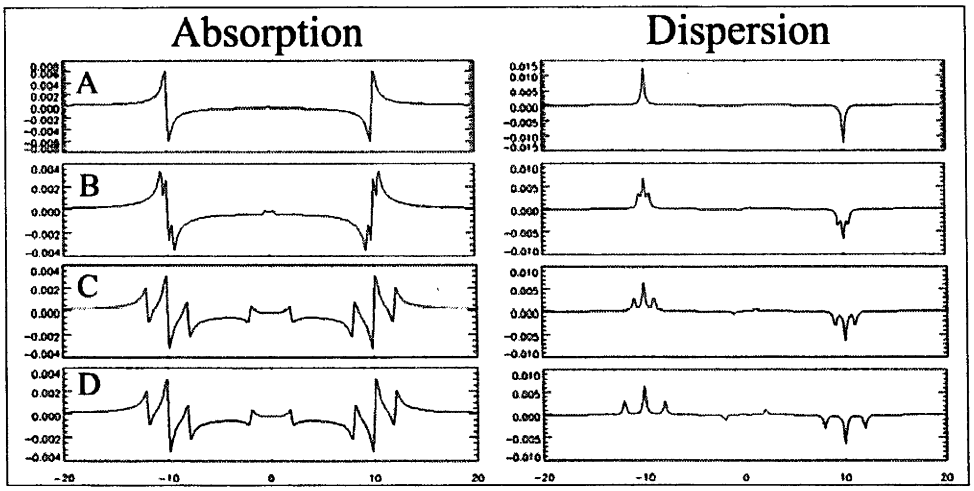

Figure 3-8: The resonant absorption and dispersion spectra. Firstly, Field$_x$ is applied on resonance with $\chi_x = 10$ MHz. Field$_z$ is then applied on resonance in increasing power with (A): No Field$_z$, (B): $\chi_z = 0.5$ MHz, (C): $\chi_z = 1.0$ MHz, (D): $\chi_z = 2.0$ MHz. The probe frequency is in terms of the probe detuning $\delta_p = \omega_p - \omega_x$.

Lorentzian	**Weight**
$L(\delta_p - \omega_z - \Omega_z)$	$-\frac{\alpha}{16}\rho_{12}^{eq} L_D(\Omega_x)$
$L(\delta_p - \omega_z + \Omega_z)$	$-\frac{\alpha}{16}\rho_{12}^{eq} L_D(\Omega_x)$
$L(\delta_p - \omega_z)$	$-\frac{\alpha}{8}\rho_{12}^{eq} L_D(\Omega_x)$
$L(\delta_p + \omega_z - \Omega_z)$	$\frac{\alpha}{16}\rho_{12}^{eq} L_D(\Omega_x)$
$L(\delta_p + \omega_z + \Omega_z)$	$\frac{\alpha}{16}\rho_{12}^{eq} L_D(\Omega_x)$
$L(\delta_p + \omega_z)$	$\frac{\alpha}{8}\rho_{12}^{eq} L_D(\Omega_x)$
$L(\delta_p - \Omega_z)$	$\frac{\alpha}{8}\rho_{12}^{eq}\frac{\Omega_z}{\Omega_x^2}$
$L(\delta_p + \Omega_z)$	$-\frac{\alpha}{8}\rho_{12}^{eq}\frac{\Omega_z}{\Omega_x^2}$
$L(\delta_p)$	0

A very simple spectrum ensues, with the same sorts of observations as seen above. In Figure 3-8, the original Mollow spectrum is split by an on-resonance Field$_z$ of increasing power, to show the effects of Field$_z$ on the standard Mollow spectrum.

The above calculations make some approximations. In the next section, the major approximations are examined to see what effect they have, and finally a formalism is briefly presented to show the numerical calculations that can be performed to include all effects.

3.5 Theoretical Improvements

Now that the basic dynamics of the system are understood, it is possible to examine the effects of the various approximations that were made along the way, in order to understand their effects and to make it possible to study the system under less stringent conditions. The approximations made include

i. The rotating wave approximation (RWA)

ii. discarding the interaction of Field_z with the Rabi of the Rabi

iii. Isotropic relaxation ($T_1 = T_2$)

The effects of each of these approximations will be examined, and then the results from a numerical simulation of the system will be presented.

3.5.1 The Rotating Wave Approximation (RWA)

In the standard Mollow case, the RWA is well understood. Keeping the anti-resonant terms results in the so-called *Bloch-Siegert shift*, in which the original transition is shifted to a slightly higher frequency. It has been shown [83] that this can be understood easily by breaking down the full interaction of the driving field into the anti-resonant and resonant part. Examining the anti-resonant part in isolation, its effect on the original transition is to generate an extreme case of the standard Mollow spectrum, where the detuning is $\omega_0 + \omega_x$. The slightly shifted Mollow sideband then interacts with the resonant interaction in an entirely normal fashion.

In the normal Mollow spectrum, a field of frequency ω_x interacts with a transition of frequency ω_0. The Mollow sidebands are then generated at $\omega_x \pm \Omega_x$. The antiresonant term (discarded in the RWA) can be thought of a field of frequency $-\omega_x$ interacting with the TLA. The detuning then becomes

$$\delta_x = \omega_0 + \omega_x$$

and so the generalised Rabi frequency becomes

$$\Omega_x^2 = \chi_x^2 + (\omega_0 + \omega_x)^2$$

The upper Mollow spectral feature is then centred at frequency

$$-\omega_x + \Omega_x$$

which is very nearly at the original transition frequency ω_0. The Bloch-Siegert shift is then the difference between these two frequencies

$$\begin{aligned}
\Delta_{bs} &= (-\omega_x + \Omega_x) - \omega_0 \\
&= -(\omega_x + \omega_0) + \sqrt{\chi_x^2 + (\omega_0 + \omega_x)^2} \\
&\simeq -(\omega_x + \omega_0) + (\omega_0 + \omega_x)\left(1 + \frac{1}{2}\frac{\chi_x^2}{(\omega_0 + \omega_x)^2}\right) \\
&= \frac{1}{2}\frac{\chi_x^2}{(\omega_0 + \omega_x)}
\end{aligned}$$

In the case of the Rabi frequency, the same sort of analysis applies. Field_z (Rabi frequency χ_z) interacts with the transition at the Rabi frequency Ω_x in the same fashion as the normal case, so the anti-resonant term will also produce the extreme case of the Rabi's Mollow spectrum. The generalised Rabi frequency of the transition driven by Field_z is given by

$$\Omega_x = \sqrt{\chi_x^2 + \delta_x^2}$$

This allows for two cases. In the simplest case, ignore the effect of the Bloch Siegert term on Field_x so that δ_x is not affected by it. In this case, the detuning of the anti-resonant term becomes

$$\delta_z = \Omega_x + \omega_z$$

and the generalised Rabi frequency for the Rabi interaction is given by

$$\Omega_z = \sqrt{(\chi_z')^2 + \delta_z^2}$$

where

$$\chi_z' = -\frac{\chi_x}{\Omega_x}\chi_z$$

so the Bloch Siegert shift for the Rabi resonance becomes

$$\begin{aligned} \Delta_{bs}^R &= (-\omega_z + \Omega_z) - \Omega_x \\ &\approx \frac{1}{2}\frac{(\chi_z')^2}{(\omega_z + \Omega_x)} \end{aligned}$$

In the more complicated scenario, note that the Bloch Siegert shift on the original transition also has an impact. In this case, δ_x (call the new detuning δ_x^{bs}) is modified

$$\begin{aligned} \delta_x^{bs} &= \omega_0 + \Delta_{bs} - \omega_x \\ &= \delta_x + \Delta_{bs} \end{aligned}$$

so that the generalized Rabi frequency is also modified to a Bloch Siegert modified term Ω_x^{bs}

$$\left(\Omega_x^{bs}\right)^2 = \chi_x^2 + (\delta_x + \Delta_{bs})^2$$

giving for the new Bloch Siegert shift in the Rabi transition

$$\tilde{\Delta}_{bs}^R \approx \frac{1}{2}\left(\frac{\chi_x}{\Omega_x^{bs}}\right)^2 \frac{\chi_z^2}{(\omega_z + \Omega_x^{bs})}$$

To put this into experimental perspective, a typical experimental scenario (see next chapter) has the following parameters (all in MHz)

$$
\begin{aligned}
\omega_0 &= 70 \\
\omega_x &= 73 \\
\chi_x &= 8.0 \\
\chi_z &= 2.0 \\
\omega_z &= 7.0
\end{aligned}
$$

which gives for the various shifts

$$
\begin{aligned}
\Delta_{bs} &\approx 0.2 \\
\Delta_{bs}^{R} &\approx 0.11 \\
\tilde{\Delta}_{bs}^{R} &\approx 0.11
\end{aligned}
$$

in general introducing an error in the detuning in the fields of the order of <0.5% for the Field$_x$ and <1.5% for Field$_z$. It is clear that the Bloch Siegert shift is a little more significant in the Rabi transition, however it is still not a significant effect by any means. There is a further interaction with the anti-resonant field, which will be discussed in the following section.

3.5.2 Interaction with the Rabi of the Rabi

In Eq. (3.9*a*, 3.9*b*) the term proportional to χ_z'', interpreted as the interaction of Field$_z$ with the Rabi of the Rabi, was dropped under the assumption that the effect would be a minor one, since Field$_z$ was (in general) well detuned from the transition.

$$
\begin{aligned}
\frac{d}{dt}\tilde{\rho}_{12} &= i\left(\delta_z + 2\chi_z'' \cos\omega_z t - \Gamma\right)\tilde{\rho}_{12} - i\frac{\chi_z'}{2}W_d - \rho_{12}^{eq}e^{-i\omega_z t} \\
\dot{W}_d &= i\chi_z'\left(\tilde{\rho}_{21} - \tilde{\rho}_{12}\right) - \Gamma\left(W_d - W_d^{eq}\right)
\end{aligned}
$$

Obviously, however, if the effects of this term are to be examined, then the term can be left

in and the transformations to the doubly dressed states can be iterated again - to the triply dressed states. Transforming these equations to the doubly dressed states (but leaving the higher order term in);

$$\begin{aligned}
\dot{\rho}_{\alpha\beta} &= (i\Omega_z - \Gamma)\rho_{\alpha\beta} - \rho_{\alpha\beta}^{eq} - \left(P_- e^{-i\omega_z t} - P_+ e^{i\omega_z t}\right) \\
&\quad +2i\cos 2\phi\chi_z'' \cos\omega_z t\rho_{\alpha\beta} - i\left(-\sin 2\phi\chi_z''\right)\cos\omega_z t W_{dd} \\
\dot{W}_{dd} &= -\Gamma\left(W_{dd} - W_{dd}^{eq}\right) + w^r\left(e^{i\omega_z t} + e^{-i\omega_z t}\right) \\
&\quad +2i\left(-\sin 2\phi\chi_z''\right)\cos\omega_z t\left(\rho_{\alpha\beta} - \rho_{\beta\alpha}\right)
\end{aligned}$$

or, using the notation $\chi_z''' = -\sin 2\phi\chi_z''$ and $\chi_z'''' = \cos 2\phi\chi_z''$

$$\begin{aligned}
\dot{\rho}_{\alpha\beta} &= (i\Omega_z - \Gamma)\rho_{\alpha\beta} - \rho_{\alpha\beta}^{eq} - \left(P_- e^{-i\omega_z t} - P_+ e^{i\omega_z t}\right) \\
&\quad +2i\chi_z''''\cos\omega_z t\rho_{\alpha\beta} - i\chi_z'''\cos\omega_z t W_{dd} \\
\dot{W}_{dd} &= -\Gamma\left(W_{dd} - W_{dd}^{eq}\right) + w^r\left(e^{i\omega_z t} + e^{-i\omega_z t}\right) \\
&\quad +2i\chi_z'''\cos\omega_z t\left(\rho_{\alpha\beta} - \rho_{\beta\alpha}\right)
\end{aligned}$$

it is obvious that the same sort of equations are arrived at. To proceed, simply go to the rotating frame, apply the RWA, drop the higher order term proportional to χ_z''''. These equations can then be solved by transforming to the *triply dressed states.* This process could be iterated indefinitely, to get the equations to the desired accuracy. The algebraic complexity of the solutions is not very edifying however, but it is obvious from the form of the equations above that it is possible to draw some conclusions intuitively about the effect of the higher order terms on the dynamics of the system given the fact that it is already understood that standard Mollow splitting will occur. Firstly, whereas in the case examined to date, the energy levels were split by Ω_z, the new generalized Rabi frequency would split the energy levels by a new generalised Rabi frequency, call it Ω_z^R

$$\Omega_z^R = \sqrt{(\chi_z''')^2 + (\Omega_z - \omega_z)^2}$$

In the case, where $\omega_z \gg \Omega_z$, χ_z then

$$\Omega_z^R \approx (\omega_z - \Omega_z)(1 + \Delta)$$

where Δ, which is small, is equal to

$$\Delta = \frac{1}{2} \frac{(\chi_z'')^2}{(\Omega_z - \omega_z)^2}$$

The effects of this can be found with the help of the following diagrams. Firstly, examine the following spectrum, produced by driving the Rabi transition slightly off resonance (same as Fig 3-3(a))

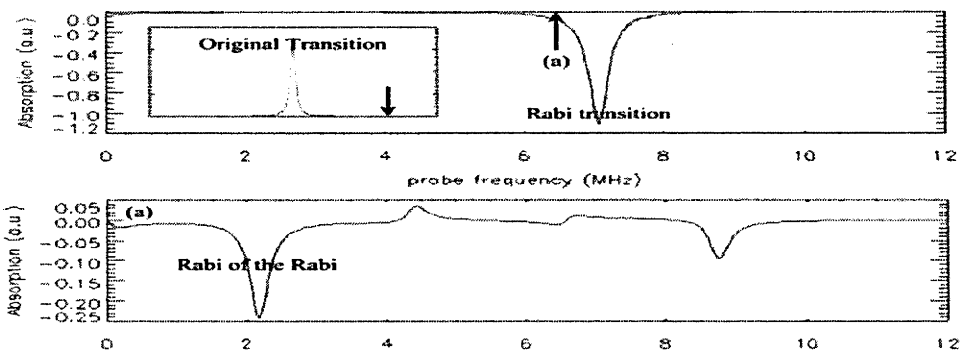

Now, examine what happens when the higher order interaction is applied. Firstly, the Field$_z$ will interact with the Rabi of the Rabi and split it in a standard Mollow fashion, shown diagrammatically here

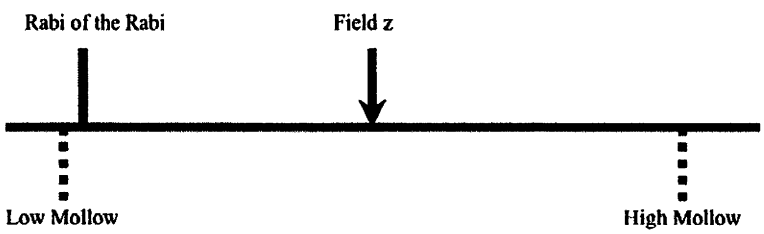

The low Mollow Lorentzian will be at frequency

$$\begin{aligned}\omega_p &= \omega_z - \Omega_z^R \\ &= \Omega_z + \Delta\Omega_z - \omega_z\Delta \\ &\approx \Omega_z - \omega_z\Delta\end{aligned}$$

and the high one at (it is expected that this is a very small peak)

$$\begin{aligned}\omega_p &= \omega_z + \Omega_z^R \\ &= \omega_z(2+\Delta) - \Omega_z(1+\Delta)\end{aligned}$$

The upshot is that the new 'Rabi of the Rabi' transition (the low Mollow peak) will be slightly shifted by the frequency $\omega_z\Delta$, and a new tiny transition will be visible at a much higher frequency. Turning attention to the split Rabi frequency, the splitting of the Rabi of the Rabi transition will also have the effect of splitting the Mollow spectrum centred at the Rabi frequency, in a fashion reminiscent of the way the Field_z splits the original transition's Mollow spectrum. In that spectrum there were Lorentzians at, for instance,

$$\delta_p = \omega_z - \Omega_z$$

and recalling that $\delta_p = \omega_p - \omega_x$ this translates to

$$\omega_p = \omega_x + \omega_z - \Omega_z$$

To take this analogy further, it is expected then that the Rabi Mollow spectrum, when split by the higher order interaction, would have a peak at

$$\begin{aligned}\omega_p &= \omega_z + \omega_z - \Omega_z^R \\ &\approx \omega_z + \Omega_z - \omega_z\Delta\end{aligned}$$

so again it appears that the higher order interaction has merely shifted the original Mollow spectral feature by the factor $\omega_z\Delta$. Likewise, another peak that would arise would be at

$$\begin{aligned}\omega_p &= \omega_z - \omega_z + \Omega_z^R \\ &\approx \omega_z - \Omega_z + \omega_z\Delta\end{aligned}$$

again shifted. The other features, all at much higher or lower frequencies, again are all expected to be quite small. In summary, the higher order interaction will (in these particular circumstances where Field_z is well detuned from the Rabi of the Rabi) merely shift (and squeeze) the original spectrum slightly.

There are circumstances where the higher order interactions will become more significant. If the Field_z frequency is stepped down away from the Rabi transition, so δ_z is becoming larger and hence Ω_z is increasing, there will come a time where Field_z will actually come close to the Rabi of the Rabi, and will split it in a more interesting fashion. This is demonstrated in Fig (3-9), a numerical 'top down' view of the dynamics. In this figure, Field_z is stepped up from low frequency, through the Rabi of the Rabi, through the Rabi transition and above it. The probe absorption spectrum is then calculated for the value of Field_z and the results are shown in an plot where the more colour there is, the higher the peak height.

This figure shows several interesting features. In particular, notice the splitting of the Rabi of the Rabi in the region where Field_z is resonant with it. The dynamics of the Mollow sidebands are clearly displayed. At the bottom of the figure, peaks 'flower' out when the Field_z frequency is very low. These transitions can be understood easily. When ω_z is small, the detuning is comparable to Ω_x, the Rabi transition's frequency. Therefore the Rabi of the Rabi will be comparable to Ω_x (i.e. $\Omega_z \approx \Omega_x$). As Field_z steps up, δ_z decreases and the Rabi of the Rabi decreases, causing the feature to fan away from the main Mollow transition as can be seen (labelled A in the diagram). There is also a peak visible (labelled B) on the other side of the Mollow sideband. This peak is an interesting one and is actually due to the inclusion of the antiresonant terms (usually discarded by the RWA) in the numerical calculation. Field_z has two components of frequencies ω_z (the resonant one) and $-\omega_z$ (the antiresonant one). Just as

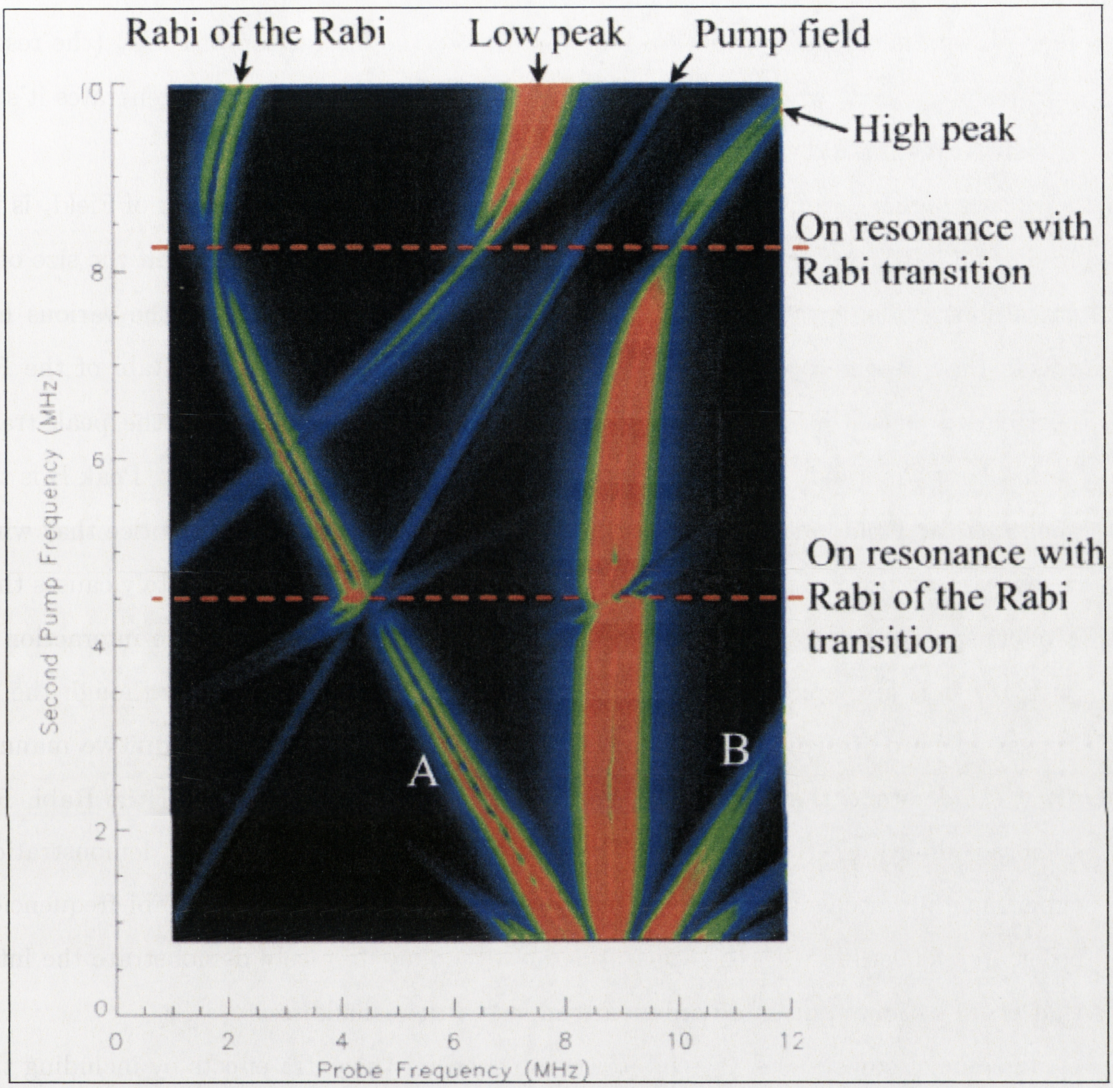

Figure 3-9: Original transition is driven by Field$_x$ with a $\chi_x = 7.85$ MHz, $\delta_x = -3$ MHz and then the Field$_z$ is scanned from 1.5 MHz, through to 10 MHz, with $\chi_z = 1.87$ MHz. The probe absorption spectrum is calculated for each Field$_z$ detuning and the isometric view is produced.

the resonant term produces a Rabi of the Rabi due to its interaction with the Rabi transition, so too does the antiresonant term. This 'antiresonant Rabi of the Rabi' is the one labelled B. As Field$_z$ steps towards the Rabi transition, the antiresonant frequency $-\omega_z$ gets *further away*, thus the antiresonant Rabi of the Rabi increases, hence the form of the peak movement in the plot. Two minor peaks below A and B are due to the interaction of Field$_z$ (the resonant and anti-resonant part) with the Rabi of the Rabi frequency, which in turn generates it's own Rabi transition (call it Rabi^3).

These higher order interactions become more marked when the power of Field$_z$ is increased. In figure (3-10), the strength of Field$_z$ is now 5 MHz, which is nearly half the size of the Rabi transition. The spectrum, which is much more complicated, shows the various high order effects that become apparent at these high powers. In peak A, the Rabi of the Rabi, it is possible to trace the spectrum up from where the Field$_z$ is low, and the peak traces out a parabola as the Field$_z$ goes through resonance with the Rabi transition. Peak B is the Rabi^3, generated by Field$_z$ interacting with peak A (the Rabi of the Rabi). Notice that when Field$_z$ is resonant with B, it splits this peak, which causes A to split and ultimately causes the original Mollow spectrum (D & E) to split. Peak C is Rabi^4, generated by the interaction of Field$_z$ with B! It is also split when Field$_z$ is resonant with it. Clearly then, though the dynamics appear to be quite complicated, they can be understood in a fairly intuitive manner if it is always understood that Field$_z$ will interact with the Rabi, the Rabi of the Rabi, Rabi^3 and so on ad infinitum. This spectrum, included here only for purposes of demonstration, is not experimentally accessible (Fig 3-9 from above is, see Chapt 4) since Rabi frequencies of this order aren't possible with the apparatus, however they do nicely demonstrate the interactions that occur as more and more orders are added to the calculations.

In some circumstances, it is important to consider the extra effects by including the higher order terms, but in the bulk of the experimental circumstances discussed in this thesis, these interactions are unimportant and the first order theory, where only the interaction of Field$_z$ with the original Rabi transition is considered, are quite adequate.

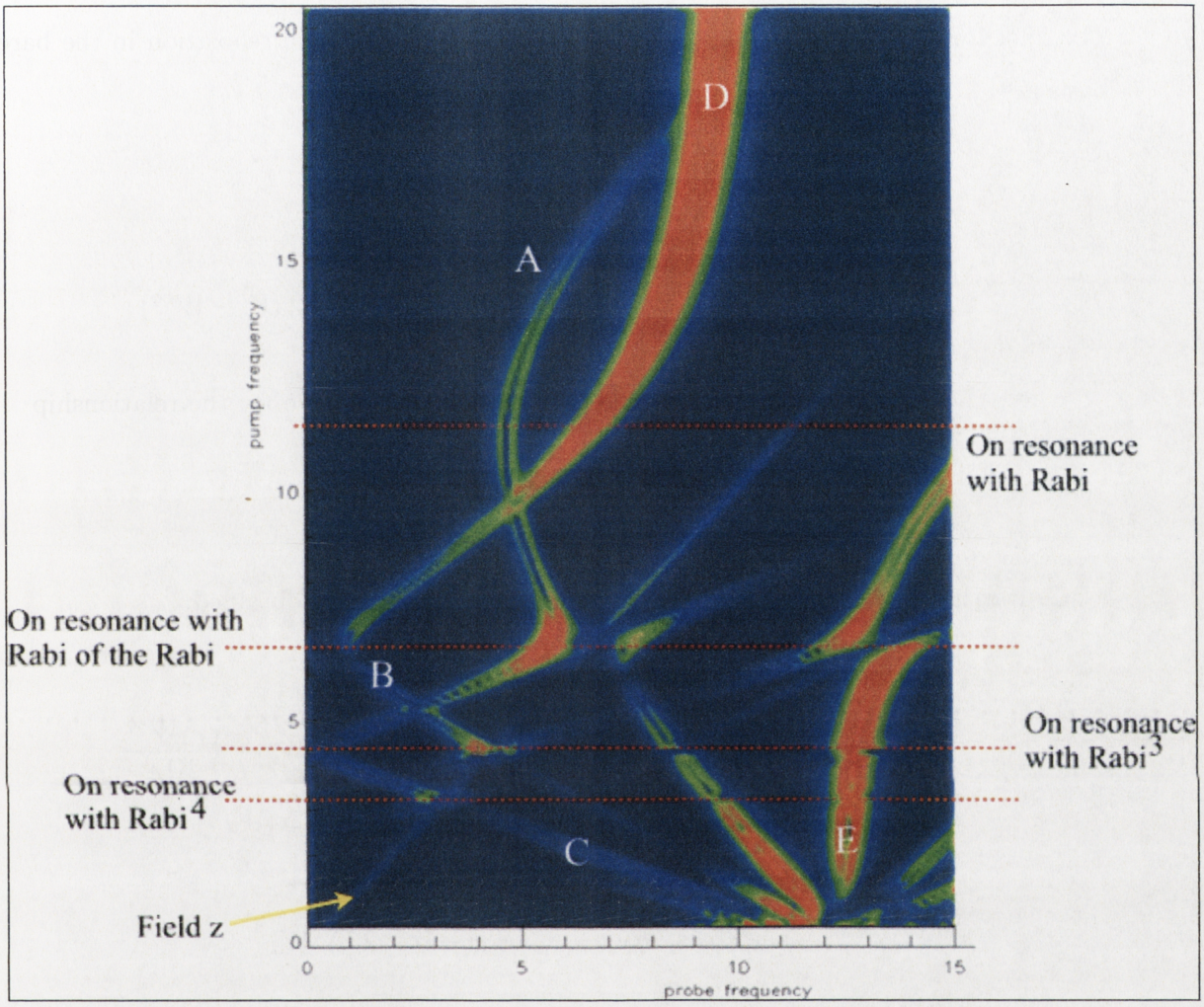

Figure 3-10: The high power case of the above spectrum. $\chi_x = 10$ MHz, $\delta_x = -3$ MHz. Field$_z$ of power $\chi_z = 5$ MHz is scanned through the Rabi transition from 1 MHz to 20 MHz and the probe spectrum is calculated for each of the Field$_z$ detunings. Peak A is the Rabi^2 (the Rabi of the Rabi) and Peak B is Rabi^3.

3.5.3 Anisotropic relaxation ($T_1 \neq T_2$)

The semiclassical dressed state basis is not useful in the case of anisotropic relaxation, as it tends to introduce further non-secular interactions. However, some progress can be made with some fairly stringent approximations (akin to the Secular approximation taken in Chapter 2). The Bloch equations for the doubly driven TLA with anisotropic relaxation in the bare state basis are

$$\begin{aligned}
\frac{d}{dt}\tilde{\rho}_{ge} &= (i\delta_x - \Gamma - 2i\chi_z \cos\omega_z t)\,\tilde{\rho}_{ge} - i\frac{\chi_x}{2}W \\
\dot{W} &= 2i\chi_x\left(\tilde{\rho}_{eg} - \tilde{\rho}_{ge}\right) - \Gamma\left(W - W^{eq}\right) - \Delta_\gamma\left(W - W^{eq}\right)
\end{aligned}$$

where the longitudinal relaxation rate γ, has been defined to obey the relationship

$$\gamma = \Gamma + \Delta_\gamma$$

Converting to the dressed states, the following equations are obtained,

$$\begin{aligned}
\dot{\rho}_{12} &= i\left(\Omega_x + 2\chi_z'' \cos\omega_z t - \Gamma\right)\rho_{12} - i\chi_z' \cos\omega_z t W_d - \frac{\chi_x \gamma W^{eq}}{2\Omega_x} \\
&\quad + \frac{1}{2}\sin^2 2\theta\Delta_\gamma\left(\rho_{12} + \rho_{21}\right) - \frac{1}{2}\sin 2\theta\cos 2\theta\Delta_\gamma W_d \\
\dot{W}_d &= 2i\chi_z' \cos\omega_z t\left(\rho_{21} - \rho_{12}\right) - \Gamma W_d + \gamma\cos 2\theta W^{eq} \\
&\quad - \sin 2\theta\cos 2\theta\Delta_\gamma\left(\rho_{12} + \rho_{21}\right) + \cos^2 2\theta\Delta_\gamma W_d
\end{aligned}$$

As can be seen, many new interactions are introduced and it is no longer generally possible to solve the equations by changing to the doubly dressed state basis. To proceed it is possible to take the secular approximation and drop the relaxation terms proportional to the populations in these equations (i.e. decouple the coherences and populations in the relaxation terms). Note this is exact in the on resonance case. Under this approximation

$$
\begin{aligned}
\dot{\rho}_{12} &= i\left(\Omega_x + 2\chi_z'' \cos\omega_z t - \Gamma\right)\rho_{12} - i\chi_z' \cos\omega_z t W_d - \frac{\chi_x \gamma W^{eq}}{2\Omega_x} \\
&\quad + \frac{1}{2}\sin^2 2\theta\Delta_\gamma\left(\rho_{12} + \rho_{21}\right) \\
\dot{W}_d &= 2i\chi_z' \cos\omega_z t\left(\rho_{21} - \rho_{12}\right) - \Gamma W_d + \gamma\cos 2\theta W^{eq} + \cos^2 2\theta\Delta_\gamma W_d
\end{aligned}
$$

Now transforming to the rotating frame, and taking the RWA, (which involves dropping terms that rotate with $e^{2i\omega_z t}$) the relaxation term proportional to ρ_{21} can be dropped. Hence

$$
\begin{aligned}
\frac{d}{dt}\tilde{\rho}_{12} &= i\left(\delta_z + 2\chi_z'' \cos\omega_z t - \Gamma'\right)\tilde{\rho}_{12} - i\frac{\chi_z'}{2} W_d - \tilde{\rho}_{12}^{eq} e^{-i\omega_z t} \\
\dot{W}_d &= i\chi_z'\left(\tilde{\rho}_{21} - \tilde{\rho}_{12}\right) - \gamma'\left(W_d - \tilde{\omega}^{eq}\right)
\end{aligned}
$$

where the modified relaxation rates are

$$
\begin{aligned}
\Gamma' &= \Gamma - \frac{1}{2}\sin^2 2\theta\Delta_\gamma \\
\gamma' &= \Gamma - \cos^2 2\theta\Delta_\gamma \\
\tilde{\rho}_{12}^{eq} &= -\frac{1}{2}\sin 2\theta\gamma W^{eq} \\
\tilde{\omega}^{eq} &= \frac{\gamma}{\gamma'}\cos 2\theta W^{eq}
\end{aligned}
$$

recovering the basic Bloch equations with the orthogonal driving term that have been examined throughout this thesis. The relaxation rates are modified by the anisotropic relaxation rates, as well as the equilibrium population differences and coherences. Writing $\gamma' = \Gamma' + \Delta_{\gamma'}$ and iterating again, the next round of equations yield the following analogous rates and equilibria

$$
\begin{aligned}
\Gamma'' &= \Gamma' - \frac{1}{2}\sin^2 2\phi\Delta_{\gamma'} \\
\gamma'' &= \Gamma' - \cos^2 2\phi\Delta_{\gamma'}
\end{aligned}
$$

$$\tilde{\rho}_{\alpha\beta}^{eq} = -\frac{1}{2}\sin 2\phi\gamma'\tilde{\omega}^{eq}$$
$$\tilde{w}^{eq} = \frac{\gamma'}{\gamma''}\cos 2\phi\tilde{\omega}^{eq}$$

Looking at the z-probe Lorentzians (in the high power limit) from the above equations, the changes follow through as

Lorentzian	**Weight**
$L^{\Gamma''}(\omega_p - \omega_z - \Omega_z)$	$-i\alpha\Delta\tilde{w}^{eq}\cos^4\phi$
$L^{\Gamma''}(\omega_p - \omega_z + \Omega_z)$	$i\alpha\Delta\tilde{w}^{eq}\sin^4\phi$
$L^{\gamma''}(\omega_p - \omega_z)$	$\frac{1}{2}\alpha\sin^2 2\theta\Delta'\tilde{\rho}_{\alpha\beta}^{eq}L_D^{\Gamma''}(\Omega_z)$
$L^{\Gamma''}(\omega_p - \Omega_z)$	$-\frac{1}{2}i\alpha\cos^2 2\theta\sin^2 2\phi\tilde{w}^{eq}$
$L^{\gamma''}(\omega_p)$	$-2\alpha\cos^2 2\theta\Delta'\tilde{\rho}_{\alpha\beta}^{eq}L_D^{\Gamma''}(\Omega_z)$

where the new Lorentzian functions are

$$L^{\gamma''}(x) = \frac{\gamma''}{(\gamma'')^2 + x^2} - i\frac{x}{(\gamma'')^2 + x^2}$$
$$L^{\Gamma''}(x) = \frac{\Gamma''}{(\Gamma'')^2 + x^2} - i\frac{x}{(\Gamma'')^2 + x^2}$$

Overall then, the anisotropic relaxation rates (at least to the rather stringent approximations made here) will affect the widths of some of the Lorentzians as well as their weights. These effects can be variable in size so obviously a more precise solution is required in many cases. In these cases, where the effects of the anisotropic relaxation are going to be significant, then a full numerical calculation must be performed.

3.5.4 Numerical Calculations

While certain approximations need to be taken analytically, the numerical solution can be obtained easily, which, and while it does not give a very good indication of the general dynamics of the situation, it at least provides an accurate representation of the solutions. The numerical calculation is easily done. Examine (for the case of the z-polarised probe) the Bloch equations

$$\begin{aligned}\dot{\rho}_{ge} &= \left(i\delta_x - \Gamma - 2i\chi_z \cos\omega_z t - 2i\alpha\cos\omega_p t\right)\rho_{ge} - i\frac{\chi_x}{2}W \\ \dot{W} &= 2i\chi_x\left(\rho_{eg} - \rho_{ge}\right) - \gamma\left(W - W^{eq}\right)\end{aligned}$$

The steady state solutions can be written in the form

$$\begin{aligned}\rho_{ge} &= \sum_{k,l=-\infty}^{\infty} \rho_{ge}^{k,l} e^{ik\omega_z t} e^{il\omega_p t} \\ \rho_{eg} &= \sum_{k,l=-\infty}^{\infty} \rho_{eg}^{k,l} e^{ik\omega_z t} e^{il\omega_p t} \\ W &= \sum_{k,l=-\infty}^{\infty} W^{k,l} e^{ik\omega_z t} e^{il\omega_p t}\end{aligned}$$

leading to the following equations

$$\begin{aligned}\left(ik\omega_z + il\omega_p - i\delta_x + \Gamma\right)\rho_{ge}^{k,l} &= -i\frac{\chi_x}{2}W^{k,l} - i\chi_z\left(\rho_{ge}^{k+1,l} + \rho_{ge}^{k-1,l}\right) \\ &\quad -i\alpha\left(\rho_{ge}^{k,l+1} + \rho_{ge}^{k,l-1}\right) \\ \left(ik\omega_z + il\omega_p + \gamma\right)W^{k,l} &= 2i\chi_x\left(\rho_{eg}^{k,l} - \rho_{ge}^{k,l}\right) + \gamma W^{eq}\delta_{k0}\delta_{l0}\end{aligned}$$

where δ_{k0}, δ_{l0} are the Kronecker delta functions. This set of equations can then be solved numerically to the desired order. The numerical calculation is entirely analogous for the $\hat{\mathrm{x}}$ probe case as well. These numerical calculations will be used several times during the thesis, and their use will be indicated when appropriate.

3.6 Summary

In this chapter, the semiclassical calculation to produce the spectra was presented. The general scheme of the calculation involves transforming to the doubly dressed states, showing the interaction of Field$_z$ with the Rabi transition. The Rabi transition is split by Field$_z$,

and when probed with a $\hat{z}$ polarised probe beam something very akin to the standard Mollow spectrum is seen. Also, the appearance of the Rabi of the Rabi transition is noted, which is understood as a natural extension of the model used.

The original transition can be probed with an $\hat{x}$ polarised probe beam, and the original Mollow spectrum is then further split by the application of Field_z to the Rabi transition. The analytical solution of the probe beam absorption spectrum is presented, and shows a natural extension of the already familiar ideas associated with the standard Mollow spectrum.

Some of the implications of the key approximations were examined, and a presentation of the numerical techniques showed the way to get a more accurate spectrum (though less edifying). Overall, the key ideas and intuitive concepts were presented, showing the way that the Rabi transition can be understood in already familiar terms from the standard TLA model and providing an analytical solution for a doubly driven system, which can be neatly extended to the triply, quadruply etc. driven states in cases where it is warranted.

Chapter 4

Experimental Results

In this chapter, the experimental results are presented which show the behaviour that has been predicted by the theoretical analysis in the preceding chapters. The experimental details of the system were covered in Chapter 1. Phase sensitive detection techniques are employed, which enables the observation of absorption and dispersion signals directly. The results of these experiments will be presented, and then compared to theoretical predictions.

4.1 The EPR transition

The bulk of the experimental data was taken at the EPR (rather than NMR) transition since the experimental setup generates a lot of noise at lower frequencies, and it is possible to bring the Rabi transition to about 10 MHz, making it easily accessible. There is some background about the EPR transition that needs to be covered before the experimental results can be understood. The EPR transition that is studied is actually composed of three distinct and significant hyperfine transitions, one for each nuclear spin projection, as shown in Fig. 4-1. The transitions are of equal strength, and the different sizes of the features are due to population differences in the transitions. For the purposes of this thesis, these transitions are considered to be three separate, non interacting transitions

The three transitions add some complication to the system. The first complication is that an on-resonance signal cannot be observed. The on-resonance signal is very much smaller than off-resonance signals. So if the on-resonance transition is at A, the biggest peak, then the

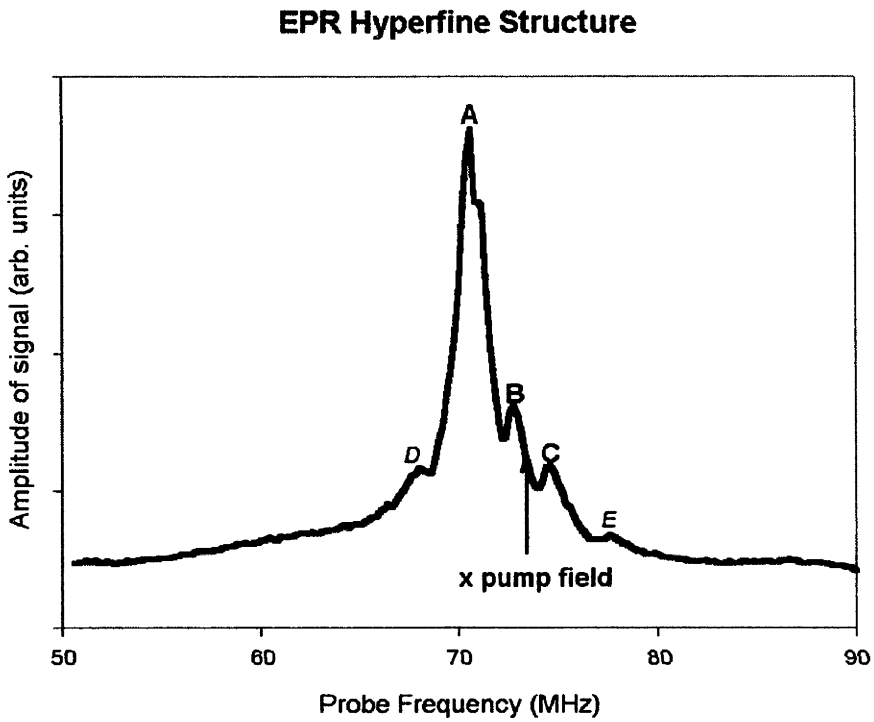

Figure 4-1: An example of the experimental plot of the EPR transitions, showing the amplitude of the probe absorption signal. Peak A is the experimentally interesting one, with contributions from peaks B,C. Peaks D,E are experimentally insignificant. The arrow shows the location of the applied Field$_x$. The alignment of the axis with the static field can be tuned such that peaks D and E are removed.

off-resonance signals due to peaks B and C will be very much bigger and will swamp out any on-resonance signal. As a result of this, only off-resonance signals are measured experimentally in this thesis.

To offset the fact that the three transitions will give three separate contributions to the overall signal, a 'sweet spot' is employed. If the pump field is placed exactly in between peaks B and C, then their contributions will be approximately equal in size (B and C are peaks with approximately the same size) however *opposite in sign.* Not only that, Field_x is now nearly resonant with them, and their signals will be heavily saturated. Therefore, their contributions will tend to cancel each other out, and leave the dominant structure in the signal to be due to the contribution from the very much larger peak A. In this fashion, it is possible to damp out contributions from the spurious hyperfine interactions, enabling the observation of the off-resonance signal from only one of the transitions, the largest one.

The results, then, of applying a single Field_x at this location can be seen in Fig 4-2. Here, the single applied field produces the familiar Mollow spectrum as the singly dressed states are created, and the probe picks up transitions between the dressed states. As can be seen, this technique produces the Mollow spectrum to a very good approximation, despite the hyperfine splitting (which is not as obvious in this experiment). This sweet spot will be employed throughout this thesis when studying the original EPR transition and also the Rabi transition that is therefore generated.

4.2 The Rabi Transition

Now that the experimental parameters for the standard Mollow spectrum have been established, the Rabi transition may be examined. A $\hat{z}$ polarised probe beam can be applied through the coil at right angles to the standard coil. With this weak field, the Rabi transition can be observed. Note that the $\hat{z}$ polarised field does not interact with the original EPR transition, so it is not possible, in the strict scenario of polarised pump and probe fields, to simultaneously observe the Rabi transition and original transition on the same plot. However to put the experimental results in context, the sample can be deliberately misaligned with respect to the coils, to mix the polarisations. Now, Field_x is not purely $\hat{x}$ polarised, but contains a small

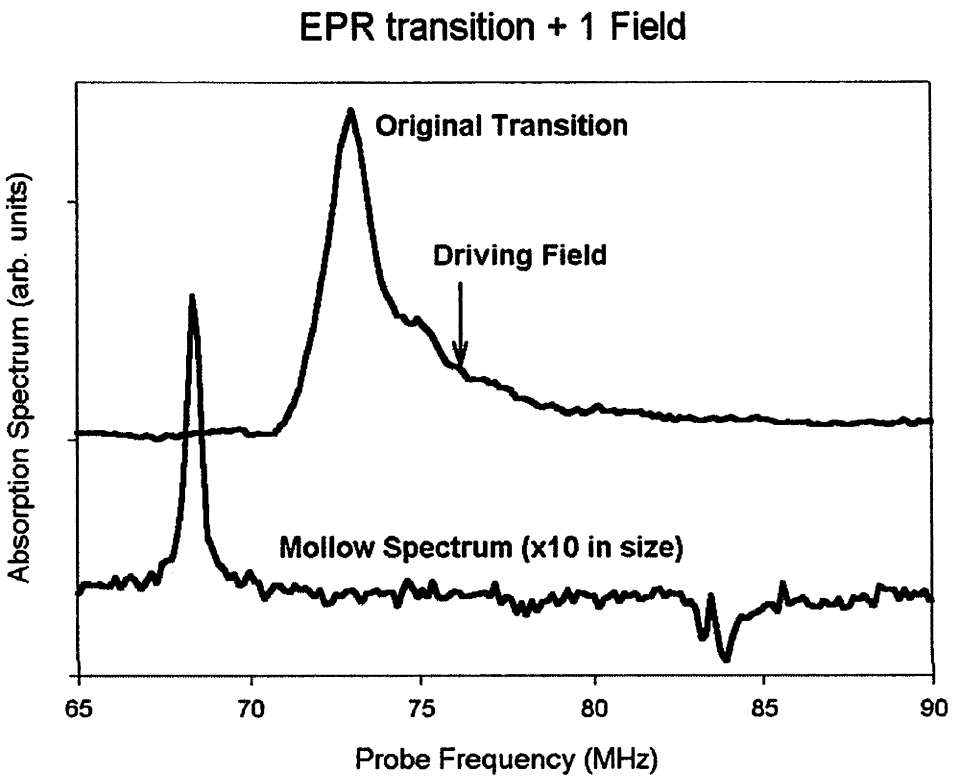

Figure 4-2: The original EPR transition (top graph) has the largest peak at 73 MHz, and is driven by a field (as indicated by the arrow) of $\omega = 76$ MHz and $\chi = 7.4$ MHz. The bottom graph is then the resultant Mollow spectrum, where the signal has been increased in size by a factor of 10.

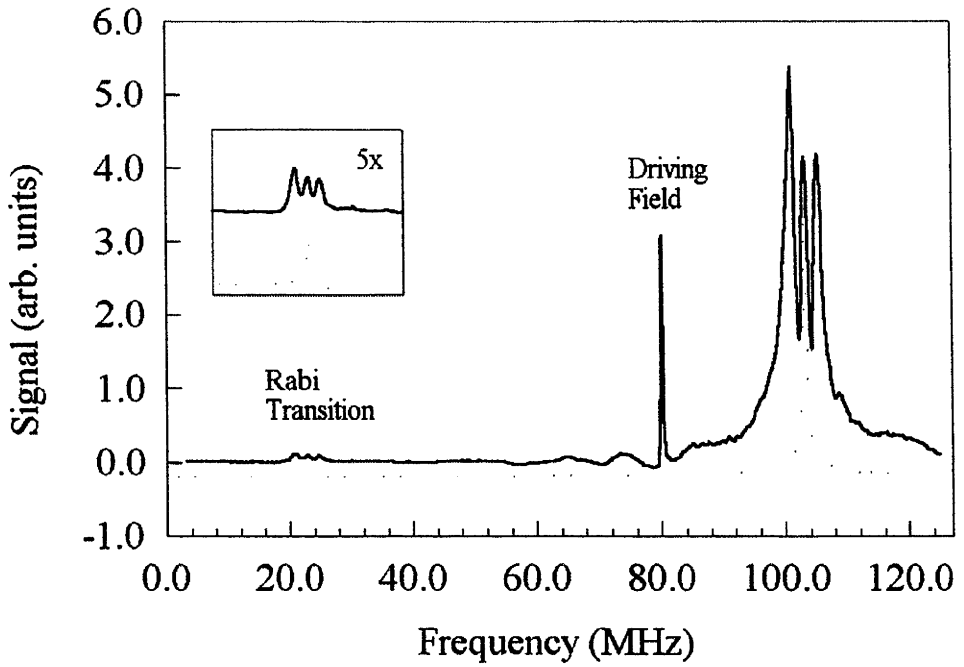

Figure 4-3: The original EPR transition, with the hyperfine structure clearly shown, is driven by a pump field at $\omega = 80$ MHz, and a misaligned probe field with both z and x polarisations shows both the Mollow spectrum due to the driven EPR transition at $\approx$ 105 MHz, and the Rabi transition at $\approx$ 24 Mhz. Figure is taken from Holmstrom *et. al. [43]*

amount of $\hat{z}$ polarisation, which allows it to interact with the Rabi transition. This scenario was used to produce fig. 4-3 which shows both the original EPR transition, and the Rabi transition. This figure is purely for illustrative purposes, but it does show the Rabi transition in relation to the original transition. The EPR transition shows the hyperfine structure clearly. The driving field drives the transition well off-resonance ($\delta_x \sim 20$ MHz) which produces the Rabi transition around the 24 MHz region. The misaligned probe field then shows both the EPR Mollow (well off resonance), as well as the Rabi transition. Note that this signal is an amplitude signal, and the detection is not phase sensitive. Notice also that the Rabi transition reflects the hyperfine structure of the EPR transition since the driving field is, in effect, driving three separate transitions, which each produce a separate Rabi transition. It is just this kind of structure that the particular 'sweet spot' from above seeks to minimise.

4.3 Driving the Rabi transition

Now that the Rabi transition has been established (it has been observed before, in [43],[44]) it is now time to move on to the central idea of this thesis, where the transition is driven by a $\hat{z}$ polarised field, and the effects are observed on both the Rabi transition, and on the original transition. Firstly, the Rabi transition itself will be probed, showing that the expected Mollow type spectrum is indeed produced in line with theoretical expectations. Then, the EPR transition will be revisited, showing the doubly driven transition effects.

4.3.1 The Driven Rabi Transition

In Fig 4-4, a Rabi transition is shown in trace (a). The original bare EPR transition had a resonance frequency of 73 MHz, and an inhomogeneous linewidth of the order of 2 MHz. Field$_x$ was applied of Rabi frequency 10.2 MHz and frequency 76 MHz (i.e. $\delta \sim -3$ MHz). In the case of a negatively detuned pump, there is more population in the higher Dressed State (fig 3.2) and so the Rabi transition is emissive in nature, and is centred at 10.6 MHz, with a linewidth of $\sim$ 400 kHz. A weak, $\hat{z}$ polarised probe is used to gather the probe absorption spectrum.

Once the Rabi transition is established, a Field$_z$ of increasing power is applied to the transition, to observe the dynamics of the Rabi transition. The field is applied with frequency $\omega_z \sim 11$ MHz as indicated by the dot in the Fig 4-4(a). As the power is increased moving down the figure (b)-(g), the expected Mollow spectrum emerges, as predicted by the theoretical treatment. This Mollow spectrum exhibits clear spectral features at $\omega_z \pm \Omega_z$ where Ω_z is the generalised Rabi frequency of Field$_z$. This gives direct observation then of the emergence of the doubly dressed states, and the peaks evident are due to transitions between the doubly dressed states. For instance, the transition in (g) on the high side (i.e.. at $\omega_z + \Omega_z$) is due to transitions between the $|\beta, n, m\rangle$ and $|\alpha, n, m-1\rangle$. The transition is absorptive since the negatively detuned Field$_z$ gives rise to a higher population is $|\alpha, n, m-1\rangle$ than $|\beta, n, m\rangle$, as is illustrated in Fig 3.2.

This demonstrates the first clear support for the idea of treating the Rabi transition as any other TLA. Other predictions include the emergence of the Rabi of the Rabi transition, and the further splitting of the original EPR transition. In Fig 4-5, the dynamics of scanning Field$_z$ through the Rabi transition is presented, in a manner similar to the numerical calculation

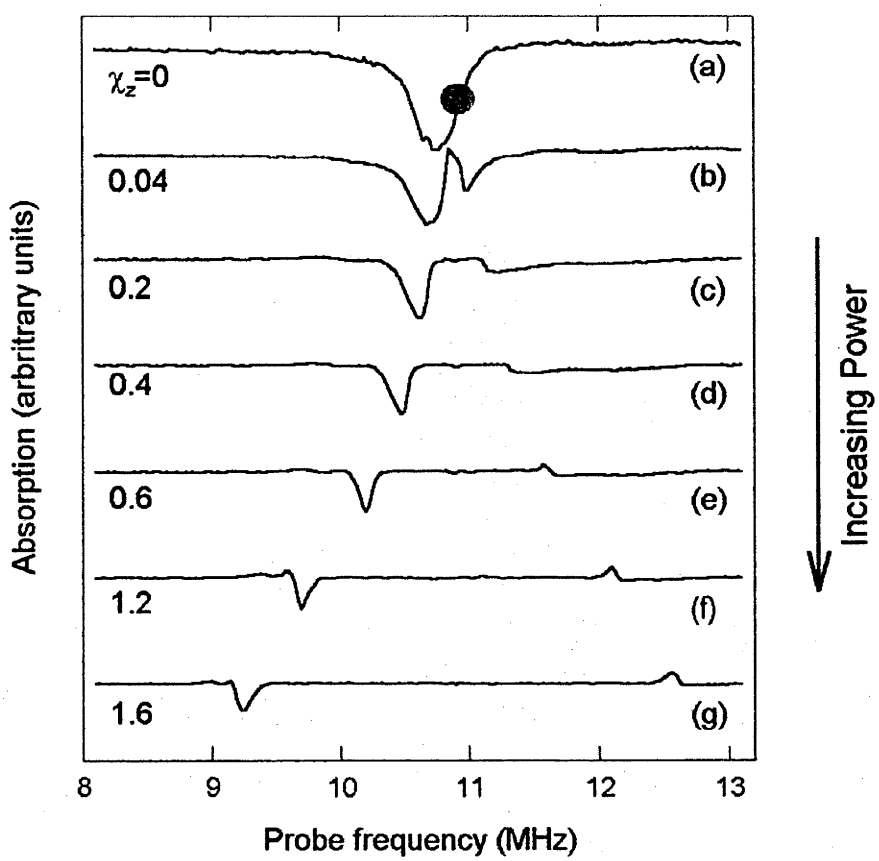

Figure 4-4: The probe absorption spectrum in the region of the Rabi transition. The Rabi transition at 10.5 MHz, shown in (a), is driven by a z polarised field ($\delta = -0.4$ MHz) of increasing strength in (b) - (g). The Rabi frequencies of the $\hat{z}$ pump are given. The spectrum exhibits the familiar AC Stark splitting. Small spectral features on the low frequency side of the left hand Mollow side band are due to hyperfine interactions which have been neglected in the analysis.

presented in chapter 3.

Here, the Rabi transition is clearly seen to undergo Mollow splitting as Field$_z$ is scanned through the transition. Also, the higher order transitions are evident as discussed in Chapter 3. In particular, higher order interactions can be seen where Field$_z$ interacts with the Rabi of the Rabi, Rabi^2(point B) and also the Rabi^3 and Rabi^4 at (C) and (D) in the experiment. These interactions are beyond the resolution of the numerical simulation, but can clearly be seen in the experimental trace.

Tracing up from the bottom of the graph, where $\omega_z \sim 1$ MHz, Field$_z$ is scanned upwards in frequency. Field$_z$ interacts with the original Rabi transition, producing the Mollow spectrum. It also generates the Rabi of the Rabi (or Rabi^2). Field$_z$ then also interacts with Rabi^2, which then generates its own Rabi transition, Rabi^3. Up to the resolution of the experiment, then, Field$_z$ also interacts with Rabi^3 to produce Rabi^4. This cascade would continue indefinitely, however here only the first four orders are seen. As Field$_z$ is scanned upwards in frequency, the Rabi transitions fan out, and at $\omega_z \sim 2$ MHz (marked as D in the figure), Field$_z$ is resonant with Rabi^4, and there is some evidence of AC Stark splitting in the transition. Note that splitting this Rabi^4 transition also causes the lower order Rabi transitions to split. Likewise, at (C), Field$_z$ is resonant with Rabi^3 ($\omega_z \sim 2.6$ MHz) and splitting of all of the resonances is again evident (a little stronger than previously). Moving Field$_z$ along, the clearest example of this splitting is seen when Field$_z$ interacts with Rabi^2, the Rabi of the Rabi, at $\omega_z \sim 4.5$ MHz. The Mollow sidebands can be clearly seen, and the effect that it has on the standard Mollow sidebands is evident as further splitting. Finally, the standard Mollow spectrum associated with the Rabi transition can be clearly seen, with the AC Stark splitting going along lines that are entirely familiar from standard TLA studies.

Clearly, then, the experimental situation is sufficiently sensitive to resolve very high order interactions. These interactions have been examined previously in Chapter 3 as a natural extension of the doubly dressed state model. They arise because the Field$_z$ can interact not only with the Rabi transition, but also with the Rabi of the Rabi (Rabi^2), Rabi^3, Rabi^4 and so on. Theoretically, these interactions are more evident in the high power numerical calculation demonstrated in chapter 3. This is clear experimental evidence of not only doubly dressed states as outlined in this thesis, but triply (where the Rabi of the Rabi is split), quadruply

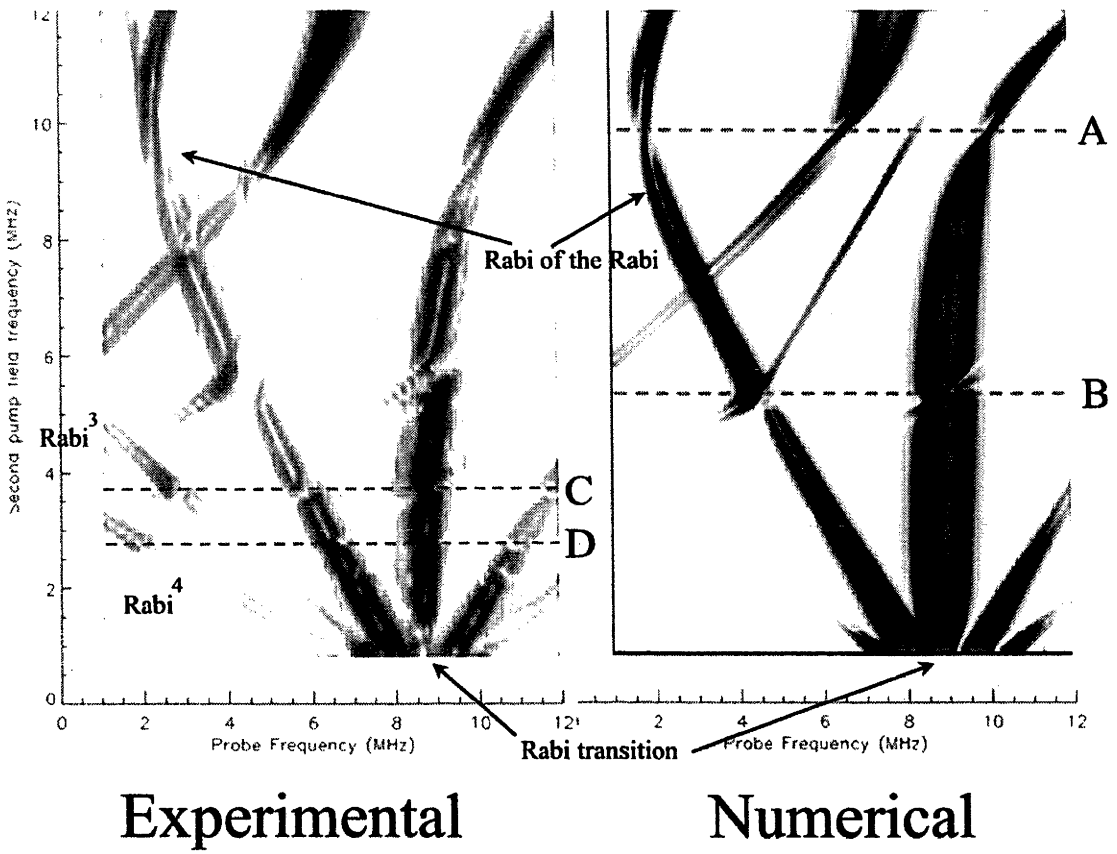

Figure 4-5: The dyanamics of the driven TLA. The left hand figure is experimental data, where Field$_z$ (χ_z~2 MHz) is scanned through the Rabi transition at 8.5 MHz. The weak probe absorption spectra are then taken for each of the Field$_z$ frequencies, and the plot shows a 'top' down view of the graphs. The right hand graph is then the numerical simulation of the same scenario. (A) shows where Field$_z$ is resonant with the Rabi transition, and (B) is where Field$_z$ is resonant with the Rabi of the Rabi, producing higher order splittings. In (C) Field$_z$ is resonant with Rabi^3 and in (D) Field$_z$ is resonant with Rabi^4.

(Rabi^3 split) and even quintuply (Rabi^4 split) dressed states. These could be modelled by a straightforward (if laborious) extension of the theoretical basis of this thesis, but these effects are certainly fully consistent with the theoretical predictions made to date within this work, as discussed in chapters 2 and 3.

To extend this idea further, an experiment was performed where the TLA was driven by three pump fields, one Field$_x$ and two Field$_z$'s. The initial EPR TLA ($\omega_0 = 66$ MHz) is driven by Field$_x$ ($\Omega_x \sim 10$ MHz, $\omega_x = 69$ MHz) which produces a Rabi transition at 10 MHz (seen in Fig 4-6(i)). Again, the transition is emissive in nature, since there is more population in the higher dressed state. Field$_z$ is then applied, slightly off resonance in Fig 4-6(ii). The Mollow spectrum is produced, with the expected behaviour in terms of populations. Also, a clear signal at the Rabi of the Rabi is observed at 1.8 MHz. Now a third pump field is applied, Field$_{zz}$, slightly detuned from the Rabi of the Rabi. This again shows a different way to generate the higher order dressed states. Previously, the interaction of Field$_z$ with the Rabi of the Rabi was strong enough to produce observable splitting when Field$_z$ was sufficiently close to the Rabi of the Rabi. In the circumstance, Field$_z$ will have only a very minor interaction with the Rabi of the Rabi, which can be effectively ignored. However, Field$_{zz}$ interacts directly with the Rabi of the Rabi, splitting it to produce triply dressed states, as seen in Fig 4-6(iii). The Rabi of the Rabi shows standard AC Stark splitting behaviour, and the Mollow spectrum associated with the Rabi transition is further split to produce six peaks.

Using an intuitive extension of the theory already proposed in this thesis, the peaks can be explained by referring to Fig 4-7. Here, the proposed energy level scheme is shown. The width of the lines denotes the populations. The singly dressed and doubly dressed state populations are known from the theoretical considerations in this thesis, and the proposed populations for the triply dressed states are then a natural extension to this theory. As can be seen, the peaks in Fig 4-6(iii) can be understood as transitions between the triply dressed states, with the population differences giving the sign of the transition. In the energy level diagrams, the red arrows refer to the two transitions ($\omega_p = \omega_{zz} \pm \Omega_{zz}$) associated with the split Rabi of the Rabi resonance, and the two blue arrows refer to the highest frequency peaks ($\omega_p = \omega_z + \omega_{zz} \pm \Omega_{zz}$) in the Fig 4-6(iii). The direction of the arrows indicates whether the transition is absorptive (upwards) or emissive (downward) in nature.

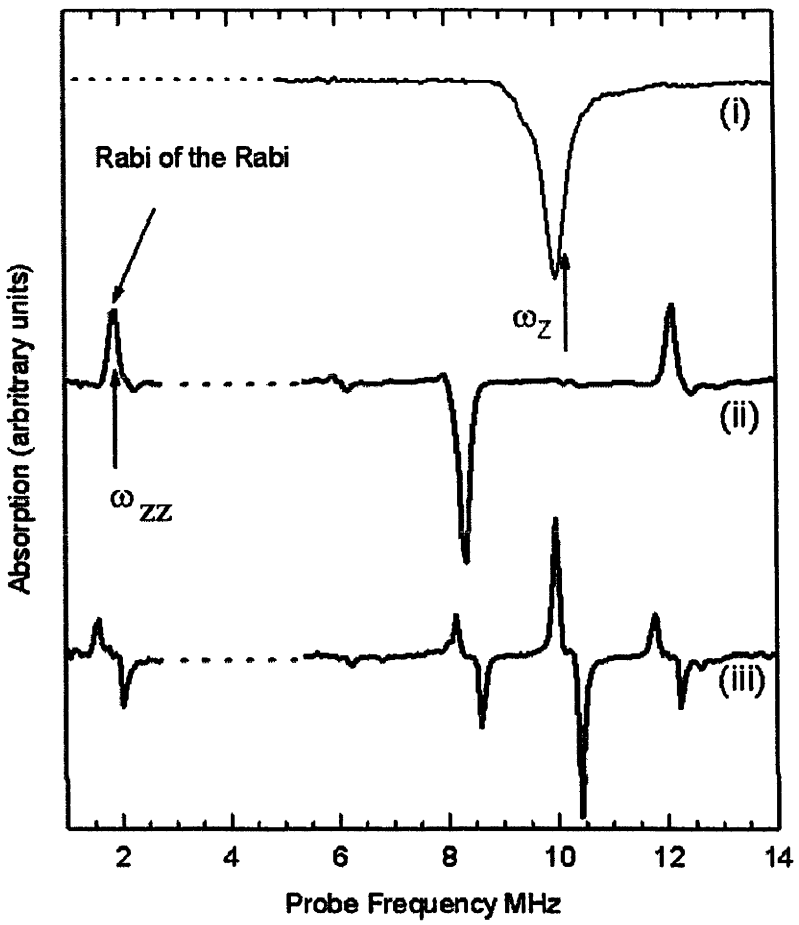

Figure 4-6: The Rabi transition, probed with a $\hat{z}$ polarized weak field. (i) the undriven Rabi transition at $\sim$ 10 MHz, where the dotted line indicats there are no spectral features of interest, (ii) the Rabi transition is driven by a $\hat{z}$ pump ($\delta_z \sim -0.5$ MHz, $\Omega_z \sim 1.8$ MHz), with its frequency indicated by an arrow in (i). The Rabi of the Rabi is highlighted at ~ 1.8 MHz and (iii) the Rabi of the Rabi is driven with a second $\hat{z}$ pump ($\delta_{zz} \sim 100$ kHz, $\Omega_{zz} \sim 200$ kHz), with its frequency indicated by an arrow in (ii).

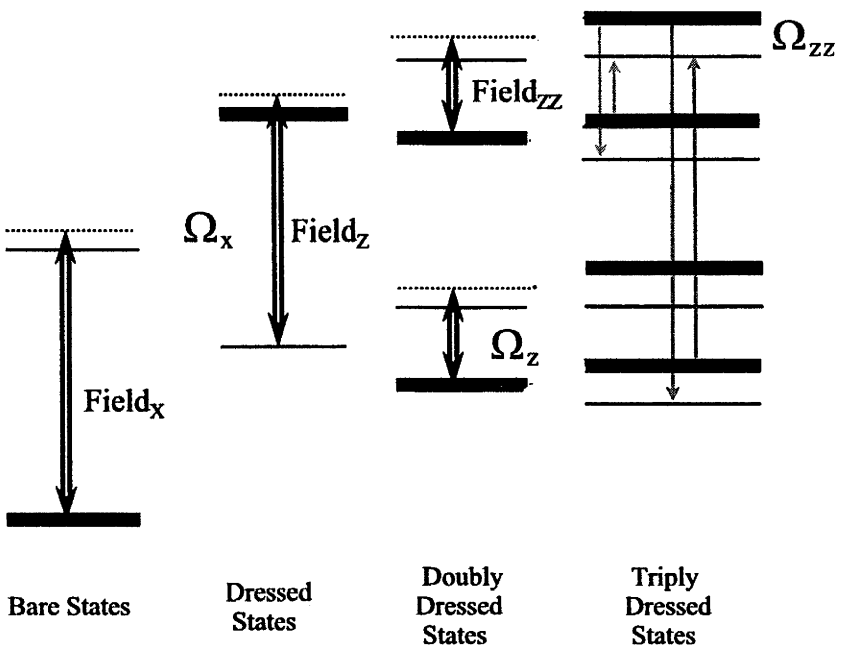

Figure 4-7: The energy level diagram for the triply dressed states. Field$_x$ is applied to the original transition, producing the Rabi transition, then Field$_z$ is applied to that. This produces the Rabi of the Rabi (from the Doubly Dressed States). A third pump field, Field$_{zz}$ (frequency ω_{zz}, Rabi frequency χ_{zz}) is applied to the Rabi of the Rabi transition, producing the triply dressed states. The width of the lines indicates the size of the populations, the thicker lines referring to the fact that the energy level has higher population. The red arrows show the Rabi of the Rabi Mollow transitions, the blue arrows show the two highest frequency transitions generated at the Rabi frequency.

To gauge the accuracy of this intuitive study, examine the Bloch equations modelling the 3 strong pump case (Field_{zz}, Field_z, Field_x),

$$\begin{aligned}\frac{d}{dt}\tilde{\rho}_{ge} &= \left\{i\left(\delta_x + 2\chi_z\cos\omega_z t + 2\chi_{zz}\cos\omega_{zz}t\right) - \Gamma\right\}\tilde{\rho}_{ge} - i\frac{\chi_x}{2}W \\ \dot{W} &= i\chi_x\left(\tilde{\rho}_{eg} - \tilde{\rho}_{ge}\right) - \Gamma\left(W - W^{eq}\right)\end{aligned}$$

where ω_{zz} and χ_{zz} are the frequency and Rabi frequency of the second pump field nearly resonant with Rabi of the Rabi. The rest of the terms are defined as they would be throughout this work. Transforming to the semiclassical dressed state basis;

$$\begin{aligned}\dot{\rho}_{12} &= i\left(\Omega_x + 2\chi_z''\cos\omega_z t + 2\chi_{zz}''\cos\omega_{zz}t - \Gamma\right)\rho_{12} \\ &\quad -i\chi_z'\cos\omega_z t W_d - i\chi_{zz}'\cos\omega_{zz}t W_d - \rho_{12}^{eq} \\ \dot{W}_d &= 2i\chi_z'\cos\omega_z t\left(\rho_{21} - \rho_{12}\right) + 2i\chi_{zz}'\cos\omega_{zz}t\left(\rho_{21} - \rho_{12}\right) - \Gamma\left(W_d - W_d^{eq}\right)\end{aligned}$$

where

$$\begin{aligned}\chi_{zz}' &= -\sin 2\theta\chi_{zz} = -\frac{\chi_x}{\Omega_x}\chi_{zz} \\ \chi_{zz}'' &= \cos 2\theta\chi_{zz} = \frac{\delta_x}{\Omega_x}\chi_{zz}\end{aligned}$$

Now, since Field_z is nearly resonant with the Rabi transition, and well detuned from the Rabi of the Rabi, and vice versa for Field_{zz}, the terms proportional to χ_z'' and χ_{zz}' can be discarded as they refer to interactions with non-resonant transitions. After transforming to the rotating frame and taking the RWA, the resultant Bloch equations are

$$\frac{d}{dt}\tilde{\rho}_{12} = i\left(\delta_z + 2\chi_{zz}''\cos\omega_{zz}t - \Gamma\right)\tilde{\rho}_{12} - i\frac{\chi_z'}{2}W_d - \rho_{12}^{eq}e^{-i\omega_z t} \tag{4.3a}$$

$$\dot{W}_d = i\chi_z'\left(\tilde{\rho}_{21} - \tilde{\rho}_{12}\right) - \Gamma\left(W_d - W_d^{eq}\right) \tag{4.3b}$$

It is now clear that it is possible to proceed from here to solve for the dynamics of this system. The above equations are transformed to the doubly dressed states, leading to

$$\begin{aligned}
\dot{\rho}_{\alpha\beta} &= \left(i\Omega_z + 2\cos 2\phi\chi''_{zz}\cos\omega_{zz}t - \Gamma\right)\rho_{\alpha\beta} + i\sin 2\phi\chi'_{zz}\cos\omega_{zz}tW_{dd} \\
&\quad -\rho^{eq}_{\alpha\beta} - \left(P_- e^{-i\omega_z t} - P_+ e^{i\omega_z t}\right) \\
\dot{W}_{dd} &= -\Gamma\left(W_{dd} - W^{eq}_{dd}\right) + w^r\left(e^{i\omega_z t} + e^{-i\omega_z t}\right) - 2i\sin 2\theta\chi'_{zz}\cos\omega_{zz}t\left(\rho_{\beta\alpha} - \rho_{\alpha\beta}\right)
\end{aligned}$$

The term proportional to $\cos 2\phi\chi''_{zz}$ refers to the interaction of Field_{zz} with the Rabi transition generated by the interaction of the field with the Rabi of the Rabi. There are clearly further cascade effects from the interaction of this second field with the Rabi of the Rabi - as discussed above. To proceed, this interaction is ignored, and a transformation to the rotating frame is performed, with the RWA applied. Defining the term

$$\begin{aligned}
\tilde{\chi}_{zz} &= -\sin 2\phi\chi'_{zz} \\
\delta_{zz} &= \Omega_z - \omega'_z \\
\rho_{\alpha\beta} &= e^{i\omega_{zz}t}\tilde{\rho}_{\alpha\beta}
\end{aligned}$$

the final form of the equations is then

$$\begin{aligned}
\frac{d}{dt}\tilde{\rho}_{\alpha\beta} &= \left(i\delta_{zz} - \Gamma\right)\tilde{\rho}_{\alpha\beta} - \frac{i}{2}\tilde{\chi}_{zz}W_{dd} - \left(\rho^{eq}_{\alpha\beta} + P_- e^{-i\omega_z t} - P_+ e^{i\omega_z t}\right)e^{-i\omega_{zz}t} \\
\dot{W}_{dd} &= i\tilde{\chi}_{zz}\left(\tilde{\rho}_{\beta\alpha} - \tilde{\rho}_{\alpha\beta}\right) - \Gamma\left(W_{dd} - W^{eq}_{dd}\right) + w^r\left(e^{i\omega_z t} + e^{-i\omega_z t}\right)
\end{aligned}$$

This is then solved by transforming to the *triply dressed states*, defined by

$$\begin{aligned}
|\Sigma\rangle &= \cos\psi\,|\alpha\rangle - \sin\psi\,|\beta\rangle \\
|\Pi\rangle &= \sin\psi\,|\alpha\rangle + \cos\psi\,|\beta\rangle
\end{aligned}$$

with the definitions

$$\cos 2\psi = \frac{\delta_{zz}}{\Omega_{zz}} \qquad \sin 2\psi = \frac{\tilde{\chi}_{zz}}{\Omega_{zz}}$$

where

$$\Omega_{zz}^2 = \delta_{zz}^2 + \tilde{\chi}_{zz}^2$$

is the frequency of the Rabi transition generated by the interaction of Field_{zz} with the Rabi of the Rabi. The general form of the Bloch equations under this transformation is then

$$\begin{aligned}
\dot{\rho}_{\Sigma\Pi} &= (i\Omega_{zz} - \Gamma)\,\rho_{\Sigma\Pi} + \sum_{k,l=-1,1} \rho_{\Sigma\Pi}^{k,l} e^{ki\omega_z t} e^{il\omega_{zz} t} \\
\dot{W}_{ddd} &= -\Gamma\left(W_{ddd} - W_{ddd}^{eq}\right) + \sum_{k,l=-1,1} W_{ddd}^{k,l} e^{ki\omega_z t} e^{il\omega_{zz} t}
\end{aligned}$$

where W_{ddd} refers to the population difference between the triply dressed states. The actual coefficients are not relevant to this study, but their values can be easily calculated by transforming the above equations. This equilibrium population difference is then given by

$$\begin{aligned}
W_{ddd}^{eq} &= \cos 2\psi \cos 2\phi \cos 2\theta W^{eq} \\
&= \frac{\delta_{zz}\delta_z\delta_x}{\Omega_{zz}\Omega_z\Omega_x} W^{eq}
\end{aligned}$$

Since $\delta_{zz}, \delta_z, \delta_x, W^{eq}$ are all negative in this experiment, then W_4^{eq} is positive, that is, there is more population in the upper triply dressed state than the lower one, as is reflected in Fig 4-7. Clearly, a similar analysis to that carried out in Chapter 3 would yield the probe absorption spectrum for this transition. However, the solution should be treated with some caution. The Rabi of the Rabi in the above experiment was only at a frequency of 2 MHz. As the frequencies of the transitions get smaller, the validity of the Rotating Wave Approximation starts to come into doubt, however there might be some value to the calculation as a future direction. It is clear from the form of the above equations, however, that at least an intuitive grasp of

what is happening is immediately apparent from the symmetry of the equations at the various interaction levels.

It should also be noted that the above equations can also be adapted for the case where the interaction of a single Field$_z$ with the Rabi transition, and the Rabi of the Rabi, are included. To see this, examine the Bloch equation for one Field$_z$ where the transformation for the first dressed state basis has been performed, and the further transformation to the rotating frame (with RWA) has been done:

$$\begin{aligned} \frac{d}{dt}\tilde{\rho}_{12} &= i\left(\delta_z + 2\chi_z'' \cos\omega_z t - \Gamma\right)\tilde{\rho}_{12} - \frac{i}{2}\chi_z' W_d - \rho_{12}^{eq} e^{-i\omega_z t} \\ \dot{W}_d &= i\chi_z'\left(\tilde{\rho}_{21} - \tilde{\rho}_{12}\right) - \Gamma\left(W_d - W_d^{eq}\right) \end{aligned}$$

In this case, the interaction of Field$_z$ with the Rabi of the Rabi remains (the term proportional to χ_z''). Comparing this with Eq 4.3a,4.3b it is clear that the triply dressed states will also provide a solution for the dynamics of this situation if it were to be pursued..

It is clear, then, that the interaction of the $\hat{z}$ polarised fields provide a rich set of dynamics, that can be intuitively understood, as well as being successfully theoretically modelled using the triply, and even higher, dressed state bases. A $\hat{z}$ polarised field interaction with the Rabi transition can be described as a cascade effect. Field$_z$ interacts with the Rabi transition, to produce the Rabi of the Rabi. It also interacts with that, producing Rabi^3, and then it interacts with that, producing Rabi^4 and so on. These interactions can be observed experimentally to the fourth order, which implies the existence of quintuply dressed states. These could be successfully modelled by extending the theoretical ideas in this thesis. This modelling has been demonstrated to at least the triply dressed states, but it is clear it could be easily extended.

4.4 Doubly Driven EPR Transition

So far, the experimental data has focused on the Rabi transition. As was explained in the theoretical analysis of the problem, interactions at the Rabi transition will also produce higher order interactions in the original transition. The original Mollow spectrum will be further split by the interaction of Field$_z$ with the Rabi transition. In this section, the EPR transition will be

examined. Because of the hyperfine structure in the EPR transition (hyperfine structure which is quenched in the Rabi transition) it is much harder to get a clean signal with the apparatus for the EPR transition, however it was possible to at least illustrate the major points raised in the theoretical section, and to provide a good comparison with theoretical predictions.

The basic experiment is then to apply Field$_x$ to the bare transition, so that the probe absorption spectrum shows the standard Mollow spectrum. The second pump, Field$_z$, is applied to the system via the second coil in the apparatus, and the effects on the probe absorption spectrum can be observed. The results are seen in Fig 4-8.

The semiclassical analytical theory as outlined in chapter 3 is used to generate the theoretical plots. In (i), the original EPR transition is shown. The right hand side of the peak is wider due to the hyperfine structure discussed earlier. Field$_x$ is applied between these two peaks ($\delta_x \sim -3$ MHz, $\Omega_x \sim 10.5$ MHz) to produce the standard AC Stark spectrum in (ii). Finally, Field$_z$ is applied to the $\hat{z}$ polarised coil, ($\delta_z \sim -1$ MHz, $\Omega_z \sim 2.7$ MHz) which results in the extra structure observable in (iii). As is well understood at this stage, this structure arises from transitions between the doubly dressed states. For instance, the transition at $\omega_p = \omega_x - \omega_z - \Omega_z$ (the left-most peak in the spectrum) is due to transitions between the $|\alpha, n, m-1\rangle$ and $|\beta, n-1, m\rangle$ dressed states. Since in this scenario the population is higher in the $|\alpha, n, m\rangle$ dressed states, the transition is emissive in nature.

In Fig 4-9 the results of a further experiment are shown where Field$_z$ is scanned through the Rabi transition. The EPR resonance is at ~71 MHz, and Field$_x$ is applied with frequency of 76 MHz ($\delta_x \sim -5$ MHz) and Rabi frequency $\chi_x \sim 7.5$ MHz. This results in a Rabi transition at $\Omega_x = 9$ MHz. For this experiment, Field$_z$ is scanned through the Rabi transition from $\omega_z = 8$ MHz through to $\omega_z = 12$ MHz, and the EPR dispersion spectrum is provided. Beneath the experimental trace, the analytical results are presented.

The theoretical results produce excellent agreement, except in the on-resonance case, at $\omega_z = 9$ MHz, where clear signals are visible. This is a good example of the hyperfine structure causing spurious signals, as discussed at the beginning of the chapter. To understand this, examine the original EPR transition used in this experiment, Fig 4-10. Here, a clear hyperfine structure is seen. The three transitions are labelled as (i),(ii) and (iii). Below, a schematic diagram shows the relative positions of the Rabi transitions that would be independently generated by

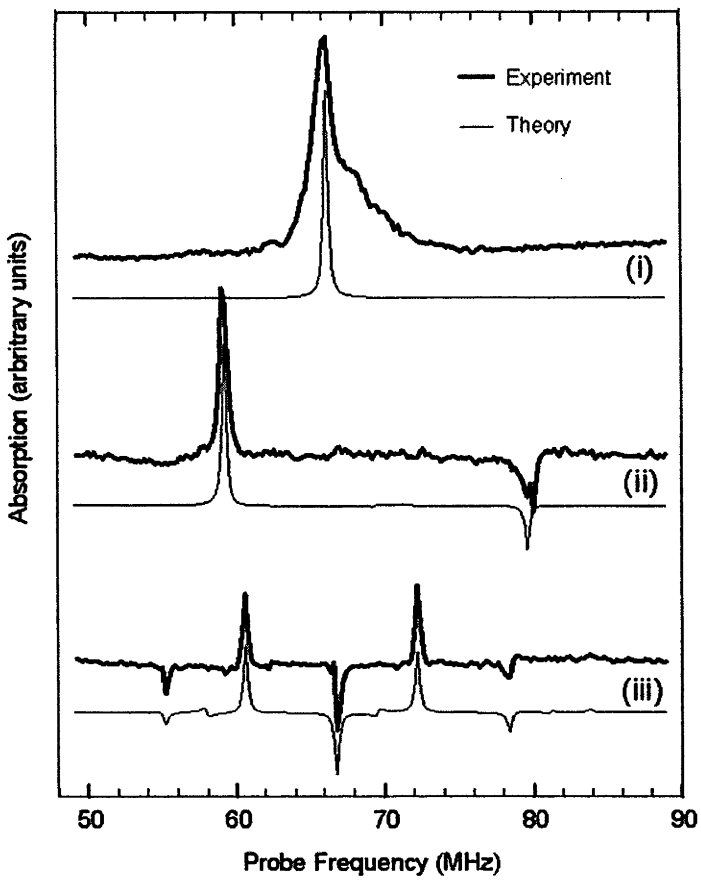

Figure 4-8: The EPR $\hat{x}$ polarized probe absorption spectrum: (i) with no $\hat{x}$ or $\hat{z}$ pump fields where the shoulder on the high frequency side of the major resonance at 66 MHz is due to weaker hyperfine features at 68 and 70 MHz, (ii) with an $\hat{x}$ pump ($\delta_x \sim -3$ MHz, $\Omega_x \sim 10.5$ MHz) midway between the two weak hyperfine lines, (iii) $\hat{x}$- plus $\hat{z}$-polarized pump ($\delta_z \sim -1$ MHz, $\Omega_z \sim 2.7$ MHz). The thick line gives the experimental results, and the thin line the theoretical results using the doubly dressed states for a single, homogeneously broadened EPR line. The extra structure in some of the features of the driven spectra is due to the neglected hyperfine lines.

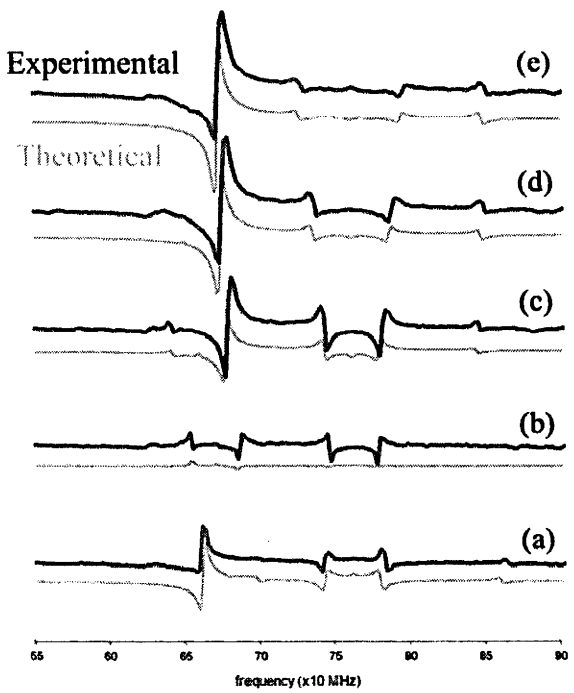

Figure 4-9: Comparison of experimental and theoretical dispersion plots for the EPR experiment where Field$_z$ is scanned through the Rabi frequency. EPR transition ($\omega_0 = 71$ MHz) is driven by Field$_x$ ($\omega_x = 76$ MHz, $\chi_x = 7.5$ MHz) producing a Rabi transition at 9 MHz. Field$_z$ ($\chi_z = 1.8$ MHz) is scanned through the transition; (a) $\omega_z = 8$ MHz, (b) 9 MHz, (c) 10 MHz, (d) 11 MHz, (e) 12 MHz.

these transitions, with their relative sizes. When Field$_z$ is on resonance with the largest Rabi transition (at 9 MHz), the EPR signal due to that transition is very small, as can be seen by the theoretical trace in Fig 4-9(b). However, Field$_z$ is now negatively detuned with respect to the smaller 'hyperfine' Rabi transitions labelled by (ii). Since the on resonance signal is so tiny, there is a significant signal generated at the EPR transition by this interaction as seen in Fig 4-9(b). The rest of the time, the signal due to Field$_z$ interacting with the (i) Rabi transition dominates because of the relative sizes of the Rabi transitions.

Other features to note in the experiment are the pair of central peaks, which tend to be very well defined, and are clearly separated by $2\Omega_z$, which changes as the detuning of Field$_z$ changes as the field scans through the transition. Note the sign change in the spectrum as Field$_z$ goes from being positively detuned ($\delta_z > 0$) to negatively detuned ($\delta_z < 0$). This is due to the fact that the populations in the doubly dressed states shift from being predominantly in the upper state $|\beta, n, m\rangle$ to the lower state $|\alpha, n, m\rangle$ as expected from the theoretical treatments.

As can be seen, there is excellent agreement with theoretical predictions from the semiclassical model. Clearly, the emergence of the dressed states, and then the doubly dressed states, is predicted and observed. The hyperfine structure causes interference of the spectra near the resonance condition, both in the Rabi and EPR transitions.

4.5 Autler-Townes Spectra

As previously seen, there is hyperfine structure within the EPR transition. The hyperfine structure arises from Nuclear Magnetic Resonance transitions within the N-V centre. These transitions can be used as TLAs in themselves. While the NMR transitions do not themselves have the hyperfine structure that complicates the EPR signals, the Rabi signal cannot be directly observed, which does make the transition less useful than the EPR one for this experiment. They are however particularly useful for performing Autler-Townes type experiments. Fig 4-11 shows the hyperfine structure of the EPR spin 0 state with the Autler Townes configuration indicated.

For the purposes of this experiment, it is quite difficult to generate the Rabi transition since it was found that in general, the NMR transition only has a very small permanent dipole

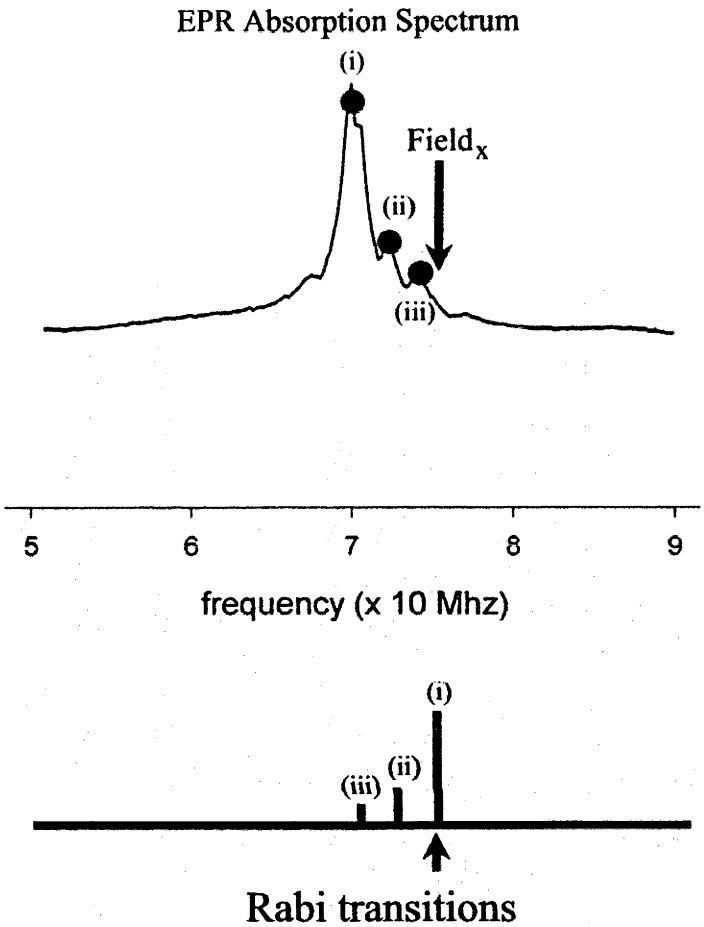

Figure 4-10: At the top, the original, undriven, EPR probe absorption spectrum is shown, with the three main hyperfine levels indicated by dots, with frequencies of (i) 71 MHz, (ii) 73 Mhz and (iii) 75 MHz. The frequency of Field$_x$ in the experiment is indicated. Below, a schematic showing the relative positions of the Rabi transitions generated by each of the transitions (due to the differing detunings of Field$_x$). The arrow indicates the on resonance Field$_z$ position ($\omega_z = 9$ Mhz).

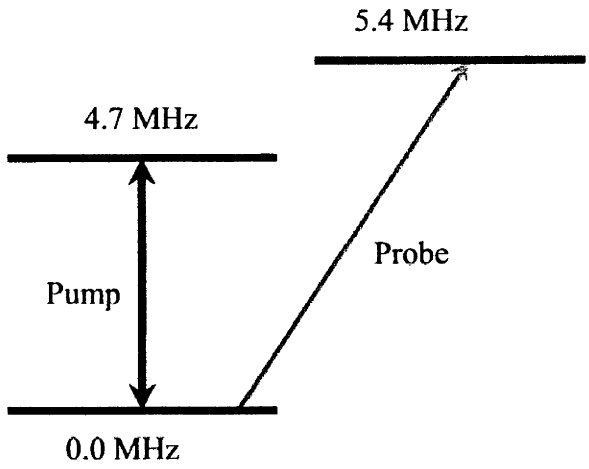

Figure 4-11: A schematic of the Autler Townes scenario for the hyperfine structure associated with the spin 0 EPR state. A pump field interacts with the 4.7 MHz transition, which is then probed via the 5.4 MHz transition.

moment. This was demonstrated by changing the static magnetic field within the cryostat, and it was observed that the NMR transition hardly moved, whereas the EPR transition exhibited large amounts of movement. However, by misaligning the static magnetic field with respect to the N-V centre's axis of symmetry [61]-[62], sufficient mixing of the EPR states could induce enough of a permanent dipole moment to allow the experiment to proceed.

The results for the Autler Townes experiment are shown in Fig 4-12. Here, a resonant Field_x is applied to the 4.7 MHz transition. The Rabi was not directly observable due to the high levels of noise that are present in the system at low frequencies, however it was measured (by the peak separation) to be 240 kHz. Field_z was applied at this frequency, and the doubly dressed state splitting then became evident, with a measured $\Omega_z = 20$ kHz. This provides a clear signal without being concerned with the hyperfine structure generating spurious signals, and it is clearly in-line with the fully quantum-mechanical calculation performed in Chapter 2.

The structure can easily be understood by referring to the doubly dressed energy level diagram for the Autler Townes scenario in section 2.5.2. Field_x splits the original transition, and gives rise to the Rabi transition, which is then further split into the doubly dressed states by the addition of Field_z to the Rabi transition. This experiment provides, once again, very clear evidence of the emergence of the doubly dressed states as postulated in the thesis, and

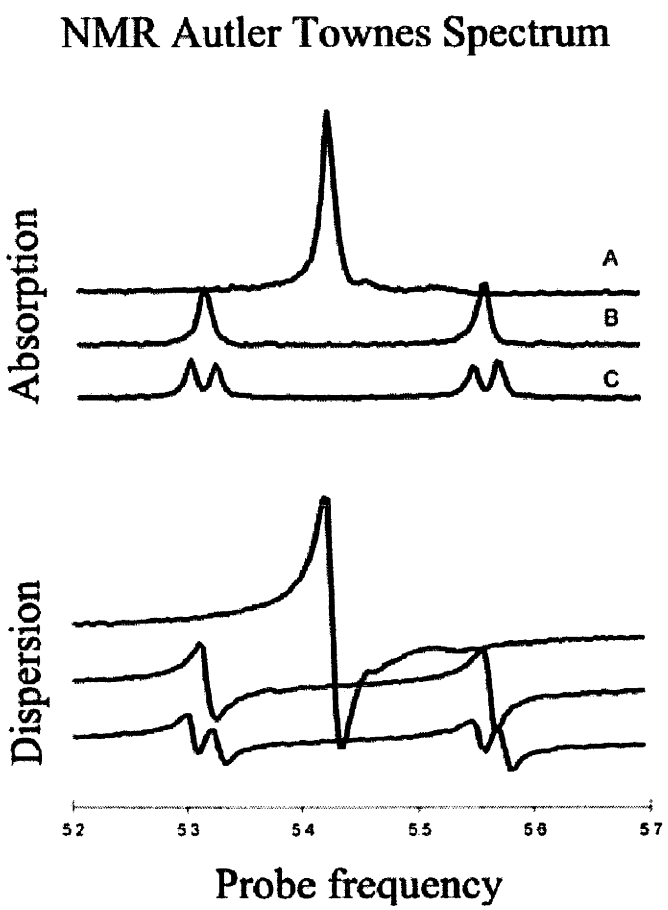

Figure 4-12: The Autler-Townes probe absorption and dispersion spectra. In (A), the original transition at ~5.4 MHz is seen. An on resonance pump field is applied, with $\chi_x = 240$ kHz in (B), causing the familiar Autler-Townes structure to emerge. Finally, Field$_z$ is applied to the Rabi transition with $\chi_z = 20$ kHz and the emergence of the doubly dressed states is then clear from (C).

the spectra are in excellent agreement with the fully quantum mechanical results outlined in Chapter 2.

4.6 Summary

In summary, this chapter presented the experimental results that have been produced in the EPR and NMR systems in the N-V Centre. The effects of doubly driving the system, with one Field_z and one Field_x have been demonstrated in the EPR, NMR and Rabi transitions, and all have been found to be in excellent agreement with theoretical predictions. Further interactions with the Rabi of the Rabi, Rabi^3 and Rabi^4 have been observed, via a cascaded effect where Field_z interacts with multiple higher order resonances. Also a third pump field has been applied to the Rabi of the Rabi, which resulted in further splitting. This is evidence for the theoretically intuitive idea of triply, quadruply and quintuply dressed states, and there was a demonstration that the theoretical treatment outlined in the thesis could be easily extended to take into account these higher order interactions.

Chapter 5

Conclusion

In this thesis, a new analysis of the doubly driven TLA is presented. It has been shown previously that when a driven TLA has a permanent dipole moment, a transition at the generalised Rabi frequency of Field_x is present, and it can be probed by a $\hat{z}$ polarised field. This transition, the Rabi transition, behaves as a TLA in its own right. In fact, this new TLA can be driven by a Field_z, and the probe absorption spectrum of this doubly driven system exhibits behaviour that is a natural extension of the standard TLA. Analytical analysis is possible if the doubly dressed states are introduced. These states, a natural extension of the well known singly dressed states, provide a powerful picture of the Rabi transition. Both the fully quantum mechanical and the semiclassical analysis are presented. Theoretical extensions could easily be applied to this theory, as demonstrated by the analysis at the end of chapter 2. Higher order interactions also became evident, and it was seen that Field_z not only interacts with the Rabi transition, but it also interacts with the Rabi of the Rabi, Rabi^3, Rabi^4 and so on indefinitely. The theoretical framework could be easily extended to include these higher order interactions. Finally, the theoretical predictions were experimentally verified in the N-V Centre in diamond. Several experiments were presented, including the doubly driven case as analysed in this thesis, and these showed excellent agreement with theoretical predictions. Also, a novel triply driven system was shown, where a third field drove the Rabi of the Rabi transition, and it was demonstrated that the concept of triply driven states might be able to model this situation successfully.

Chapter 6

Appendix - the complete solution for the doubly driven TLA

In this appendix, the complete solution for the dynamics of the doubly driven atom is presented. In this case, as described in Chapter 3, one strong pump (Field_x) is applied to the original transition and another pump, Field_z, is applied to the Rabi transition produced by Field_x. The results are broken down into two sections, firstly where the system is probed with a $\hat{z}$ polarised probe field, to provide the spectrum for the split Rabi transition. The second section presents the results for the $\hat{x}$ polarised probe field, to show the double splitting of the original transition.

6.1 $\hat{z}$ polarised probe field

The procedure to produce the probe absorption spectrum is well documented in Chapter 2. Here, the results will simply be presented. The probe absorption spectrum is given by

$$\begin{aligned} W^{0,1} = & -\sin 2\theta \left(\cos^2\phi \rho_{\alpha\beta}^{-1,1} L_{-1,1}^{-} - \sin^2\phi \rho_{\beta\alpha}^{-1,1} L_{-1,1}^{+} + \frac{1}{2}\sin 2\phi w^{-1,1} L_{-1,1} \right) \\ & -\sin 2\theta \left(-\sin^2\phi \rho_{\alpha\beta}^{1,1} L_{1,1}^{-} + \cos^2\phi \rho_{\beta\alpha}^{1,1} L_{1,1}^{+} + \frac{1}{2}\sin 2\phi w^{1,1} L_A \right) \\ & +\cos 2\theta \left(-\sin 2\phi \left(\rho_{\alpha\beta}^{0,1} L_{0,1}^{-} + \rho_{\beta\alpha}^{0,1} L_{0,1}^{+} \right) + \cos 2\phi w^{0,1} L_{0,1} \right) \end{aligned}$$

with the notation

$$\begin{aligned} L^{\pm}_{k,l} &= L\left(k\omega_z + l\omega_p \pm \Omega_z\right) \\ L_{k,l} &= L\left(k\omega_z + l\omega_p\right) \end{aligned}$$

Of these 9 Lorentzians, only 5 are experimentally significant (i.e. where the Lorentzian peak is at a positive frequency). Those five Lorentzians are then:

Lorentzian	**Weight**
$L\left(\omega_p - \omega_z - \Omega_z\right)$	$-\sin 2\theta \cos^2\phi \rho^{-1,1}_{\alpha\beta}$
$L\left(\omega_p - \omega_z + \Omega_z\right)$	$\sin 2\theta \sin^2\phi \rho^{-1,1}_{\beta\alpha}$
$L\left(\omega_p - \omega_z\right)$	$\frac{1}{2}\sin 2\phi w^{-1,1}$
$L\left(\omega_p - \Omega_z\right)$	$-\cos 2\theta \sin 2\phi \rho^{0,1}_{\alpha\beta}$
$L\left(\omega_p\right)$	$\cos 2\phi w^{0,1}$

So it only remains to present these components-

$$\begin{aligned} \rho^{-1,1}_{\alpha\beta} &= \frac{1}{2} i\alpha \sin 2\theta \left(\cos^2\phi W^{eq}_{dd} - \sin 2\phi \rho^{eq}_{\alpha\beta} L\left(-\Omega_z\right)\right) \\ &\quad + i\alpha \cos 2\theta \cos^2\phi \rho^{eq}_{12} \left(\cos 2\phi L\left(-\omega_z - \Omega_z\right) + 2\sin^2\phi L\left(-\omega_z\right)\right) \\ \rho^{-1,1}_{\beta\alpha} &= -i\frac{1}{2}\alpha \sin 2\theta \left(\sin^2\phi W^{eq}_{dd} + \sin 2\phi \rho^{eq}_{\alpha\beta} L\left(-\Omega_z\right)\right) \\ &\quad - i\alpha \cos 2\theta \sin^2\phi \rho^{eq}_{12} \left(\cos 2\phi L\left(\omega_z - \Omega_z\right) - 2\cos^2\phi L\left(\omega_z\right)\right) \\ w^{-1,1} &= \alpha i - \sin 2\theta \rho^{eq}_{\alpha\beta} \left(L_A\left(\Omega_z\right) - i\cos 2\phi L_D\left(\Omega_z\right)\right) \\ &\quad + \alpha i \cos 2\theta \sin 2\phi \rho^{eq}_{12} \left(\sin^2\phi L\left(-\omega_z + \Omega_z\right) + \cos^2\phi L\left(-\omega_z - \Omega_z\right)\right) \\ \rho^{0,1}_{\alpha\beta} &= \frac{1}{2} i\alpha \sin 2\phi \cos 2\phi \Delta_{cc} \left(1 - \Gamma L\left(-\Omega_z\right)\right) \\ &\quad + \frac{1}{2} i\alpha \sin 2\phi \frac{1}{2}\Gamma\Delta_{ss} \sin^2\phi \left(L\left(-\omega_z\right) - L\left(\omega_z - \Omega_z\right)\right) \\ &\quad + \frac{1}{2} i\alpha \sin 2\phi \frac{1}{2}\Gamma\Delta_{ss} \cos^2\phi \left(L\left(-\omega_z - \Omega_z\right) - L\left(\omega_z\right)\right) \\ w^{0,1} &= -i\Gamma\frac{\alpha}{2}\left(\sin^2 2\phi \Delta_{cc} \left(L\left(-\Omega_z\right) - L\left(\Omega_z\right)\right)\right) \\ &\quad - i\Gamma\frac{\alpha}{2}\Delta_{ss} \sin^4\phi \left(L\left(\omega_z - \Omega_z\right) - L\left(-\omega_z + \Omega_z\right)\right) \\ &\quad - i\Gamma\frac{\alpha}{2}\Delta_{ss} \cos^4\phi \left(L\left(-\omega_z - \Omega_z\right) - L\left(\omega_z + \Omega_z\right)\right) \end{aligned}$$

with the definitions

$$\begin{aligned}\Delta_{cs} &= \cos 2\theta \sin 2\theta W^{eq} \\ \Delta_{cc} &= \cos^2 2\theta W^{eq} \\ \Delta_{ss} &= \sin^2 2\theta W^{eq}\end{aligned}$$

In Chapter 3, these rather complicated coefficients are considerably simplified. To calculate the absorption and dispersion spectra, it is then just a matter of taking the imaginary and real parts respectively of $W^{0,1}$.

6.2 $\hat{\mathbf{x}}$ polarised probe field

The $\hat{\mathbf{x}}$ polarised probe absorption spectrum is given by

$$\begin{aligned}\rho_{ge}^{0,1} = \; & \cos^2\theta\left(\cos^2\phi\rho_{\alpha\beta}^{1,-1} - \sin^2\phi\rho_{\beta\alpha}^{1,-1} + \frac{1}{2}\sin 2\phi w^{1,-1}\right) \\ & -\sin^2\theta\left(-\sin^2\phi\rho_{\alpha\beta}^{1,1} + \cos^2\phi\rho_{\beta\alpha}^{1,1} + \frac{1}{2}\sin 2\phi w^{1,1}\right) \\ & +\frac{1}{2}\sin 2\theta\left(-\sin 2\phi\left(\rho_{\alpha\beta}^{1,0} + \rho_{\beta\alpha}^{1,0}\right) + \cos 2\phi w^{1,0}\right)\end{aligned}$$

which has 9 experimental Lorentzians

Lorentzian	Weight
$L(\delta_p - \omega_z - \Omega_z)$	$\cos^2\theta\cos^2\phi\rho^{1,-1}_{\alpha\beta}$
$L(\delta_p - \omega_z + \Omega_z)$	$-\cos^2\theta\sin^2\phi\rho^{1,-1}_{\beta\alpha}$
$L(\delta_p - \omega_z)$	$\frac{1}{2}\sin 2\phi\cos^2\theta w^{1,-1}$
$L(\delta_p + \omega_z - \Omega_z)$	$\sin^2\theta\sin^2\phi\rho^{1,1}_{\alpha\beta}$
$L(\delta_p + \omega_z + \Omega_z)$	$-\sin^2\theta\cos^2\phi\rho^{1,1}_{\beta\alpha}$
$L(\delta_p + \omega_z)$	$-\frac{1}{2}\sin 2\phi\sin^2\theta w^{1,1}$
$L(\delta_p - \Omega_z)$	$-\frac{1}{2}\sin 2\theta\sin 2\phi\rho^{1,0}_{\alpha\beta}$
$L(\delta_p + \Omega_z)$	$-\frac{1}{2}\sin 2\theta\sin 2\phi\rho^{1,0}_{\beta\alpha}$
$L(\delta_p)$	$\frac{1}{2}\sin 2\theta\cos 2\phi w^{1,0}$

where the components are then equal to

$$
\begin{aligned}
\rho^{1,-1}_{\alpha\beta} &= i\frac{\alpha}{2}\left(\cos^2\theta A^0 + \sin 2\theta D^{-1}\right)\\
\rho^{1,-1}_{\beta\alpha} &= -i\frac{\alpha}{2}\left(\cos^2\theta B^0 + \sin 2\theta D^{-1}\right)^\star\\
\rho^{1,1}_{\alpha\beta} &= -i\frac{\alpha}{2}\left(\sin^2\theta B^0 - \sin 2\theta D^{1}\right)\\
\rho^{1,1}_{\beta\alpha} &= i\frac{\alpha}{2}\left(\sin^2\theta A^0 - \sin 2\theta D^{-1}\right)^\star\\
\rho^{1,0}_{\alpha\beta} &= i\frac{\alpha}{2}\left(\sin 2\theta D^0 + \cos^2\theta A^1 - \sin^2\theta B^{-1}\right)\\
\rho^{1,0}_{\beta\alpha} &= -i\frac{\alpha}{2}\left(\sin 2\theta D^0 - \sin^2\theta A^1 + \cos^2\theta B^{-1}\right)^\star\\
w^{1,-1} &= -i\frac{\alpha}{2}\left(\sin 2\theta\sin 2\phi E^{-1} - 2\cos^2\theta C^0\right)\\
w^{1,1} &= -i\frac{\alpha}{2}\left(\sin 2\theta\sin 2\phi E^{1} - 2\sin^2\theta\left(C^0\right)^\star\right)\\
w^{1,0} &= -i\frac{\alpha}{2}\left(\sin 2\theta\sin 2\phi E^{0} - 2\cos^2\theta C^1 - 2\sin^2\theta\left(C^{-1}\right)^\star\right)
\end{aligned}
$$

The components in these terms are given by

component	value
A^{-1}	$\sin 2\phi \cos^2 \phi \rho_{12}^{eq} \left(L\left(-\omega_z - \Omega_z\right) - L\left(-\omega_z\right)\right)$
A^{1}	$-\sin 2\phi \rho_{12}^{eq} \left(\sin^2 \phi L\left(\omega_z - \Omega_z\right) + \cos^2 \phi L\left(\omega_z\right)\right)$
A^{0}	$\sin 2\phi \rho_{\alpha\beta}^{eq} L\left(-\Omega_z\right) - \cos^2 \phi W_{dd}^{eq}$
B^{-1}	$\sin 2\phi \rho_{12}^{eq} \left(\cos^2 \phi L\left(-\omega_z - \Omega_z\right) + \sin^2 \phi L\left(-\omega_z\right)\right)$
B^{1}	$-\sin^2 \phi \sin 2\phi \rho_{12}^{eq} \left(L\left(\omega_z - \Omega_z\right) - L\left(\omega_z\right)\right)$
B^{0}	$\sin 2\phi \rho_{\alpha\beta}^{eq} L\left(-\Omega_z\right) + \sin^2 \phi W_{dd}^{eq}$
C^{-1}	$-\frac{1}{4} \sin^2 2\phi \rho_{12}^{eq} \left(L\left(-\omega_z + \Omega_z\right) - L\left(-\omega_z - \Omega_z\right)\right)$
C^{1}	$\rho_{12}^{eq} \left(\cos^4 \phi L\left(\omega_z + \Omega_z\right) - \sin^4 \phi L\left(\omega_z - \Omega_z\right)\right)$
C^{0}	$\rho_{\alpha\beta}^{eq} \left(\cos^2 \phi L\left(\Omega_z\right) + \sin^2 \phi L\left(-\Omega_z\right)\right)$
D^{-1}	$\rho_{12}^{eq} \left(\cos 2\phi \cos^2 \phi L\left(-\omega_z - \Omega_z\right) + \frac{1}{2} \sin^2 2\phi L\left(-\omega_z\right)\right)$
D^{1}	$-\rho_{12}^{eq} \left(\cos 2\phi \sin^2 \phi L\left(\omega_z - \Omega_z\right) - \frac{1}{2} \sin^2 2\phi L\left(\omega_z\right)\right)$
D^{0}	$-i\frac{1}{2} \sin 2\phi W_{dd}^{eq} \Omega_z L\left(-\Omega_z\right)$
E^{-1}	$-\rho_{12}^{eq} \left(\sin^2 \phi L\left(-\omega_z + \Omega_z\right) + \cos^2 \phi L\left(-\omega_z - \Omega_z\right)\right)$
E^{1}	$\rho_{12}^{eq} \left(\cos^2 \phi L\left(\omega_z + \Omega_z\right) + \sin^2 \phi L\left(\omega_z - \Omega_z\right)\right)$
E^{0}	$-2i\rho_{\alpha\beta}^{eq} L_D\left(\Omega_z\right)$

The absorption and dispersion spectra can then be derived from the imaginary and real parts respectively of ρ_{ge}^{1}.

Bibliography

[1] A. Abragam, *Principles of Nuclear Magnetism,* (Oxford, 1961); L. Allen and J. Eberly, *Optical resonance and two-level atoms*, (Dover, N.Y., 1987); P. Meystre and M. Sargent III, *Elements of Quantum Optics*, (Springer-Verlag, 1991)

[2] S.H. Autler and C.H. Townes, Phys. Rev. **100**, 703 (1955)

[3] B.R. Mollow, Phys. Rev. A **5**, 2217 (1972)

[4] F.Y. Wu, S. Ezekiel, M. Ducloy and B.R. Mollow, Phys. Rev. Lett. **38**, 1077 (1977)

[5] G. Grynberg and C. Cohen-Tannoudji, Opt. Commun **96**, 150 (1993)

[6] F. Schuda, C.R. Stroud Jr. and M. Hercher, J. Phys. B **7**, L198 (1974)

[7] F.Y. Wu, R. E. Grove and S. Ezekiel, Phys. Rev. Lett. **35**, 1426 (1975)

[8] B.R. Mollow, Phys. Rev. **188**, 1969 (1969)

[9] C. Cohen-Tannoudji and S. Reynaud, J. Phys. B **10**, 345 (1977)

[10] C. Cohen-Tannoudji and S. Reynaud, J. Phys. B **10**, 365 (1977)

[11] C. Cohen-Tannoudji and S. Reynaud, J. Phys. B **10**, 2311 (1977)

[12] C. Cohen-Tannoudji, J. Dupont-Roc, and G. Grynberg, *Atom-Photon Interactions* (Wiley, New York, 1992)

[13] P. R. Berman, Phys. Rev. A **53**, 2627 (1996)

[14] N. Lu and P. R. Berman, *ibid.* **36**, 3845 (1987)

[15] P. R. Berman and R. Salomaa, *ibid.* **25**, 2667 (1982)

[16] F. Bloch and A.J.F. Siegert, Phys. Rev. **57**,522 (1940)

[17] H. Friedmann and A.D. Wilson-Gordon, Phys. Rev. A **36**, 1333 (1987)

[18] A.D. Wilson-Gordon and H. Friedmann, Phys. Rev. A **38**, 4087 (1988)

[19] G.S. Agarwal and N. Nayak, Phys. Rev. A **33**, 391 (1988)

[20] H. Freedhoff and Z. Chen, Phys. Rev. A **41**, 6013 (1990)

[21] W.M. Ruyten, Phys. Rev. A **46**, 4077 (1992)

[22] Z. Ficek and H.S. Freedhoff, Phys. Rev. A **48**, 3092 (1993)

[23] M.F. Van Leeuwen, S. Papademetriou and C.R. Stroud Jr., Phys. Rev. A **53**, 990 (1996)

[24] Z. Ficek and H.S. Freedhoff, Phys. Rev. A **53**, 4275 (1996)

[25] K. Koch, B.J. Oliver, S.H. Chakmakjian, C.R. Stroud Jr. and L.W. Hillman, J. Opt. Soc Am. B **6**, 58 (1989)

[26] G.S. Agarwal and N. Nayak, J. Opt. Soc. Am. B **1**, 164 (1984)

[27] T.G. Rudolph, H.S. Freedhoff and Z. Ficek, Phys. Rev. A **58**, 1296 (1998)

[28] T.G. Rudolph, H.S. Freedhoff and Z. Ficek, J. Opt. Soc. Am. B **15**, 2325 (1998)

[29] H. Wang, V.N. Freire and X-G Zhao, Phys. Rev. A **58**, 1531 (1998)

[30] T.G. Rudolph, Z. Ficek and H.S. Freedhoff, Opt. Comm. **147**, 78 (1998)

[31] G.Y. Kryuchkyan, M. Jakob and A.S. Sargsian, Phys. Rev. A **57**, 2091 (1998)

[32] P. Bucci and S. Santucci, Phys. Rev. A **2**, 1105 (1970)

[33] A.M. Bonch-Bruevich, T.A. Vartanyan and N.A. Chigir, Sov. Phys. JETP **50**, 901 (1979)

[34] G.I. Toptygina and E.E. Fradkin, Sov. Phys. JETP **55**, 247 (1982)

[35] S. Papademetriou, S. Chamakjian and C.R. Stroud Jr, J. Opt. Soc. Am. **9**, 1182 (1992)

[36] Q. Wu, D.J. Gauthier and T.W. Mossberg, Phys. Rev. A **50**, 1474 (1994)

[37] Y. Zhu, Q. Wu, S. Morin and T.W. Mossberg, Phys. Rev. Lett. **65**, 1200 (1990)

[38] N.B. Manson, C. Wei and J.P.D. Martin, Phys. Rev. Lett. **76**, 3943 (1996)

[39] H.S. Freedhoff and M.E. Smithers, J. Phys. B **8**, L209 (1975)

[40] H.S. Freedhoff, J. Phys. B **11**, 811 (1978)

[41] B.J. Dalton and M. Gagen, J. Phys. B **18**, 4403 (1985)

[42] T.E. Barrett, N.G. Woodard and G.P. Lafyatis, Phys. Rev. Lett. **69**, 422 (1992)

[43] S.A. Holmstrom, C. Wei, A.S.M. Windsor, N.B. Manson, J.P.D. Martin and M. Glasbeek, Phys. Rev. Lett. **78**, 302 (1997)

[44] A.S.M. Windsor, Changjiang Wei, Scott A. Holmstrom, John P.D. Martin and Neil B. Manson, Phys. Rev. Lett. **80**, 3045 (1998)

[45] Y. Zhu, Q. Wu, A. Lezama, D.J. Gauthier and T.W. Mossberg, Phys. Rev. A **41**, 6574 (1990)

[46] C.C. Yu, J.R. Bochinski, T.M.V. Kordich, T.W. Mossberg and Z. Ficek, Phys. Rev. A **56**, R4381 (1997)

[47] L.S. Gaida and S.A. Pulkin, Opt. Spec. (USSR) **67**, 446 (1989)

[48] S. Papademetriou, M.F. Van Leeuwen and C.R. Stroud Jr., Phys. Rev. A **53**, 997 (1996)

[49] A.D. Greentree, C. Wei, S.A. Holmstrom, J.P.D. Martin, N.B. Manson, K.R. Catchpole and C. Savage, J. Opt. B **1**, 240 (1999)

[50] A.D. Greentree, C. Wei and N.B. Manson, Phys. Rev. A **59**, 4083 (1999)

[51] Z. Ficek and H.S. Freedhoff, Prog. Opt. **XL**, 389 (2000) and references within

[52] Z. Ficek and H.S. Freedhoff, Phys. Rev. A **53**, 4275 (1996)

[53] H.S. Freedhoff and M.E. Smithers, J. Phys. B **8**, L209 (1975)

[54] H.S. Freedhoff, J. Phys. B **11**, 811 (1978)

[55] B.J. Dalton and M. Gagen, J. Phys. B **18**, 4403 (1985)

[56] A.G. Redfield, Phys. Rev. **98**, 1787 (1955)

[57] J.R. Franz and C.P. Slichter, Phys. Rev. **148**, 287 (1966)

[58] Y. Prior, J.A. Kash and E.L. Hahn, Phys. Rev. A, **18**, 2603 (1978)

[59] T.E. Barrett, N.G. Woodard, and G.P. Lafyatis, Phys. Rev. Lett. **69**, 422 (1992)

[60] S.A. Holmstrom, C. Wei, A.S.M. Windsor, N.B. Manson, J.P.D. Martin, and M. Glasbeek Phys. Rev. Lett. **78**, 302 (1997)

[61] X.F. He, *Raman Heterodyne detected magnetic resonance of the nitrogen-vacancy centre in diamond,* Ph.D. Thesis, Australian National University (1991)

[62] C. Wei, *Optical-radio frequency double-resonance studies of two- and three-level systems* PhD. Thesis, Australian National University (1994)

[63] S.A. Holmstrom, *Characterising the dressed states: A study of the driven two level system* Ph.D. Thesis, Australian National University (1997)

[64] N.R.S. Reddy, N.B. Manson and E.R. Krausz, J. Lumin. **38.** 46 (1987)

[65] D.A. Redmon, S.W. Brown, and S.C. Rand, J. Opt. Soc. Am. B **9**, 768 (1992)

[66] K. Holliday, N.B. Manson, M. Glasbeek, and E. van Oort, J. Phys. Condens. Matter **1** 7093 (1989)

[67] E. van Oort, N.B. Manson and M. Glasbeek, J. Phys. C. **21**, 4385 (1988)

[68] N.B. Manson, X.-F. He, and P.T.H. Fisk, Opt. Lett. **15**, 1094 (1990)

[69] D.A. Redman, S. Brown, R.H. Sands, and S.C. Rand, Phys.Rev. Lett. **67**, 3420 (1991)

[70] I. Hiromitsu, J. Westra, and M. Glasbeek, Phys. Rev. B **46**, 10600 (1992)

[71] M. Yoshimi, Phys. Rev. B. **53,** 11360 (1996)

[72] J.H.N. Loubser and J.A. van Wyk, Rep. Prog. Phys. **41**, 1201 (1978)

[73] A.T. Collins, J. Phys. C. **16**, 2177 (1983)

[74] A. Lenef, S.W. Brown, D.A. Redman, and S.C. Rand, Phys. Rev. B **53**, 13427 (1996)

[75] A. Lenef and S.C. Rand, Phys. Rev. B **53**, 13441 (1996)

[76] H. Hanzawa *et al.*, Physica B **184**, 137 (1993)

[77] G. Davies and M.F. Hamer, Proc. R. Soc. London A **348**, 285 (1976)

[78] J. Walker, Rep. Prog. Phys. **42**, 1605 (1979)

[79] A.T. Collins, M.F. Thomas and Maria Isabel B. Jorge, J. Phys. C. Solid State Physics **16**, 2177 (1983)

[80] J. Mlynek, N.C. Wong, R.G. DeVoe, E.S. Kintzer, and R.G. Brewer, Phys. Rev. Lett. **50**, 993, (1983)

[81] N.C. Wong, E.S. Kintzer, J. Mlynek, R.G. DeVoe, and R.G. Brewer, Phys. Rev. B **28**, 4993 (1983)

[82] J.P.D Martin, N.B. Manson, D.C. Doetschman, M.J. Sellars, R. Neuhaus and E. Wilson, J. Lumin. **86**, 355 (2000)

[83] C. Wei, A.S.M. Windsor and N.B. Manson, J. Phys. B **30**, 4877 (1997)